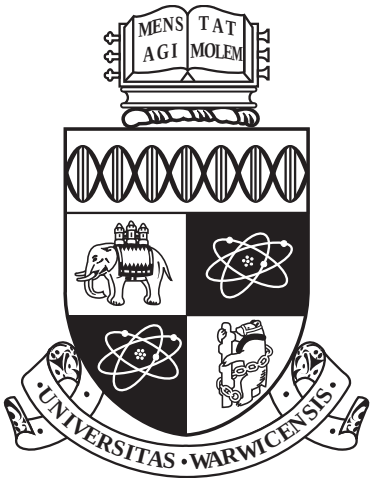

Swarming

by

Daniel J. G. Pearce

Thesis

Submitted to the University of Warwick

for the degree of

Doctor of Philosophy

Department of Physics

September 2014

THE UNIVERSITY OF
WARWICK

Contents

Acknowledgments

	Supervision	Guidance	Academic Support	Financial Support	Emotional Support	Good Times	Spoof	Reading my thesis	Examining my thesis
Prof. Matthew Turner	✔	✔	✔	✔	✔	✔	✔	✔	
Prof. George Rowlands	✔	✔	✔		✔	✔	✔	✔	
Dr. Kevin Moffat	✔		✔						
EPSRC				✔					
MOAC		✔	✔	✔		✔	✔		
Family		✔			✔	✔	✔	✔	
Julia		✔			✔	✔			
PS0.01		✔	✔		✔	✔	✔	✔	
Glendale		✔			✔	✔	✔		
RLT Crew					✔	✔	✔	✔	
WUCC						✔	✔		
Warwick Snow						✔	✔		
Prof. Paul Chaikin								✔	✔
Prof. Rudolf Roemer								✔	✔

Thank you so much to Prof. Matthew Turner, who has been an excellent supervisor, mentor and friend throughout the last four years. Thank you to my family for supporting me in so many ways throughout my life. And finally thank you to Julia, we made it.

"I saw Starlings in vast flights, borne along like smoke, mist - like a body unindued with voluntary power - now it shaped itself into a circular area, inclined - now they formed a Square - now a Globe - now from complete orb into an Ellipse - then oblongated into a Balloon with the Car suspended, now a concave Semicircle; still expanding, or contracting, thinning or condensing, now glimmering and shivering, now thickening, deepening, blackening!"

- Samuel Taylor Coleridge

Declarations

This thesis is submitted to the University of Warwick as my application towards the degree of Doctor of Philosophy. The content of this thesis is my own work, unless stated otherwise, and has been carried out under the supervision of Prof. Matthew Turner and Dr. Kevin Moffat at the University of Warwick. No part of the thesis has been submitted for a degree at any other institution.

The following work has been submitted to refereed journals for publication:

- D.J.G. Pearce and M.S. Turner, "Differentiating swarming models by mimicking a frustrated anti-Ferromagnet", submitted to *Phys.Rev.Lett.*
- D.J.G. Pearce and M.S. Turner, "Density regulation in strictly metric-free swarms", *New J.Phys.*, **16**, 082002 (2014).
- D.J.G. Pearce, A.M. Miller, G. Rowlands and M.S. Turner, "Role of projection in the control of bird flocks", *Proc. Nat. Ac. Sci.*, **111**, 10422 (2014).

Abstract

Swarming is a conspicuous behavioural trait observed throughout the animal kingdom. It is thought to improve collective awareness and offer protection from predators. Self propelled particle (SPP) models are often compared with animal swarms and involve the hypothesis that information coordinating motion is exchanged between neighbours. We identify that minimal models for swarming must achieve a few key properties such as, polarisation, the global alignment of velocities, cohesion, high density that is robust to perturbation. These constraints still leave considerable freedom in the structure of these models. To tackle this degeneracy, and better distinguish between candidate models for polarisation, we first study swarms of SPPs circulating in channels where we permit information to pass through windows between neighbouring channels. Co-alignment between particles then couples the channels so that they tend to counter-rotate. We study channels arranged to mimic a geometrically frustrated antiferromagnet and show how the effects of this frustration allow us to better distinguish between SPP models. There is now experimental evidence that nearest-neighbour interactions in many swarms are *metric free*, but the models that control density rely on attractive and repulsive forces with associated length scales. We propose a solution that involves a metric-free motional bias on those individuals that are topologically identified to be on the surface of the swarm. We find a novel power-law scaling of the real-space density with the number of individuals N as well as a familiar order-to-disorder transition. We argue that local interactions alone are insufficient to explain the organisation of large flocks of birds and expand the strictly metric free model to mimic the information set and abilities of a starling in a murmuration. We postulate that large flocks self-organise to the maximum density at which a typical individual is still able to see out of the flock in many directions; such flocks are marginally opaque. The emergence of marginal opacity constrains how individuals interact with each other within swarms. It also provides a mechanism for global interactions: An individual can respond to the projection of the flock that it sees. We then present evidence for marginal opacity in starling murmurations observed around the UK.

List of Figures

Chapter 1

Introduction

1.1 Collective motion in animals

Swarming behaviour is one of the most impressive features of the natural world. It is a trait present in many species across the animal kingdom with examples from birds, fish, mammals, insects, micro-organisms and of course humans. When many animals come together into one of these congregations it follows that there is likely some benefit over solitary behaviour. In some cases the advantages are more apparent, migratory birds have been observed to fly in a V formation which helps to conserve energy much like cyclists in a peloton[1], or colonies of leaf cutter ants clear paths through the jungle floor between sources of food and the hive[2]. In this thesis I will restrict myself to examining how social swarming could provide increased protection from predation. These types of behaviour come at a significant cost, they require a lot of energy, are very conspicuous and reduce the probability of an individual finding food. It follows that there are likely some benefits as an anti-predation strategy that outweigh these costs.

Observing highly organised groups of animals has inspired researchers for many years. The field was initially the realm of naturalists, artists and writers describing what they saw in the field. Arguably one of the earliest accounts of people trying to explain the behaviour of starling murmurations in a scientific manner would be that of Gilbert White in his letters to other naturalists, published in "The Natural History and Antiquities of Selbourne" [4]. Here he postulates that the driving forces behind the murmurations are that of love and hunger, namely any bird wants to be

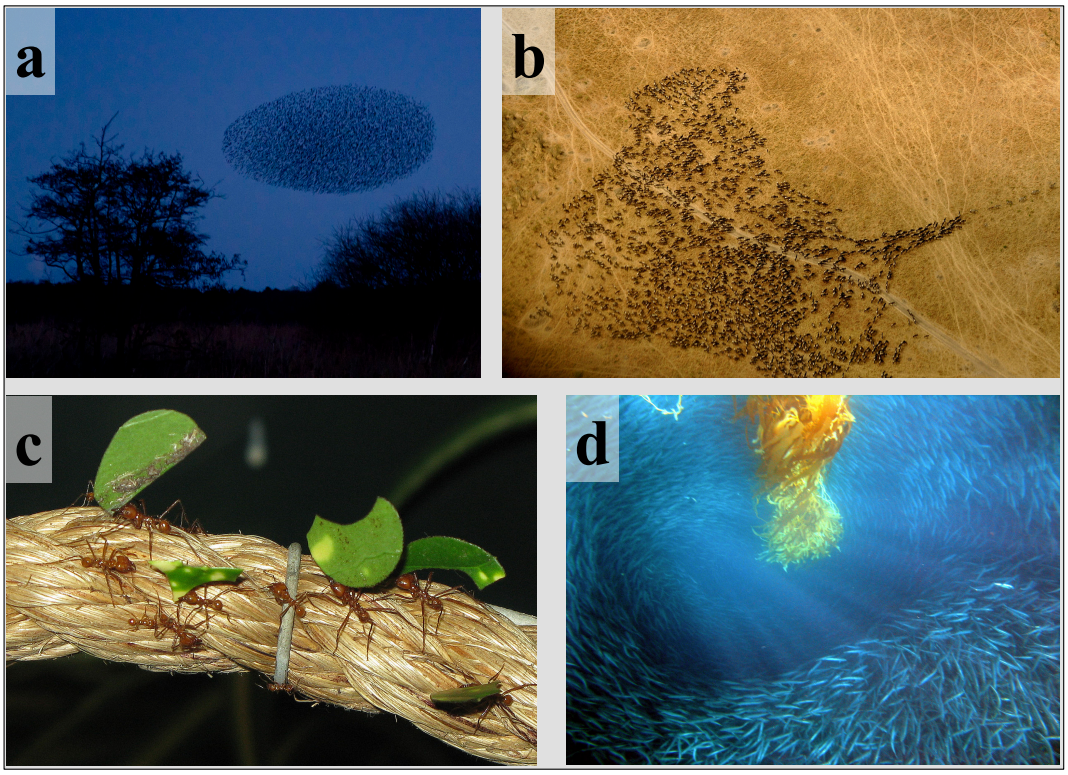

Figure 1.1: Examples of collective behaviours in the animal kingdom. (a) Starling murmurations over roosting sites prior to sunset in Suffolk (UK) (b) Herd of wildebeest and zebra in Masai Mara (Kenya) (c) Leaf cutter ants in Bristol Zoo (UK) (d) Pacific Jack milling around a loose piece of kelp. All images were sourced from wikimedia commons[3].

near the edge of the swarm where there is less competition for food, but also close to many other birds to increase its chance of finding a mate. This is particularly interesting as it hypothesises that the density of a murmuration is a balance of two opposing forces and also that there is no central organisation; it is an emergent behaviour. Similar to Gilbert White, the earliest observers of the collective motion of animals were more interested in the question of "why?" rather than "how?".

1.2 Why do animal aggregates form?

In order to understand how animals form large organised groups, it is useful to first look at why they perform such a conspicuous and taxing behaviour. For the examples we are considering we assume that a primary drive to form large animal

aggregates is safety from predation, indeed it is a behaviour seen almost exclusively in prey species. There are numerous theories as to why exactly, organised group behaviour emerges as an effective anti-predation strategy.

1.2.1 Predator evasion strategies

Dilution effect

Being part of a large group of similar individuals provides anonymity and a reduced probability of being caught by a predator. This is because each individual is only one of a large number of potential targets, an effect known as target degeneracy or the dilution effect[5;6;7]. It follows that as more individuals are added to the group the effect increases. While large animal aggregates often feature individuals interacting with other animals of the same species (conspecifics), the dilution effect would also be advantageous to any group of animals that share a common predator[8;9].

Selfish herd

The dilution effect is often expanded upon by modelling a "selfish herd" [10]. This assumes that the predator will target the prey that it is nearest to, hence it is beneficial for an individual to position itself between other members of the group minimising its exposure[11;10]. For example, consider individuals drinking from a pond containing a predator that is equally likely to emerge at any point on the pond's perimeter. Any individual can maximise its own safety by positioning itself between two other members of the group. If all individuals were to follow this strategy, the result would be a highly dynamic, out of equilibrium system in which individuals constantly circulate away from the edge of the swarm[10;11*]. This hypothesis has formed the basis of models that can recreate some aspects of a group response to a predator, for example insects, fish and even sheep avoiding a sheep dog[12;13;14]. It is not however applicable to all collective animal behaviour as not all swarming behaviour emerges in direct response to the presence of a predator and not all animals can easily change their position within a swarm, for example starlings in a murmuration[15].

Confusion effect

This is a predator evasion strategy which assumes that coordinated motion in prey can confuse the predator and make it difficult for it to single out an individual

*It is of course possible to have all individuals on the interior of a 3D swarm if it is in space that is curved in 4D, we assume the animals are not aware of this.

target[7]. This requires large coordinated motion from the group, necessitating the individuals to effectively work together. Individuals here must take cues from the rest of the flock and cannot just act selfishly as in the example above. Typically this would require cohesion and co-alignment, hence a sharing of information leading to highly polarised swarms. The confusion effect takes advantage of perceptual bottlenecks suffered by predators[16]. There is also evidence that this effect also deters predators from targeting large swarms as the confusion may leave them more vulnerable to predation themselves[17]. This effect has been observed in fish, primates, birds and insects[18;19;20;21;7].

Many eyes hypothesis

The many eyes hypothesis postulates that all individuals within a swarm make observations that add to their collective knowledge. The group having more information on its surroundings leaves it better equipped to deal with predation[7;22;23]. Indeed it has been shown that animals are more efficient at avoiding model predators[24] and obstacles[25], finding food[26] and following concentration gradients[27] by sharing information within groups. As well as efficiently sharing information, the many eyes hypothesis also requires that the group is able to make collective decisions, indeed there is evidence that larger groups are better at making decisions based on the information of an informed subset of the swarm[28].

Bottom-up organisation

Many predator evasion strategies rely on the idea that any individual can contribute information or help make a decision for the whole swarm. This would mean that there is no one leader; this is referred to as bottom up, self organised behaviour[29]. This is part of what makes these systems so appealing to physicists, they are an example of emergent behaviour; we observe the bulk properties of the system which is the result of many independent agents each reacting to some pre defined set of rules governing its behaviour. The converse would be top-down, centralised organisation in which one individual takes the role of leader and makes all the decisions for the whole swarm[29]. Both methods of group organisation can be effective and distinguishing between them is not trivial, the main difference being the response of the group to perturbations[29]. Consider a swarm in which individuals only react to the signals of a leader, therefore the behavioural fluctuations of two (non leader) individuals are independent. In this case the group will not initialise a response to

a perturbation unless it (or its effect on an individual) is detected by the leader. Therefore swift collective responses to external perturbations is indicative of bottom up, self organised behaviour[30]. A fast, collective response to perturbation is crucial for groups of animals under pressure of predation[31;32], for this reason this study will concentrate on bottom up organisation. It is worth noting that there are examples of top down organisation within the animal kingdom, for example the hierarchical structure observed in an bee colony[33] or pack animals such as a pride of lions[34].

1.3 Observations

Since Gilbert White observed large starling murmurations in the 18^{th} century there have been many advances in science that have allowed for more detailed observations and measurements on swarming animals to be made. These studies go through the animal kingdom at every length scale, from bacterial colonies to humans, and even in many non animal systems, such as chemotaxins, liquid crystals and molecular motors[35;36;7].

1.3.1 Insect swarms

One of the most studied examples of collective behaviour is in large insect groups. There may be two reasons behind this. First, it is possible to keep and study large numbers of insects in a controlled environment in a lab. Secondly, locust damage to crops has a serious impact in many areas of the world, both economic and social. For example, the 2004 locust infestation in North and West Africa caused damage with an estimated cost of over $400 billion[37;38]. Insects represent an incredibly diverse set of organisms, while some species lead a solitary life, many display different types of collective motion[39]. Insects swarm for many reasons, including having hive-like societies such as ants, termites and honey bees[40], migratory behaviour observed in many species of butterflies[41], or swarms moving between food sources, like those observed in locusts[42]. There are many ways for insects to achieve this, some notable examples include ant pheromone trails[43] and bees "dancing" communication[40]. We are concerned with less structured, emergent behaviour, for which marching bands of locusts are a well studied example[44;45;46;47].

Locust swarms form when many juvenile locusts gather and enter the "gregarious" phase, rather than the "solitarious" phase. When this occurs they form large, highly polarised marching bands that can be many kilometres long[47]. This is an

important stage in the formation of a swarm as it happens on the ground, where the locusts are far more easily managed. If the marching bands recruit enough locusts, then a swarm will form in which they will fly to other areas of food and can destroy vast areas of farmland. Recent observations indicate that the formation of marching bands is based on the density of the locusts and the level of food available. When the density is high enough and the food levels are low enough, cannibalistic interactions will drive the formation of highly polarised marching bands[44;45;46]. This is tested by removing the ability for individual locusts to detect the approach of others or detect being bitten, which leads to the marching bands no longer forming[46;44]. Locusts are also more likely to bite conspecifics that are approached side on and stationary, hence it drives local alignment[45].

The link between density and the onset of collective motion was most elegantly explored by putting swarms of locusts in a circular track, the argument being that the locusts were not aware of the curvature and this was essentially an infinitely long tube[42]. When the density is sufficiently high, the locusts go from uncorrelated random walks to highly polarised marching bands. Due to the nature of the enclosure these are either clockwise or anticlockwise. For such polarised marching bands, there is an associated switching time between anticlockwise and clockwise polarised motion which increases with the density, until eventually becoming fixed[42]. This was shown to closely resemble the results of a one dimensional self propelled particle model in which particles co-align with neighbours within a certain distance[42;48]. This study was the inspiration for the work outlined in Chapter 2.

1.3.2 Fish schools

Fish schools are another well studied example of swarming species. Fish provide a significant proportion of our diet with the human race consuming around 19kg of fish per capita per year. The worlds fisheries produce 158 million tons of fish per year and 12% of the world's population depend on the industry for their livelihood[37]. Similar to insects, there is a huge diversity in species of fish, particularly in physical size. Despite this, schooling behaviour is surprisingly prevalent, observed in some 50% of all bony fish species, suggesting it originated very early in vertebrate evolution[49]. Small schooling fish, such as golden shiners, can be studied in a lab with the correct equipment, whereas larger schooling fish, for example tuna, can only realistically be studied in large groups in the wild.

Many studies have been performed to measure the shape and size of large

fish schools in the wild. Originally it was thought that fish schools had no internal structure[50], then it was hypothesised that fish occupy positions on a crystal lattice[51]. Modern methods have made it possible to make accurate measurements on the internal structure of schools and revealed many structural features. These include anisotropic nearest neighbour distribution with fish less likely to directly follow other fish, rather arranging themselves slightly off centre[52;53] and certain preferred nearest neighbour separation[53;54;55]. Fish schools can also come in a wide range of morphologies, including spheroids, paraboloids and vortices[52;53;56;55], see Fig. 1.1d.

Studying schools of smaller species of fish in the lab allows detailed observations to be made. In particular the concurrent trajectories of all fish in a swarm can be obtained with a high level of accuracy. This has allowed the direct observation of a density dependent order transition in some species of fish[57]. By confining fish in a ring shaped enclosure, much like the one described above with locusts[42], it was shown that models considering the topological arrangement of the fish, as well as their numerosity, more accurately describe the schools[58]. The concurrent trajectories of interacting fish has been used to establish that the polarisation of schools of golden shiners depends on speed regulation rather than co-alignment, and that two body interactions alone are insufficient to explain the observed dynamics[59].

Information sharing can also be studied in fish schools in a lab. Larger groups of fish have been observed to more efficiently follow concentration gradients[27], find food[26] and avoid predators[24], indeed fish that cannot see a predator will take evasive action if the behaviour of conspecifics indicates a predator is near[60]. By presenting choices with mutually exclusive outcomes it has been shown that schools are also better than solitary fish at making decisions based on their surroundings[60;24]. The observation that larger groups make more effective decisions suggests that there is some sort of group decision making process. Many studies have tried to probe how a school manages to reach a consensus action based on the information and influence of all the fish[61;62;63]. It has been observed that a pre-trained subset of fish (leaders) within a group can effect the behaviour of the school by leading it toward previously learnt feeding sites[64]. Also, when a fish school must decide between two, competing subsets of leaders, having a larger number of uninformed individuals increases the efficiency with which the school identifies the largest subset of leaders[28]; this supports the idea that the decision making process is performed as a group. Another method to assess how schooling fish react to one another is to introduce replica conspecifics, which has been used to demonstrate that groups of fish are more likely to significantly change their behaviour when the number of leaders reaches some threshold[62].

1.3.3 Bird flocks

Keeping large flocks of birds to study in controlled environments is very difficult. For this reason all studies on large bird flocks are done in the wild, which brings its own set of difficulties. Until recently visual observations (and those from photographs or video) were all that could be used, with the 3D position and velocity of individual birds being unobtainable. The reason for this is technical, to obtain full 3D positions one would need concurrent video from (at least) two positions. Each individual must then be identified in all concurrent images and these images then used used to triangulate the full 3D position of each bird. A tracking algorithm must then follow each bird over subsequent frames of the video to recover a full trajectory. Due to the nature of this technique some luck is also needed, as flocks must fly in front of multiple static cameras at the same time and be disperse enough for the tracking algorithms to identify every individual bird from multiple angles. Early attempts at these techniques managed to track the positions of tens of birds, but these were often small groups moving to or from roosting sites[65;66;67]. It was not until the STARFLAG project[68;69] that the detailed analysis of large bird flocks was achieved, allowing statistical techniques to be employed on large murmurations.

Analysis of the 3D positions of the birds within the flocks confirmed that they have a quasi-2D morphology, taking the shape of a (curved) sheet[70]. It was observed that the velocities of neighbouring starlings are highly correlated and that the correlation range is proportional to the size of the flock[70;71]. For example, the velocities of two birds separated by 1m within a 10m wide flock are as strongly correlated as the velocities of two birds separated by 10m within a 100m wide flock. Hence the interactions ruling the behaviour of the birds are scale free. It was suggested that starlings co-align with their nearest neighbours within a flock, but that these neighbours are selected topologically rather than metrically[70;71;30]. Detailed analysis of the trajectories suggest that it is likely each starling within a flock co-aligns with its six or seven nearest neighbours, regardless of separation[71]. This would result in more robust flocks that are less likely to fragment[30]. It was observed that the interacting neighbours within a flock also have an anisotropic angular distribution, occurring more often to the sides rather than in front or behind each other[70;71]. There is also a detectable difference in the behaviour of birds on the surface of the flock from those in the bulk[70]. This give rise to an apparent inflow of information from the surface, which promotes mixing within the flock and the exchange of neighbours[72]. It has recently been shown that when a flock of birds performs a turn, this

is initiated by a small region of densely packed birds between which there is a very rapid flow of information. This makes it appear that they decide to turn at almost the same time. The resulting turn has been observed to propagate through the flock at a constant speed, which does not depend on the density of the flock[73].

There has been significant work on the collective motion of other types of birds. Using GPS data loggers to obtain the positions of birds during flight it has been observed that flocks of homing pigeons are more efficient at finding a path home than solitary pigeons. It has been suggested that this may be related to the flock averaging over the known routes of the individuals[74]. Surf scoters form large groups on the water surface, making their flocks, and interactions, two dimensional. This makes very high precision data easier to obtain and has been used to fit a model with with different angular and radial interaction zones able to explain the patterns seen in the flock[75].

Flying as part of a large swarm is highly computationally demanding and many studies suggest that the ocular and cognitive capabilities of birds are well adapted to the task. Pigeons have been shown to be capable of accurately discriminate and follow sets containing up to six or seven objects[76]. This supports the observation that birds co-align with their six or seven nearest neighbours[71]. When starlings are in flight their eyes are pointing nearly 150 degrees in different directions[77] giving them a very wide viewing angle. While this affords greater awareness[78;79;80], the amount of binocular vision, and therefore depth perception, is greatly reduced.

1.4 Modelling Approaches

Arguably the first attempt at recreating the collective motion of animals is the "Boids" model developed by Reynolds[81] in 1987. This model was proposed for use in computer animation as an alternative to scripting the exact path for every individual in a swarm. It was used to great effect in the 1992 film *Batman Returns* to create animations of bats and penguins moving through Gotham City. Reynolds employed a technique called agent based modelling in which the macroscopic behaviour of a complex system is simulated using many interacting, autonomous agents, often referred to as particles. This technique is clearly suited to modelling self organised animal behaviour. By simulating many agents that interact at the micro-scale, and observing the emergent behaviour at the macro-scale, we can use this approach to learn more about the underlying mechanisms of swarming.

When using agent based models to study collective animal behaviour an evolution equation is specified for the position and velocity of each agent, which determines how it gathers and utilises information from its environment at any one time. Typically this describes the social influences acting on the agent at a microscopic level. For example, the Boids model involved local co-alignment, short ranged repulsion and long ranged attraction between agents (referred to as "boids")[81]. A large number of these agents are then studied by iterating their positions over time, the emergent behaviour of the swarm is the result of the choice of rules assigned to each agent. In the present study we concern ourselves with minimal models; i.e. those that aim to simulate only the decisions made by the individuals within a large swarm. The predator evasion strategies outlined earlier highlighted a few key features of swarms that should be central to developing a minimal model: Cohesion, ordering and rapid information transfer. A minimal model capable of recreating these features can be expanded to include external influences on swarms, such as predation or flight physics[82;83;1;84].

1.4.1 Ordering within swarms

Arguably the best known model for polarised collective motion is that of Vicsek et al.[48]. In this model, groups of Self-Propelled Particles (SPPs) move off lattice with a constant speed within a periodic box. The future direction of each particle is taken to be the average of its neighbouring particles' directions combined with a random contribution with adjustable weight. This random contribution is used to introduce perturbations to the system, such as would arise in flocking organisms due to deterministic and stochastic factors affecting their motion. This is commonly referred to as statistical "noise" and will be referred to as such throughout the thesis. The neighbours with which a particle interacts are selected as those within a certain pre-defined metric radius, see Fig. 1.2a. When many of these particles interact within a periodic box they display an ordered state, in which all particles' velocities are aligned, and a disordered state, in which all particles explore seemingly independent random walks. The transition between the two states is controlled by the density and the maximum magnitude of the noise. Principally this teaches us that local co-alignment interactions are sufficient to create global order within a swarm of fixed density.

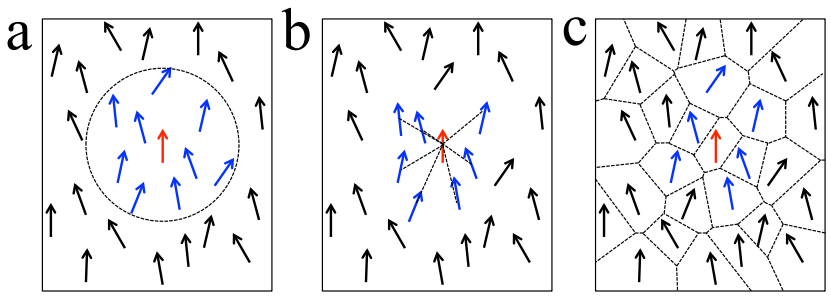

Figure 1.2: Different example of how the red individual can assign the neighbours with which it co-aligns (blue), (a) all neighbours within a metric radius, (b) the nearest n_c (in this case 7) nearest neighbours regardless of separation, (c) all neighbours who are connected under a delaunay triangulation.

Since the initial Vicsek model, many more models for creating ordered swarms have been developed, indeed it is easy to think of different selection criteria for the neighbouring particles. Recent experiments on flocks of starlings[70;30], fish[58] and human crowds[85] have shown that the controlling interactions are more likely metric free, at least in large murmurations. This naturally constrains the underlying models to also have a metric-free character, ushering in a new class of metric-free models[86;87;71;88]. In the metric-free Vicsek model[71], neighbours are selected as the n_c nearest neighbours, regardless of separation, see Fig. 1.2b. This gives rise to swarm velocity correlation ranges that scale with the size of the swarm, as observed in birds, and make the swarm more robust to fragmentation. This approach makes it impossible for an individual to become isolated from the swarm because it always interacts with its nearest n_c neighbours. At most the flock can be fragmented into subgroups containing at least $n_c + 1$ individuals. The topological Vicsek model[86] differs from the original, metric-based, version in that neighbours are assigned to be those that form the first shell in a Voronoi tessellation, equivalent to being connected by edges under a Delauny triangulation[89], see Fig. 1.2c. This procedure has the advantage that it is completely metric free and it is now impossible to fragment the group. It also has the satisfying feature that it has one less control parameter, lacking an interaction radius or number of nearest neighbours.

These models all show that local co-alignment between autonomous agents is sufficient to create swarms with long range polarisation, but they all share one flaw. Without any terms in the model controlling the separation of the agents, they are unable to establish a cohesive swarm with a well defined density unless confined to

a periodic box[86;35].

1.4.2 Cohesion of swarms

Another primary feature of swarms is cohesion, essentially the ability of the swarm to stay together and not fragment. Cohesion has been introduced in a multitude of ways using agent based models. The previous section introduced the idea of confining the swarm to a periodic box, hence fixing its density, but this merely avoids the issue and does not explain how cohesion might be achieved in animal groups.

The most commonly used method of creating cohesion within SPP models in unbounded space takes the form of a motional bias applied pairwise between particles. This is often a combination of long ranged attraction and short ranged repulsion which in turn introduces some preferred inter particle distance[90;91;92;93]. In one representative study[90] an individual will feel a repulsion from all individuals within a certain radius, $r \in [0, r_R]$, in order to prevent collisions. Individuals co-align with individuals within an intermediate range, $r \in (r_R, r_O]$, which will lead to global polarisation provided the density is sufficiently high. Agents are also attracted to all individuals at a greater range, $r \in (r_O, r_A]$, such a long ranged attraction will prevent fragmentation of the flock. Concentric zones like this give the particle-particle interaction a discontinuous nature, this can of course be modified to utilise any attraction/repulsion function, for example a Lennard-Jones type potential can result in a cohesive swarm[94]. These types of models all introduce a preferred separation from nearest neighbours, effectively fixing the density. They also involve an individual performing a calculation based on the exact position of all neighbours within a certain radius just to achieve flock cohesion.

1.5 Statistical mechanics of swarming

Agent based models can exhibit self organisation. Each agent's responses are based only on local rules but we get an emergent globally quantifiable behaviour. We use numerical methods to realise these models as they cannot yet be easily solved analytically; the set of coupled dynamic equations for a large swarm are too numerous to be realistically manageable. This has lead to the study of the physics of global features of these systems using approaches from statistical physics.

1.5.1 Order transition

In SPP models the disordered state is one in which the velocities of the individuals are randomly orientated and the ordered state is one in which the velocities of the particles are all aligned, see Fig. 1.3. The external parameter controlling the state the system is the noise amplitude, i.e. the maximum value the random addition can take. When the noise amplitude is low there is very little noise interfering with the interactions between particles and they are all able to co-align, giving a highly polarised swarm with a significant net motion. When the noise amplitude is high the particles are essentially on independent random walks and the system is disordered. To quantify this we define the order parameter as the normalised velocity of the centre of mass of the swarm

$$P = \frac{1}{N}\left|\sum_{i=1}^{N} \hat{\underline{v}}_i\right|. \tag{1.1}$$

Here, and throughout, a hat $\hat{}$ denotes a normalised vector and $\underline{v}_i$ is the velocity of individual i of a swarm of N particles, which give $0 \leq P \leq 1$. When the system is perfectly ordered, with all velocities aligned, this gives $P = 1$. For a disordered system, in which the velocities are randomly orientated it will give $P \sim O\left({}^{1}/_{\sqrt{N}}\right)$, see Fig. 1.3.

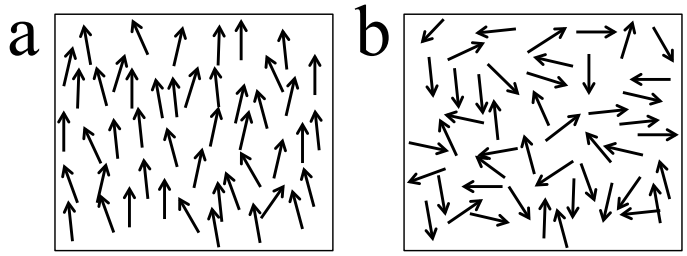

Figure 1.3: Example of SPP particles in the (a) ordered ($P > 0.9$) and (b) disordered state ($P < 0.1$). The order parameter is a measure of alignment, therefore symmetric velocity fields with no net alignment, for example divergent, convergent or circular fields, have $P \approx 0$.

The order transition involves a sudden symmetry breaking of the system. Upon adopting the ordered state a preferred direction of motion for the entire swarm

is spontaneously adopted. This transition can be either discontinuous (first order like) or continuous (second order like) with respect to variation of the noise amplitude. The nature of this, and similar, transitions have been studied in depth and have been the subject of much debate [48;95 96;97 98;99 100;101 102;103]. Recent studies took advantage of the rotational symmetry of the system to show that if the velocity of the particles is large, artefacts related to the boundary conditions can lead to an erroneous description of the order transition [102] and confirmed its continuous nature [98;99;100]. The nature of the transition has also been shown to depend intimately on the type of noise added to the particles [104]. The original Vicsek model featured "angular" noise, where a random angle is added to the orientation of the velocity of a particle and has a continuous order transition. If the model is modified to feature "vectorial" noise', in which a random unit vector is added to the velocity of a particle the order transition takes on a discontinuous character [96;105].

1.5.2 Correlation functions

Correlation functions can be used to asses the degree to which two series of data are related, essentially measuring their similarity. A cross correlation function can be used to asses the correlation between two functions at different phase shifts (δt). For two data series $A(t)$ and $B(t)$ taken over time $t \in [0, T]$, with means μ_A and μ_B and variances σ_A and σ_B, respectively, the cross correlation function is here defined as the following equation.

$$C_{AB}(\delta t) = \frac{\sum_{t=0}^{t=T-\delta t}[(A(t) - \mu_A)(B(t + \delta t) - \mu_B)]}{(T - \delta t)(\sigma_A \sigma_B)} \tag{1.2}$$

This function gives a maximum at the phase shift, δt, at which the functions are most congruous. This can also be used to asses how self similar a data series is by defining the autocorrelation function.

$$C_{AA}(\delta t) = \frac{\sum_{t=0}^{t=T-\delta t}[(A(t) - \mu_A)(A(t + \delta t) - \mu_A)]}{(T - \delta t)(\sigma_A \sigma_A)} \tag{1.3}$$

This can be used to measure de-correlation timescales, denoted τ, essentially a measure of how quickly a system changes and relaxes from perturbations. .

1.6 Outline of the thesis

In this thesis we will study minimal models for how large groups of animals interact. Chapter 2 will address the issue of metric vs. metric free interactions in the co-alignment term between agents. To do this, we will employ ring shaped enclosures, similar to those described previously for locusts and fish[42;58]. By setting up a system in which agents pass information between rings it is possible to "frustrate" them, much like spins in an antiferromagnetic triangular lattice[106]. This is used to discriminate between similar flocking models in a new way. Chapter 3 addresses the issue of metric free cohesion by employing interactions based on only topological relationships. This leads to the first completely metric and scale free model for swarming. We expand this idea further in Chapter 4 in which we relate cohesion in flocking models to how birds obtain information from their surroundings, i.e. as a 2D projection of the world onto their retina. We call this a hybrid projection model. This model leads to several interesting predictions including the marginal opacity of flocks of birds. In Chapter 5 we present data collected on starling flocks in the wild to test the predictions of the hybrid projection model.

Chapter 2

Distinguishing methods of nearest neighbour identification

Much of the work in this chapter is under review, it is also available online in the article 'Differentiating swarming models by mimicking a frustrated anti-Ferromagnet' by Pearce et al.[107].

There is a huge amount of freedom in how we construct an agent based model able to recreate swarming behaviour, evidenced by the various models proposed to recreate this effect[94;36;35]. In these models a simple set of rules for the behaviour of an individual agent is specified. When enough of these identical agents are introduced the result is a swarm with some macroscopic collective behaviour that depends on the selection of the microscopic rules. It can be very difficult to refine the "microscopic" rules for each individual by studying data for the collective "macroscopic" behaviour. The essential difficulty is that model building is an inverse problem in which no techniques yet exist to perform this inversion. In this chapter I will introduce a way of frustrating swarms of interacting particles using a physically restricted geometry that takes inspiration from frustrated anti-ferromagnets. This method reveals new "macroscopic" behaviours that can be used to distinguish between two very similar (but fundamentally different) SPP models for polarised swarms.

Swarms of animals are often highly ordered, this feature is generated in agent based models through the co-alignment between particles. This involves each agent updating its velocity based on the velocities of those around it. To create global order it is sufficient for each individual within a swarm to co-align with a subset of the swarm. There is considerable freedom in the selection criteria for this subset.

The finite ranged velocity correlations observed in swarming animals suggest that this interaction is local, i.e. individuals co-align with their nearest neighbours within the swarm. There are many suggested methods by which these nearest neighbours can be selected and distinguishing between them is a deceptively difficult task [71;86;48].

Recent experiments have employed constrained environments to further probe swarming behaviour [42;62;58;108] even managing to create behaviour that mimics logic gates [109;110]. The work in this chapter was primarily motivated by one such experiment performed on locusts enclosed in a ring-like track [42]: As the density of locusts was increased they were observed to undergo a transition from a state of random motion to a polarised state in which they co-aligned to create coherent, circulating swarms. Due to the ring-shaped enclosure (track) the swarm can polarise into clockwise or anticlockwise circulation, giving it a binary or spin-like nature, see the *isolated system* panels Fig. 2.1. It was shown that this behaviour can be reproduced by a simple one dimensional SPP model with periodic boundary conditions [42]. Here the polarisation transition and the spontaneous polarisation switching time could be related to the parameters of the model. However, it is hard to draw any definite conclusions concerning the structure of the model as there remains considerable freedom to choose different structurally and parametrically distinct SPP models that could be capable of reproducing this behaviour, as I will show in this chapter.

2.1 Find out how it works by breaking it

Our approach is to seek to break the behavioural degeneracy between models. In order to achieve this we first consider two ring-shaped channels arranged near to one-another that share a (section of) boundary through which the individuals can pass information, but cannot physically cross. This could be realised experimentally by connecting the rings by a window. In animals that mainly depend on their sense of vision a transparent window would be appropriate; for animals that use touch a limited physical opening might be used. This window is assumed to provide a coupling between the two rings. Here we extend the interactions between individuals to include neighbours that are visible through the window, as well as those that are visible inside the same ring, and use the same behavioural rule for both cases. For highly polarised swarms, driven by co-alignment, we would then expect a ring polarised anticlockwise (an "up" spin) to be most stable when it is adjacent to

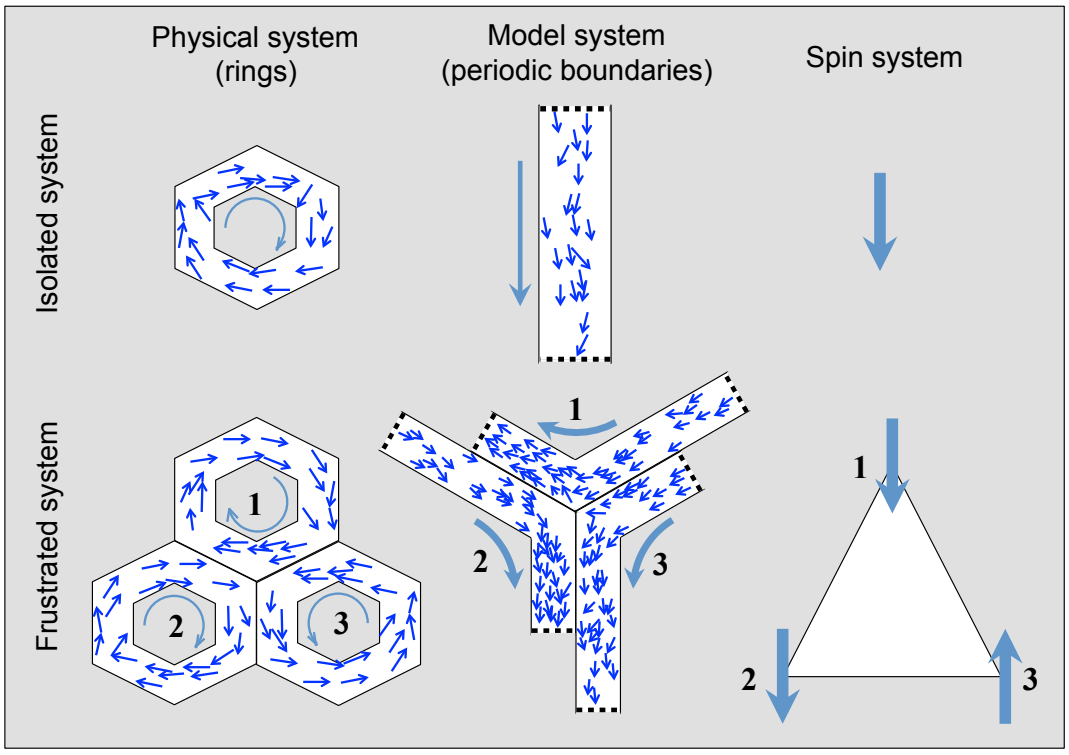

Figure 2.1: Different SPP models are studied in confined tracks. **Isolated system**: The macroscopic behaviour of a ring containing swarming animals is approximated by interacting agents moving in a linear, semi-periodic channel, for simplicity. Clockwise/anticlockwise collective motion in the ring, analogous to a spin, corresponds to motion up/down the semi-periodic channel. **Frustrated system**: The motion within three rings arranged on a triangular lattice is frustrated when interactions are permitted across windows between the tracks. This is again simulated using linear semi-periodic channels for the SPP model (which remain linear but are shown as kinked in the middle panel for clarity; periodic linear channels with windows between all pairs cannot easily be represented in a 2D image). This system can be interpreted as analogous to a geometrically frustrated anti-ferromagnet.

a ring polarised clockwise (a "down" spin), or vice-versa: Only in this situation would neighbours connected through the window also find themselves co-aligned. The coupling across the window is therefore analogous to being *antiferromagnetic* in character.

Inspired by the extensive literature that exists in condensed matter physics on geometrically frustrated antiferromagnetic systems[111;112;106] we analyse motion in three rings arranged so they each each share a boundary with the other two, see

the *frustrated system* panels Fig. 2.1. In this way we create a system similar to geometrically frustrated antiferromagnetic atoms on a triangular lattice. It is now not possible for all three rings to remain highly polarised and co-aligned across all windows. As in the analogous magnetic system we no longer expect a unique (trivial) ground state to exist, see Fig. 2.1. This affords us additional information from the resulting behaviour, whatever it may be, that can be used to better distinguish microscopic models. In this chapter I will compare the behaviour of two different SPP models frustrated in this way in order to obtain new behavioural information with which to discriminate between them.

2.2 Model Details

In what follows we compare two different SPP models frustrated in this way. Apart from the boundary conditions both our SPP models take a fairly standard form in which N particles move in a (3D) periodic box with a constant speed v_0. At each discrete time step every particle orientates its velocity along the average direction of its neighbours (combined with some vectorial noise). The only difference between the two models studied here will be how these neighbours are identified. Writing those neighbours to the i^{th} particle as $\mathcal{N}_i$ the equation of motion involves the normalised average velocity of its neighbours $\widehat{\langle \underline{v}_j^t \rangle}_{j\in\mathcal{N}_i} \equiv \frac{\sum_{j\in\mathcal{N}_i} \underline{v}_j^t}{|\sum_{j\in\mathcal{N}_i} \underline{v}_j^t|}$. Noise is introduced by randomly orientated unit vectors $\hat{\underline{\eta}}_i^t$ that are uncorrelated between individuals and in time $\langle \hat{\underline{\eta}}_i^t \cdot \hat{\underline{\eta}}_j^{t'} \rangle = \delta_{ij}\delta_{tt'}$. The position, r_i, and velocity, v_i, of particle, i, within a swarm are then given by the following equations, where the parameter $0 \leq \phi_n \leq 1$ controls the relative weighting of the noise term and angular brackets $\langle \cdots \rangle$ denote an average over the subset indicated. The particles here move a fixed distance per time step, v_0 (equivalent to a length of time step Δt), which we set to unity, $v_0 = 1$.

$$\underline{v}_i^{t+1} = (1-\phi_n)\widehat{\langle \underline{v}_j^t \rangle}_{j\in\mathcal{N}_i} + \phi_n \hat{\underline{\eta}}_i^t \tag{2.1}$$

$$\underline{r}_i^{t+1} = \underline{r}_i^t + v_0 \hat{\underline{v}}_i^t \tag{2.2}$$

For the remainder of this chapter we restrict our attention to two leading classes of SPP models. The first of these is a model which selects nearest neighbours according to a **metric**-based measure of distance (the model due to Vicsek and coworkers[48] is often cited as a prototype of this class of models). Here a particle co-aligns with others that lie within a fixed interaction range R. Individuals can have as few as zero or as many as $N-1$ neighbours within this definition. The second model

selects nearest neighbours according to a **metric-free** scheme, recalling the evidence for interactions with this character in bird flocks[30;71]. In this model each particle aligns with the n_c nearest particles, irrespective of absolute separation. Both these models exhibit two distinct states, *ordered*, in which the particles achieve a high level of polarisation and all their velocities are highly aligned, and *disordered*, in which there is no net polarisation and the velocities of individuals are largely uncorrelated. The transition from the disordered to the ordered state is primarily controlled by two quantities: the noise weighting ϕ_n and the density of particles. For sufficiently low noise ϕ_n and high density, this system achieves a high level of polarisation in which the velocities of all the individual particles are highly aligned. As the noise is increased (or the density is decreased) the system undergoes a transition into a disordered state in which there is no net alignment of the particles' velocities. Here, we simulate these swarms in a semi-periodic box. We take N particles in a box of width W, height H and length L in the x, y and z direction respectively. This is an unconventional SPP system in that it is only periodic in the z direction. If a particle reaches a boundary perpendicular to the x or y directions it undergoes an elastic collision where the component of its velocity perpendicular to that boundary is reversed. In this way the swarm is effectively confined to a long, thin (periodic) channel. For simplicity we set $v_0 = 1$ and fix $W = H$ and $L = 10W$. The choice of L here is somewhat arbitrary provided it is large enough. Since the box is periodic in the z direction the primary significance of the value of L is only in that it controls the density of particles $\rho = N/(L \times H \times W)$, provided $L >> v_0$ and $L >> R$ for the metric model. This leaves three control parameters, the number of particles N, the noise weighting ϕ_n and the interaction range (R for the metric and n_c for the metric-free models).

It is worth mentioning here that there is a need to carefully map the $\pm z$ direction in the channels containing the SPP particles and the clockwise/anti-clockwise polarisation of the insects in the 3 ring frustrated system. For this reason agents in adjoining channels perceive adjacent swarms with a reflection that reverses their z coordinates, $z \to -z$, meaning they anti-align in real space. This allows the frustration to be established in a symmetric manner between the three channels and a direct map from $\pm z$ to clockwise/anticlockwise.

Consider the following example. We have three rings, modelled by three periodic channels. Each ring can be polarised clockwise or anticlockwise, and each channel can be polarised in the $\pm z$ direction. If the z coordinate *is not* switched between adjacent channels, all channels can co-align in the $+z$ direction with no

frustration. This is clearly not equivalent to the frustrated ring system. Conversely, if the z co-ordinate *is* inverted for adjacent channels, channel 1 polarised in the $+z$ direction will align with channel 2 polarised in the $-z$ direction (ring 1 clockwise with ring 2 anti-clockwise). Now channel 3 would have to polarise in the $-z$ direction (ring 3 anti-clockwise) to align with channel 1, or the $+z$ direction (ring 3 clockwise) to align with channel 2. Hence the system is frustrated.

All simulations were performed using software written in C++ by the author. The initial conditions for the particles were with randomised positions and orientations within their allocated channel. The simulations were pre-equilibrated for at least 10,000 time steps, which is significantly longer than the density and polarisation autocorrelation times which are of the order of 1000 time steps (where the polarisation is able to switch within the timescales accessible by simulation) see Fig. 2.2. The resulting behaviour was then analysed over a period of 100,000 time steps. For observations of the spatial inhomogeneity, the results were based on ten separate observations each 10,000 time steps because the system is weakly ergodic for low noise configurations.

Measured Quantities

Due to the nature of the semi-periodic box, the swarm cannot sustain a high level of polarisation unless it is aligned parallel, or anti-parallel, to the z axis. This is because a net alignment in either the x or z direction will cause the swarm to quickly interact with a non-periodic boundary and the members of the swarm will rapidly change direction in an incoherent fashion until order along z re-emerges. For this reason it is possible to quantify the polarisation of the system using only the z-component of velocity, analogous to the polarisation of circulation.

$$P_z^t = \frac{1}{N} \sum \underline{v}_i^t \cdot \hat{\underline{z}} \tag{2.3}$$

For disordered swarms $P_z^t \approx 0$, and for highly ordered swarms $P_z^t \approx \pm 1$. We can also define a persistence time for the polarisation of ordered swarms, τ_P, by taking the time at which the autocorrelation of P_z^t reduces to a half, i.e. $C_{P_z,P_z}(\tau_P) = 0.5$.

We also measure the extent to which the particles are clumped into high density areas. We define the spatial inhomogeneity, ξ, as the maximum variance in the number of particles occurring within a section of the channel of (any) length ΔL, normalised by the square root of the total number of particles. This definition was inspired by work on giant density fluctuations in SPP models[113]. The maximum

usually occurs when $\Delta L \approx L/2$ and varies between $\xi \sim 1$, for a roughly uniform distribution of particles within the channel, and $\xi \gg 1$ for a highly inhomogenious distribution. For the spatial inhomogeneity measurements ten independent realisations were observed because the density variations are weakly ergodic for low noise.

2.3 Both SPP models recreate the same behaviour in an isolated channel

Swarms of SPPs confined in these channels support both ordered and disordered states (with high and low polarisations, respectively), with a transition between the two around $\phi_n \sim 0.5$, see Fig. 2.2. Near this transition the swarms are polarised, $P_z^t \sim \pm 0.5$, and have a bi-stable direction of motion along the channel, i.e. there is still sufficient noise that the swarm can spontaneously switch direction. This is evidenced by the autocorrelation times for P_z^t. As ϕ_n is decreased, the rate of these directional switches decreases and eventually the direction of polarisation becomes permanently locked, at least on the timescale that we can access our simulations. As the interaction range is increased the location of the order transition (and the onset of fixed direction of polarisation) occurs at slightly higher levels of noise. This is the same for both SPP models provided the density is sufficiently high so as not to cause fragmentation in the metric model. The metric model is known to exhibit a breakdown of global polarisation when the expected number of particles within the interaction radius, R, becomes too small. This is not an issue for the metric free model. The behaviour of both models is similar over a large range of densities and interaction ranges, and reproduces the behaviour seen for insect swarms enclosed in a ring and previous simulations thereof[42]. The single channel simulations do not readily provide information that we could use to easily distinguish between these two models, even under variation of the density and interaction radii.

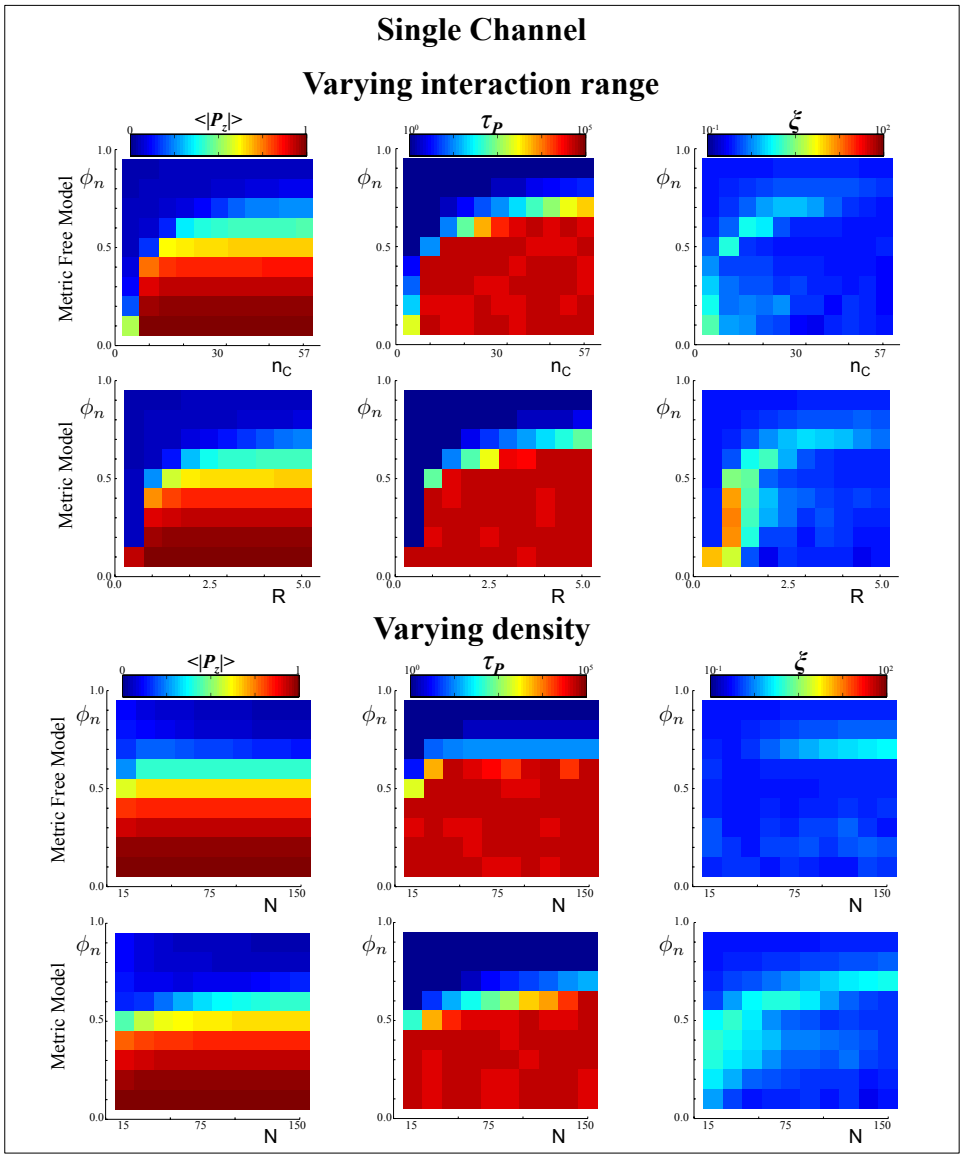

Figure 2.2: Metric and metric free models are difficult to distinguish when constrained to a channel. The average polarisation (left column), polarisation correlation, or switching, time (middle column), and the spatial inhomogeneity (right column) are shown as the (rows 1 and 2) interaction range (R or n_c for metric or metric-free models respectively) and (rows 3 and 4) number of particles, hence density, are varied for different levels of noise (ϕ_n) for an isolated channel of particles. Each point is the average over 90,000 time steps after a 10,000 time step pre-equilibration. Rows 1&2 are realised with $N = 100$ particles, rows 3&4 are realised with $n_c = 27$ and $R = 2.5$. For the spatial inhomogeneity ten realisations each of 10,000 time steps were used because the density variations are weakly ergodic for low noise.

2.4 Three frustrated channels

In order to introduce a coupling between the polarisation of two adjacent channels we position them alongside each other so that they share a face normal to the x axis (say), i.e. particles in channel 1 are restricted to $x \in [0, W]$ and particles in channel 2 have $x \in [-W, 0]$. This means that the minimum distance that could occur between two particles from different channels is zero, therefore particles from channel 1 could have a contribution to the alignment term of particles from channel 2 if the line of sight between them passes through a region designated as a window, see Fig. 2.3. Transport of particles across the window is not allowed, so there is no mixing of the swarms. This creates a coupling between the two swarms in which they tend to co align their polarisation due to the passage of directional information across the boundary. We can adjust the coupling between two channels by adjusting the length of the window, that is to say changing the length of the region in which information can be shared between two swarms. With pairwise coupling between three channels we can arrange them to be mutually frustrating, as shown in Fig. 2.1.

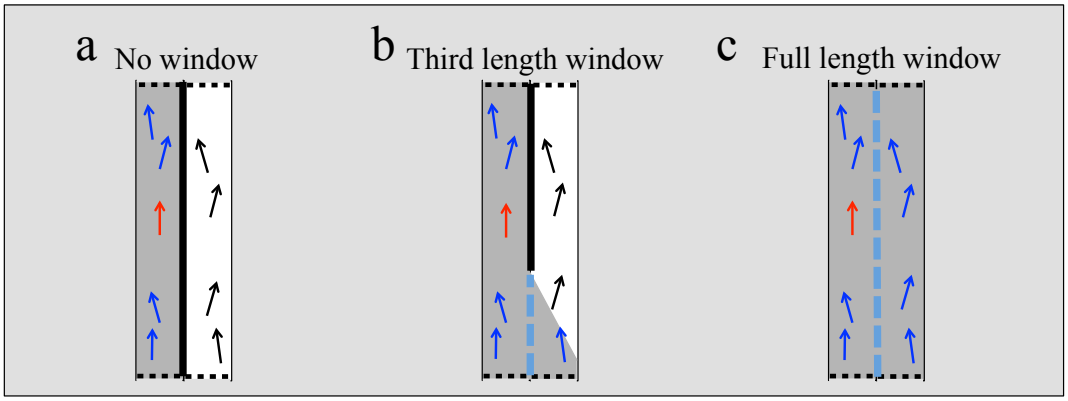

Figure 2.3: Sketch showing the interaction between adjacent channels with (a) no windows, (b) windows that are a third the length of the channel, and (c) windows that are the full length of the channel. The red individual is able to interact with any of the (blue) individuals to which there is an unbroken (by a boundary) line of sight, i.e. within the grey areas.

2.4.1 Fully-frustrated system creates distinct behaviour from candidate SPP models

Since we are not restricted by physical geometrical considerations in these simulations, it is possible to extend this shared boundary to the full length of the channel, see Fig. 2.3c. In this case the "windows" extend along the full length of the channel and each channel shares two such boundaries with each of the other channels, we refer to this as the fully frustrated system. For weak interactions (short ranges R or small number n_c) little difference is observed in the behaviour of the swarms, see Fig. 2.4. However, when the interaction becomes stronger, systems of SPPs with metric-based interactions are no longer able to reach long lived states with constant polarisation. When the interaction range becomes comparable to the width of the channels, $W \sim R$, two swarms in adjacent channels cannot pass by each other without significant interaction. This results in highly polarised swarms that are unable to pass each other without one of them changing direction. Since the leading edge of a swarm is the first to be affected by an adjacent swarm, the directional changes are initiated at the front of the swarm pushing them into high density bands. This results in a shuttle like motion of highly compact swarms appearing to "bounce" back and forth (see supplementary movie 2.1). By contrast the metric free model does not see a reduction in switching time or increase in local density (see supplementary movie 2.2). This is because the coupling between adjacent channels is weaker, even when n_c is very high, the metric free co-alignment term is dominated by particles from the same channel.

The polarisation and switching times of both models are largely unaffected by varying the density of particles within the channels (at the observed interaction radii $R = 2.5$ and $n_c = 27$); marginally higher switching times and polarisation are observed for very high density within the metric model. As the density is increased the metric model shows increased spatial inhomogeneity. This is because it has adopted the switching behaviour observed for the given interaction range ($R = 2.5$) again pushing the particles into high density bands. Since the larger swarms are pushed to bands of the same size, they exhibit a higher density fluctuation, hence ξ.

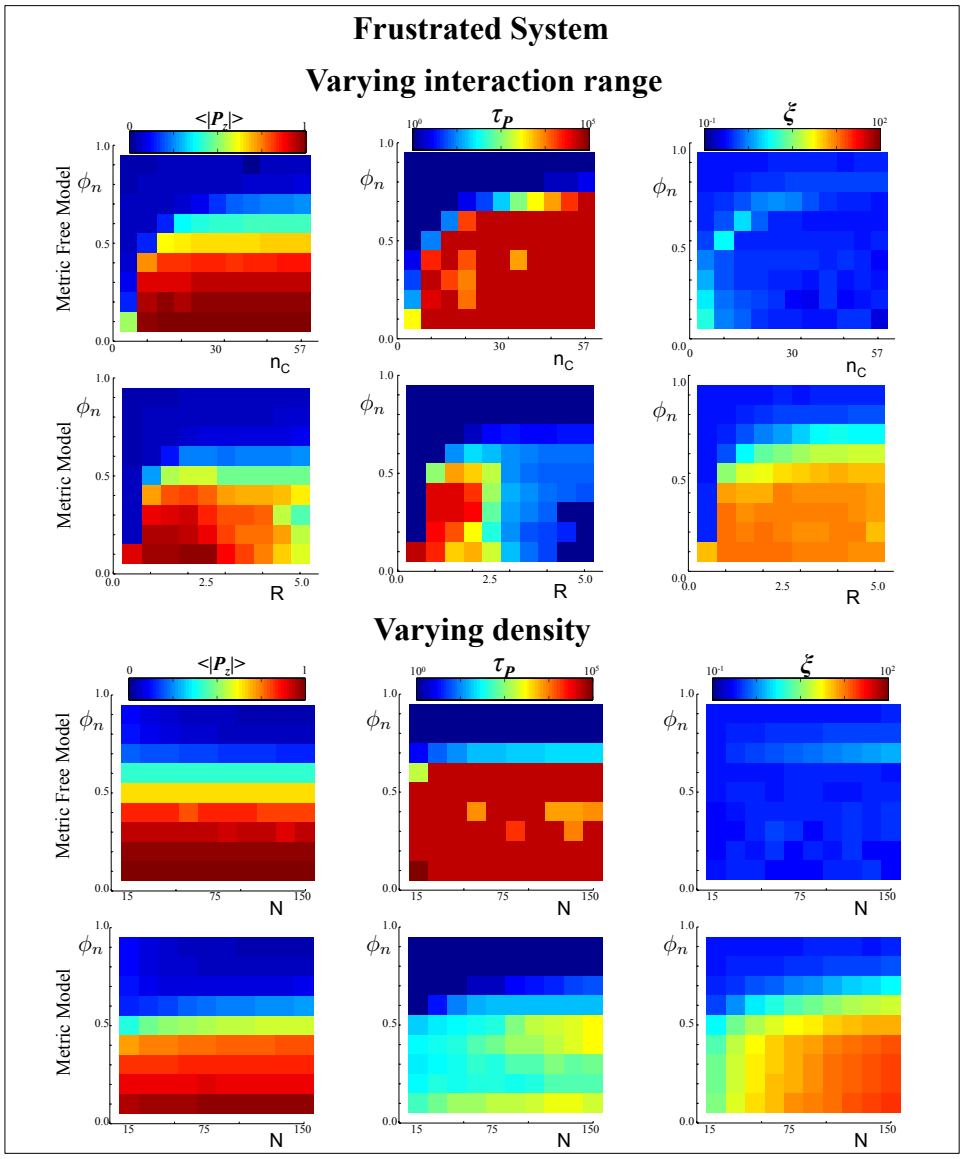

Figure 2.4: Frustrating the system introduces a new behaviour transition in the metric model. The average polarisation (left column), polarisation correlation, or switching, time (middle column), and the spatial inhomogeneity (right column) are shown as the (rows 1 and 2) interaction range (R or n_c for metric or metric-free models respectively) and (rows 3 and 4) number of particles, hence density, are varied for different levels of noise (ϕ_n) for a system of three fully frustrated channels of particles. Each point is the average over 90,000 time steps after a 10,000 time step pre-equilibration. Rows 1&2 are realised with $N = 100$ particles, rows 3&4 are realised with $n_c = 27$ and $R = 2.5$. For the spatial inhomogeneity ten realisations each of 10,000 time steps were used because the density variations are weakly ergodic for low noise.

2.4.2 Shorter inter-channel windows reveal additional behaviour

The window length between adjacent channels can be varied. We define a partially-frustrated system to be one in which the windows extend over only a third the length of the entire channel, see Fig. 2.3b, although a continuum of such choices clearly exist. In this configuration channel 1 (say) shares a window with channel 2 over the first third of its length, a window with channel 3 over the second third and the final third has no window. This geometry more closely resembles the physical version of the frustrated system shown in Fig. 2.1(bottom left).

For this partially-frustrated system both metric and metric-free swarms give rise to highly polarised swarms with long persistence times, see Fig . 2.5. The drop in persistence times for metric swarms with high interaction radii that was observed for fully frustrated systems, see Fig. 2.4, is not seen here. This is due to the emergence of a new behavioural phenotype that we describe as localised *trains* of particles (see supplementary movie 2.3). In the ordered state, particles clump together into high density bands, leading to the increase in ξ observed for low noise, Fig. 2.5. Clumping like this reduces the time that the swarm takes to pass a window. In this way, one swarm can pass a window while the adjacent swarm is in another region of its channel, significantly reducing the coupling between the two swarms. The reduced coupling leads to the increased persistence times observed for metric swarms. The *trains* phenotype emerges in the metric based model as a response to the geometry of the semi frustrated system. In the fully frustrated system the advantages gained by the *trains* phenotype are not possible, hence the significantly reduced persistence times for metric swarms. Reducing the length of the windows has less effect on the behaviour of the metric free model. A slight increase in the spatial inhomogeneity is observed, again since this reduces the coupling between adjacent channels, see supplementary movie 2.4.

Varying the density has a smaller effect on the behaviour of the swarm than varying the interaction range. At the given interaction ranges, both swarms are able to form highly polarised swarms with long persistence times, Fig. 2.5. This is again due to the onset of the *trains* phenotype in the metric model described earlier. As the number of particles in the channel is increased, larger values of spatial inhomogeneity are observed for both swarms, this is because a larger number of particles are occupying similarly sized region of the channel.

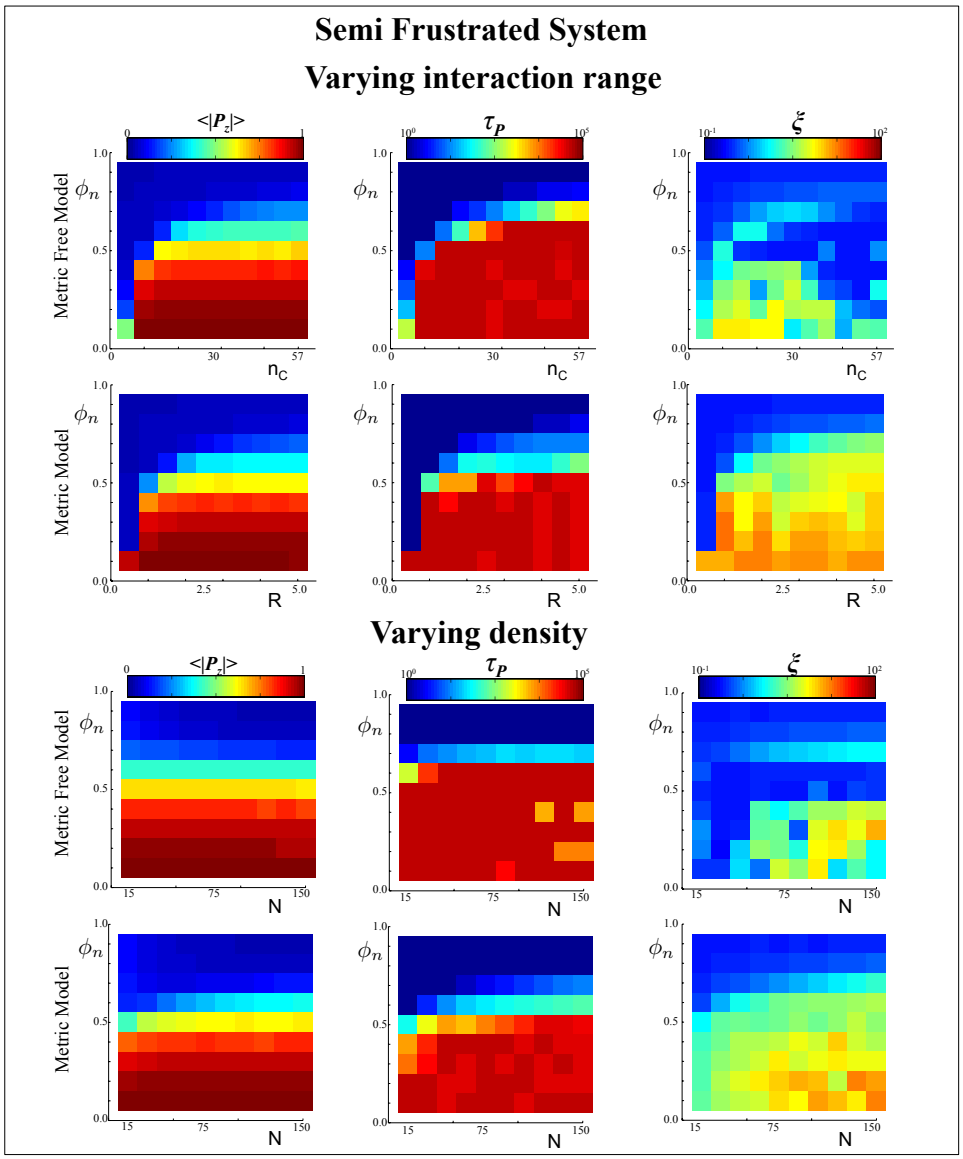

Figure 2.5: The average polarisation (left column), polarisation correlation, or switching, time (middle column), and the spatial inhomogeneity (right column) are shown as the (rows 1 and 2) interaction range (R or n_c for metric or metric-free models respectively) and (rows 3 and 4) number of particles, hence density, are varied for different levels of noise (ϕ_n) for a system of three partially frustrated channels of particles. Each point is the average over 90,000 time steps after a 10,000 time step pre-equilibration. Rows 1&2 are realised with $N = 100$ particles, rows 3&4 are realised with $n_c = 27$ and $R = 2.5$.

2.5 Building a logic gate from a system of self propelled particles

In the final part of this chapter we explore further the implications of the spin-like nature of the motion within these channels to construct an information processing device. First we define our "bit" as

$$m = \begin{cases} 1 & \text{if } P_z > 0 \\ 0 & \text{if } P_z < 0 \end{cases} \tag{2.4}$$

Hence for polarised swarms, $m = 1$ or $m = 0$ for those aligned parallel or antiparallel to the z-axis, respectively.

We now consider the arrangement of channels shown in Fig. 2.6. Here we assume that the **Out** channel reacts to the polarisations of channels **In 1**, **In 2** and **L** in order to minimise the frustrations. The values of m for the **Out** channel that minimise the frustration in the system for every combination of polarisations of **In 1** and **In 2** are shown in the table in Fig. 2.6. These are the same as those given by a logic OR gate which takes the **In 1** and **In 2** as its inputs.

To test whether the logic table shown in Fig. 2.6 is indeed realised we employ an SPP model with metric based interactions. This choice is due to the stronger coupling between adjacent channels evidenced by the frustrated systems explored earlier, see Figs. 2.4, 2.5. We require that all particles are identical, hence have the same interaction radii (R) and noise (ϕ_n). Therefore the shape of the enclosure and the density of the particles must dictate the different behaviours of the **In** and **Out** channels. Swarms at lower density, contained in channels that have a width less than (or comparable to) the interaction radius are more likely to rapidly change their direction of polarisation when induced by the swarm in an adjacent channel (2.4). Therefore, in order to obtain a rapid response in the **Out** channel it would be sensible to assign it a reduced width. Conversely, in order to prevent the swarms in the **In** and **L** channels switching polarisation in response to the swarm in the **Out** channel it is sensible to assign them a width greater than the interaction radius. This would result in a unidirectional flow of polarisation information from **In** channels to **Out** channels. Hence the system would mimic an essentially deterministic logical output, rather than one that is only realised statistically.

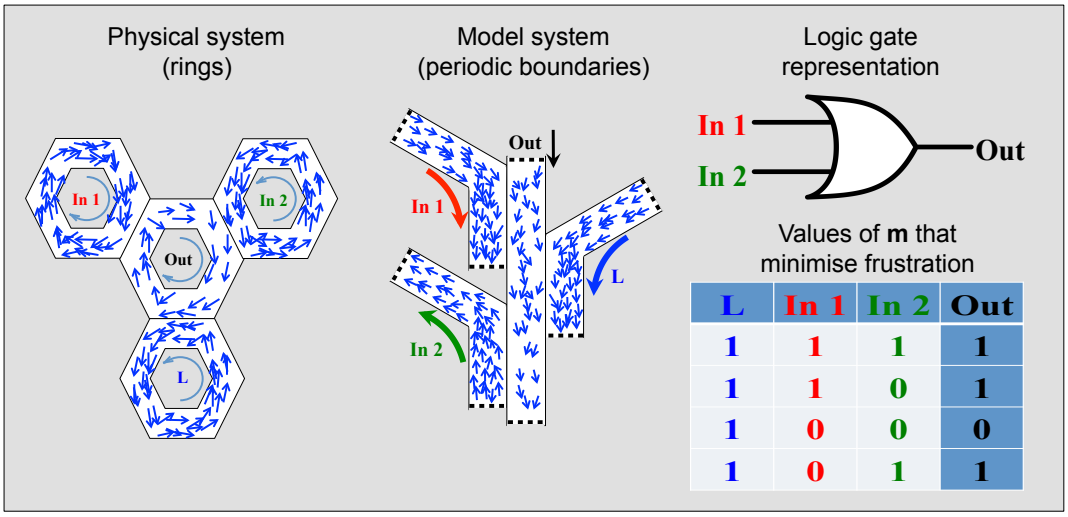

Figure 2.6: Arrangement of rings of animals expected to give a logical OR type behaviour when the direction of polarisation of the **Out** ring is considered the output, and **In 1** and **In 2** are considered inputs. This corresponds to a simple arrangement of channels for the SPP system. The table shows the values for m that minimise the frustration for each possible combination of input polarisations, this is identical to that expected from an OR gate.

2.5.1 Identifying suitable inputs and outputs for a logic gate

This criteria identifies a wide range of possible configurations for constructing a logic gate. As explained earlier all particles in the system are identical, so the shape of the channels and the density of the particles must dictate the different behaviours of the **In** and **Out** channels. We have selected $R = 2.5$ and $\phi_n = 0.5$. We have defined our input (**In**) channels to contain $N = 100$ particles with $W = 5$, $H = 1.9$ and $L = 75$, whereas output **Out** channels here have $N = 75$, $W = 1.75$, $H = 1.9$ and $L = 75$. In the absence of frustration this would lead to polarised swarms with long persistence times, see Fig. 2.2.

To confirm this was a suitable choice we simulated an **In** channel and an **Out** channel alongside each other, see Fig. 2.7a. This system was then simulated them until the system reaches a steady state. This is a state in which the swarms are co-aligned and there is no spontaneous switching. In order to observe how the system reacts to perturbation, we periodically invert the velocity of the every particle in either channel. We observe that this results in the swarm in the **Out** channel to reverse its polarisation in order to recover a co-aligned state, see Fig. 2.7b. This response is independent of which swarm was initially inverted. This confirms that

polarisation information flows from the **In** channel to the **Out** channel only, making them suitable for use in a logic gate.

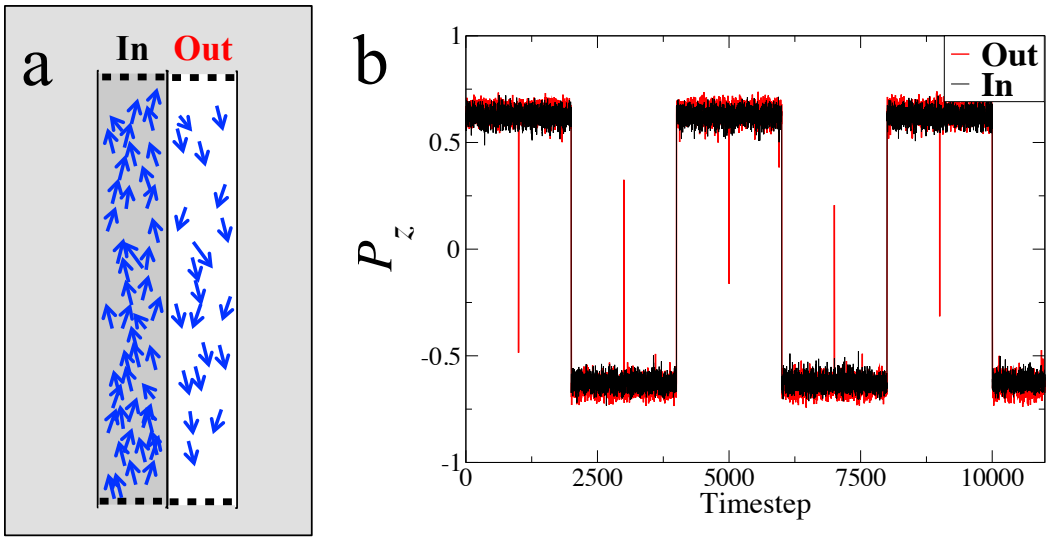

Figure 2.7: (a) Arrangement of two parallel channels. Channel **Out** has the configuration $N = 75$, $W = 1.75$, $H = 1.9$ and $L = 75$ and **In** has the configuration $N = 100$ particles with $W = 5$, $H = 1.9$ and $L = 75$. All particles in the system have $R = 2.5$ and $\phi_n = 0.5$. (b) The polarisation of both channels are periodically switched, whichever swarm has its direction switched, the swarm in the channel **Out** will reverse its direction to ensure the two channels are aligned. The transient spikes in the **Out** polarisation are when its polarisation is artificially switched and swiftly reverses again to realign with the **In** channel.

2.5.2 The certain channel geometries mimic the behaviour of a logical OR

The specific geometry and densities the **In** and **Out** channels explored above to were used to construct the arrangement of channels outlined in Fig. 2.6. This system was then simulated and allowed to reach a stable configuration in which all swarms were aligned. In order to probe the system's response we periodically invert the direction of all particles in either of the **In** channels. This allows us to access all possible configurations of polarisation for the swarm in the **In** channels and the corresponding response of the swarm in the **Out** channel. Fig. 2.8a confirms the logical OR like response of the swarm in the **Out** channel. Fig. 2.8b shows that

swarms contained in this particular geometry responds rapidly enough that the rate of switching can be increased and the logical OR like response is unchanged. In both fast and slow switching regimes the swarm in the **Out** channel is observed to have the correct polarisation to mimic a logical OR for $> 99\%$ of time steps. By employing the correct geometric constraints we have made the complex behaviour of a swarm predictable, in this case in accordance with the output of a logical OR. Although not intended to be used as an actual information processing device, this approach provides another way to probe the behaviour of a swarm and compare directly with experiments on swarming animals that have achieved the same effect [109;110].

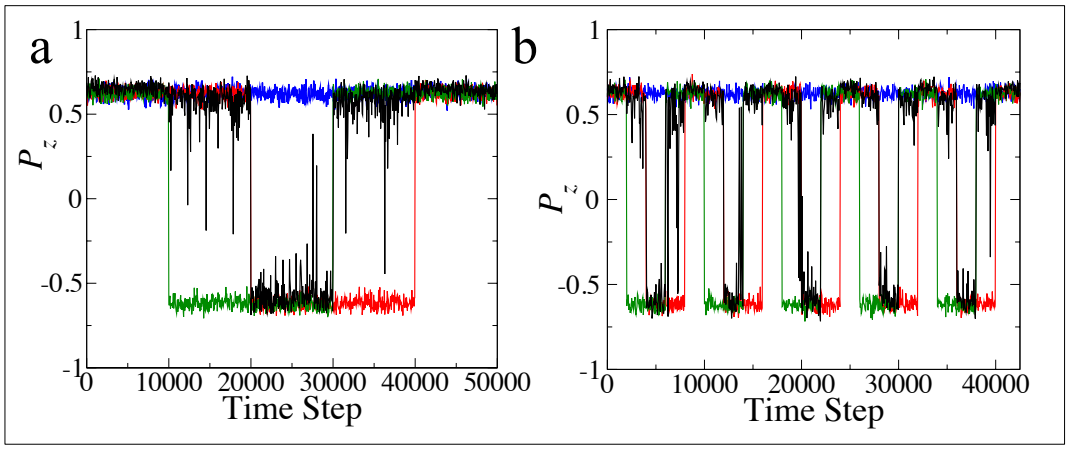

Figure 2.8: Polarisation of SPP model in a set of channels arranged as in Fig. 2.6 over the course of a simulation in which the **In 1** and **In 2** channels are artificially switched at intervals of (a) 10,000 and (b) 2,000 time steps. The system relaxes into a state where the polarisation of the **Out** channel has the reaction of a local OR (shown inset) by spontaneously switching when necessary. The **Out** channel gives the correct sign for $> 99\%$ of time steps for both the slow (a) and fast (b) switching of inputs.

2.6 Summary

Distinguishing between candidate models can be a difficult task. This is especially true when multiple structurally distinct models can give rise to very similar global behaviour. We have shown that different models for swarming can better be distinguished when the particle (animal) motion is frustrated. We achieved this by introducing windows through which particles confined to different channels can interact. By then employing a channel geometry that mimics a geometrically frustrated an-

tiferromagnet we were able to break the behavioural degeneracy of two similar SPP models. This approach promises to allow one to better distinguish between models for animal behaviour by comparing them with experimental data that is itself obtained in frustrated geometries. Ultimately this could lead to an improved insight into the behavioural mechanisms that lead to swarming, one of the prototypical examples of emergent order in nature.

Finally, we use a spin analogy to propose confining geometries in which the swarm(s) perform the operation of a universal logic gate. These could be combined to perform more complex computational tasks, placing a bound on the computational capability of animal swarms, at least those that are artificially confined in this way, to that of a Turing machine. Although the computation that is being performed in this class of confining geometries is unlikely to be more than very loosely related to the computation that is being performed in swarms of unconfined animals our results underline the fact that there is no known limit to the emergent computational power of a swarm. It also demonstrates how it is possible to take a typically complex and hard to predict system and by applying the correct constraints make its behaviour predictable.

Chapter 3

Strictly metric free density regulation

Much of the work in this chapter is published in the article 'Density regulation in strictly metric-free swarms' by Pearce et al.[114].

As was established earlier, many of the interactions between swarming animals, particularly birds, have been observed to be metric free[70;71;30;85]. By this we mean that there is no associated length scale for the interactions between individuals. This should be taken into account when trying to develop a model for swarming behaviour. As has been shown in Chapter 1, and numerous previous studies[86;87;71;88], metric free solutions for the selection of neighbours are possible. Local co-alignment between neighbours selected in this manner can give rise to global polarisation in a metric free swarm, provided the swarm is unable to fragment. Fragmentation is often prevented by confining the swarm to a limited volume by employing periodic boundaries[86;71;30]. Global polarisation, however, is only one physical requirement for a swarm. Another, equally important feature of swarms is slightly harder to introduce in a scale invariant way, and that is cohesion.

Bird flocks have a finite density. When a large flock is observed for a period of time it maintains a cohesive whole with relatively stable edges, even when individual birds leave and join the group. The birds may target some spacing that is close enough to provide protection from predators, but sufficiently disperse to avoid collisions with others within the flock. This could be recreated in a model by some kind of short ranged repulsion (in order to avoid collisions) and a long ranged attraction (to prevent fragmentation). Models that follow just this type of reason-

ing are well established and numerous[94;91;92;93], but they have a few disadvantages. This approach introduces a metric to the model in the form of a preferred separation between agents. Therefore the model is no longer metric free, regardless of how polarisation is obtained. Also, the velocity correlations in the resulting swarm would no longer be scale free. This is because an individual's topological or metric free nearest neighbours (such as those explored in Chapter 2) would, on average, be at the preferred separation. Hence the distance between co-aligning neighbours, and hence the velocity correlation length, are independent of the size of the swarm. Of course, this can be rectified by having some kind of scaled preferred separation, wherein the bird is roughly aware of the total size of the flock and adjusts its behaviour accordingly. This would now run the risk of over parameterising the model with terms that represent calculations that are unrealistic for a bird to perform.

We can find a potential solution for this problem by asking ourselves a simple question: are the birds not aware they are part of a larger flock? Local only, particle-particle type interactions, in which a bird only reacts to its nearest neighbours, are unlikely to give rise to interactions that scale with the total size of the flock. This is because any small section of the flock is essentially independent of any other sufficiently distant section. This is exactly why these types of interactions can be (and so often are) studied in periodic environments, mimicking some infinitely large flock with no edges. But this is obviously not the case in real life, where large flocks of birds clearly have well defined and stable edges that represent a very different environment for an individual than being somewhere near the centre. Is it possible that birds might act differently on the edge?

3.1 The strictly metric free (SMF) model

The topological Vicsek model[86] differs from the original, metric-based[48], version in that individuals co-align with neighbours that are assigned to be those that form the first shell in a Voronoi tessellation; this equivalent to being connected by edges under a Delauny triangulation[89]. This procedure has the advantage that it is completely metric free. It also has the satisfying feature that it has one less control parameter, lacking an interaction radius or number of nearest neighbours. When the resulting collective motion is studied in a periodic box (with vectorial noise) the system is found to support both a low noise, ordered state of aligned particles and a high noise, disordered state[86]. As the system size is increased (at constant density) the transition between the disordered and ordered states has been shown to take on a

continuous character[86]. The topological Vicsek model does not include any terms to control the density, so when simulated in unbounded space the swarm undergoes constant expansion. However, due the completely topological nature of the model the swarm is able to generate highly polarised swarms regardless of the inter particle spacing.

Our essential insight is that we can exploit a Dealunay triangulation to also define the edge of a swarm when it is in unbounded space. This will allow us to propose a fully 3D, strictly metric free (SMF) model that also controls the density of a system of self-propelled particles in unbounded space. The topological Vicsek model supports global alignment order, regardless of swarm density. To this structure we introduce a metric free surface term which, in behavioural terms, would correspond to individuals on the swarm exterior behaving differently. We first identify all individuals that could make a topological connection to a hypothetical individual separated to infinity (in any direction). These individuals lie on the convex hull of the swarm[89]. We refer to these as being on the *edge*, while all others are referred to as being in the *bulk*. We next introduce a metric-free inward motional bias for those on the edge. This is somewhat reminiscent of the effect of a surface tension in a thermodynamic system, an analogy that we will explore later. For those on the edge we define "inwards" as the average of the vectors pointing to the Voronoi neighbors to that individual that are also on the convex hull.

While other choices are possible, including the average of vectors to *all* neighbours, we believe that our choice is simple and has the property that the inward motional bias vanishes for individuals on a surface that has no convexity. This is in qualitative agreement with the existence of large swarms with relatively stable edges and also mimics the physics of a surface under tension. It is feasible for an individual on the edge of the swarm to identify others on the edge by first projecting the relative positions of all others (onto its retina), mapping them to points on the surface of a unit sphere, see Fig. 3.1a. For an individual on the *edge*, all these points will fall within one hemisphere, notifying that the individual is on the convex hull of the swarm, see Fig. 3.1b. The convex hull of the points on the unit sphere (in S^2) identifies the nearest neighbours who are also on the *edge* of the swarm, see Fig. 3.1b. Essentially the neighbours of an individual on the convex hull of the swarm which are also on the convex hull can be easily be identified as lying on the boundary of the portion of the unit sphere containing these points. Indeed edge detection is known to be performed in the neural hardware of the visual cortex in higher animals[115;116], a feature that we will return to in Chapter 4. Because this model was motivated by

the observed metric free nature of starling flocks[70;30], we restrict ourselves to motion in 3D so as to best compare with large murmurations of birds such as starlings (although the same model is easily applied in 2D).

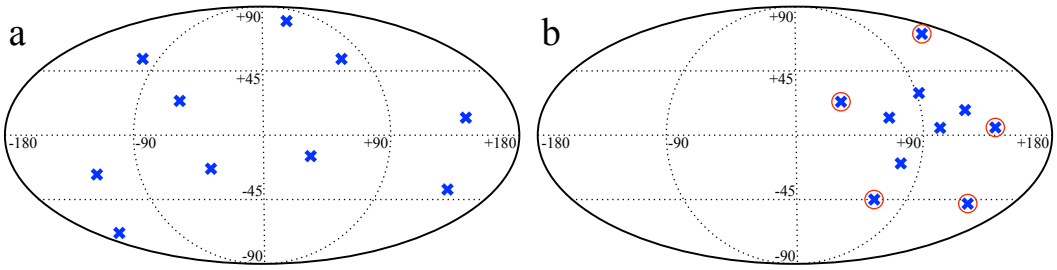

Figure 3.1: A sketch that shows: (a) The angular positions of the nearest neighbours (shown as crosses) of an individual in the *bulk* of the swarm. (b) Angular positions of the neighbours of an individual on the *edge* of a swarm all fall within one hemisphere. The convex hull (in S^2) of those positions identifies those neighbours also on the *edge* (circled in red).

The SMF model has a number of features that are appealing in behavioural terms. First, its metric free character means that an animal isn't required to accurately judge and compare distances. It only requires that an individual recognise when it is on the *edge* and identify its neighbours with the most extremal (angular) positions within its view. Secondly, the position of neighbours also on the edge give each of them information on the boundary, and hence the shape of the swarm as a whole; something that is not available from local interactions in the bulk. Finally, giving the control of density to those that reside on the edge also gives it to those that are most exposed to predation. Those in the bulk are the safest from predation[13], so are least likely to try to change their relative position or the properties of the swarm as a whole[10]. Individuals on the edge are in the most danger and have the best information on the global structure of the swarm. It seems reasonable that they should be those that select the swarm structure. Recent studies on large starling flocks have also noted that there is a local rise in bird density toward the edge of flocks, which would tend to support some distinction between edge and bulk, such as we introduce here[70;117]. It also promotes mixing within the flock since particles on the edge of the swarm change their behaviour in order to rejoin the bulk, hence reducing the rearrangement time of the Voronoi mesh. This is similar to the observed inflow of information from the boundary of flocks to their bulk[72;117]. We propose a minimal model to address the question of metric free density control

in large flocks[15;70], but the model could easily be expanded to capture many more features of bird flocks by the inclusion of additional refinements such as blind angles, flight physics etc.

Our SMF model is defined as follows. At discrete time t, particle i has position $\underline{r}_i^t$ and direction of motion $\hat{\underline{v}}_i^t$, with $\hat{\underline{r}}_{i,j}^t$ representing the unit vector pointing from particle i toward particle j at time t. These are updated every time step according to equations (3.1) - (3.4). The neighbours, B_i, are those forming the first shell around particle i in a Voronoi tessellation constructed from the particle positions at time t. If particle i is in the set C of all those on the convex hull of the system, the neighbours, $S_i = B_i \cap C$ are those that also lie on the surface, see Fig. 3.2a. The model is controlled by two parameters. First ϕ_e, the strength of the "edge" effect, is the relative weight of alignment to the inward movement bias for particles on the edge. The second parameter is the strength of the noise, ϕ_n. See Eqs. (3.1) - (3.4).

$$\underline{r}_i^{t+1} = \underline{r}_i^t + v_0 \hat{\underline{v}}_i^t \tag{3.1}$$

$$\underline{v}_i^{t+1} = (1-\phi_n)\hat{\underline{\mu}}_i^t + \phi_n \hat{\underline{\eta}}_i^t \tag{3.2}$$

$$\underline{\mu}_i^t = (1-f_i)\frac{\langle \hat{\underline{v}}_j^t \rangle_{j\in B_i}}{|\langle \hat{\underline{v}}_j^t \rangle_{j\in B_i}|} + f_i \langle \hat{\underline{r}}_{ij}^t \rangle_{j\in S_i} \tag{3.3}$$

$$f_i = \begin{cases} \phi_e & \underline{r}_i^t \in C \\ 0 & \text{otherwise} \end{cases} \tag{3.4}$$

again $\hat{\underline{\eta}}$ denotes a random unit vector and v_0 is the speed with which the particles move.

We structure our model so that every individual experiences a similarly weighted noise contribution, controlled by ϕ_n in Eq. 3.2. According to Eq. 3.3 each individual first decides a (deterministic) direction before any noise is introduced. This direction is determined by either (a) simply co-aligning with neighbours - in the case where the i^{th} individual is not on the surface ($f_i = 0$ according to Eq. 3.4). Or (b), resolving a linear combination of the co-alignment direction and the one that arises from the metric free surface term, these being weighted by factors $1-\phi_e$ and ϕ_e respectively - when i is on the surface ($f_i = \phi_e$ according to the same Eq. 3.4). This means that the combination of a deterministic "preferred" direction and a random noise vector is similar for each individual, irrespective of location.

Fig. 3.2a shows an example of the topological constructions included in Eq. 3.3.

The metric free surface term for each individual is taken as the average of the unit vectors pointing to adjacent points that are on the convex hull ($\langle \hat{\underline{r}}_{ij}^t \rangle_{j \in S_i}$). This has a magnitude in [0,1] and is greatest when the angle between the $\hat{\underline{r}}_{ij}$ is small. Therefore individuals that are 'exposed' outliers associated with the sharpest kinks in the convex hull, will have a stronger drive to rejoin the swarm. This construction is shown in more detail in Fig. 3.2b.

3.2 SMF model can recreate a coherent, ordered swarm

This set of equations can be solved iteratively and gives rise to a coherent and ordered swarm in both two and three dimensions, see Fig. 3.2c,d and supplementary movies 3.1 and 3.2 for simulations of $N = 100$ and $N = 500$ particles, respectively. Because the equations are completely metric free, the choice of units is somewhat arbitrary. The only dimensional unit is the distance travelled per time step, v_0 which is set to unity, thereby defining our unit of length. If we set $\phi_e = 0$ we obtain the topological Vicsek model[86], which in unbounded space is found to support either an ordered or a disordered state depending on the noise level, ϕ_n, with a continuous transition between the two. This is despite the fact that, without a term acting at the edge to bound the swarm it is undergoing continuous spatial expansion and a corresponding decrease in density[86]. Although this is not a realistic model for swarms it does provide a benchmark global order (and order-disorder transition) for a swarm in the absence of modifications that suppress fracture and is shown as $\times$'s on Fig. 3.3a and Fig. 3.4a,b (there is no such data on Fig. 3.3b since the continuous spatial expansion does not produce a non-zero steady state density). Here, and in what follows, we set $\phi_e = 0.5$ for simplicity, providing equal weighting to co-alignment and inward bias in Eq. 3.3 for individuals on the edge of the swarm. The effects of varying ϕ_e itself are covered further in 3.7.1. This leaves only one free control parameter, the noise strength ϕ_n. The similarity between the benchmark properties of the models shown in Fig. 3.3-3.4, both with and without the new surface term, are included merely as supporting results to show that the introduction of the surface term doesn't "break" the other well known properties of the model.

When analysing the performance of the model we primarily look at two qualities, cohesion and ordering. In order to study these we need to define robust quantitative measures of these. For ordering we use the order parameter, P^t, given by the equation $P^t = |\frac{1}{N}\sum \underline{v}_i^t|$; the symbol P denotes the average over the course of a simulation $P = \langle P^t \rangle$. In order to assess the spatial cohesion of the swarm we first

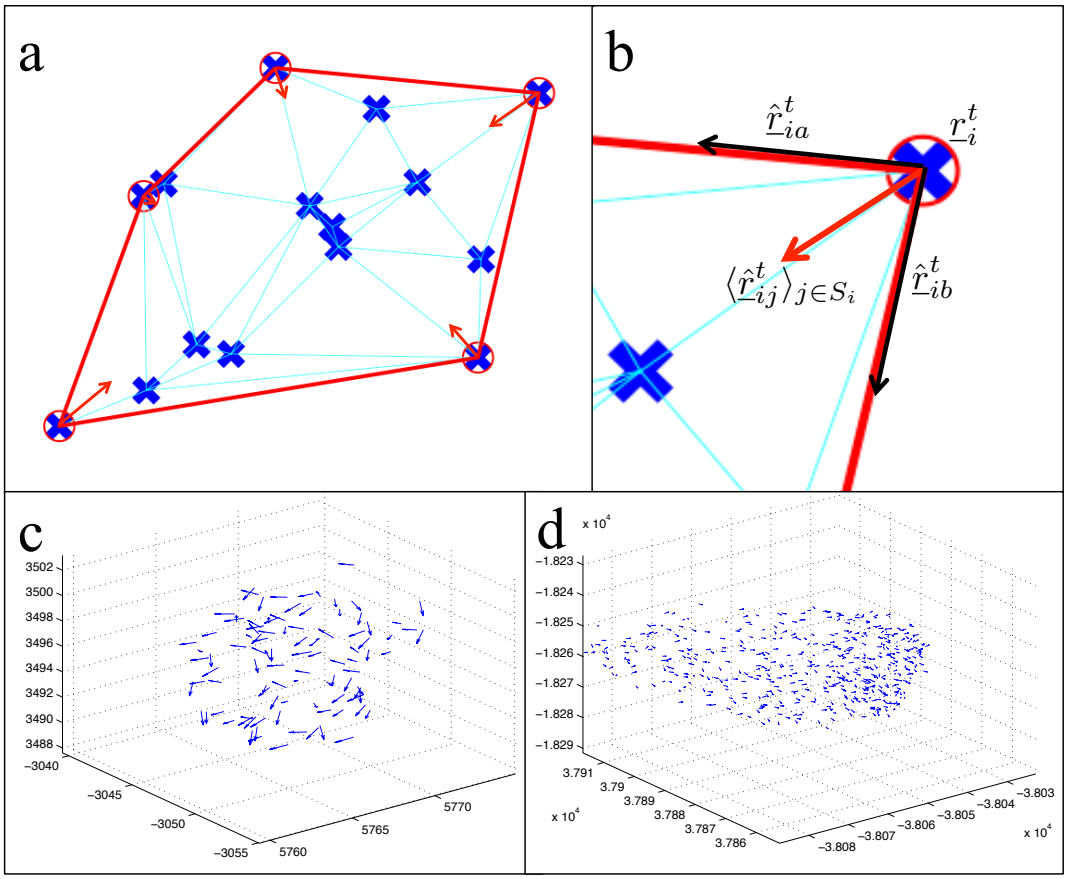

Figure 3.2: (a) A sketch showing of the topological constructions included in Eq. 3.3. Here an arrangement of points ($\underline{r}^t_i$) are shown as crosses in the 2D plane, for simplicity (the model is fully 3D), with those lying on the convex hull circled in red (for which $f_i \neq 0$ in Eq. 3.4). The Delaunay triangulation is shown in cyan, and the red lines denote the subset which connects points on the convex hull. Therefore, points connected by a cyan (or red) line are those in B_i, hence will co-align, and points connected by a red line are those in $S_i = B_i \cap C$, hence contribute the the metric free surface term (displayed as a red arrow for each point on the convex hull.) (b) Detailed sketch showing how the metric free surface term appearing in Eq. 3.3 is constructed for a general particle i. This depends on the vector $\langle \hat{\underline{r}}^t_{ij} \rangle_{j \in S_i}$ (red arrow) which is the average of unit vectors to adjacent individuals *that are also on the convex hull*, $\underline{r}^t_{ia}$ and $\underline{r}^t_{ib}$ for particles a and b, respectively (black arrows). (c) and (d) Snapshot of a realisations of the model for 100 and 500 particles, respectively. Both have a noise weighting of $\phi_n = 0.45$ and give rise to a polarisation of $P \approx 0.75$.

define the swarm's spatial extent, R, as the average nearest neighbour separation R_1 multiplied by the cube route of the number of individuals, i.e. $R = R_1 N^{1/3}$.

While alternative definitions are possible this measure has the attractive feature that it isn't strongly biased by a single outlying individual that may, by chance, have moved some distance away from the others. All simulations were performed using software written by the author in C++. The triangulation algorithms from the Computational Geometry Algorithm Library (C.G.A.L.) were used[118]. The initial conditions for the N individuals are that they started with random positions in a square region of space of area N^2 (in units of the distance travelled per time step, v_0) with randomly orientated velocities.

3.2.1 Global polarisation is independent of the swarm size

Swarms generated by our SMF model can achieve highly ordered states. A high global order parameter P emerges naturally when the noise is sufficiently low, see Fig. 3.3a. Note that the precise value of P is roughly independent of the size of the number of individuals in the swarm, N. The swarm therefore maintains a particular level of global order without the need for the individual members to comprehend (and respond to) the size of the swarm in which they reside. This could explain how relatively simple animals can participate in swarms which vary in size by several orders of magnitude without the swarms qualitatively changing their behaviour[70].

The surface term also has very little effect on how the swarm forms an ordered state: large swarms ($N \gtrsim 500$) reach roughly the same global order as the topological Vicsek model with an average difference of 0.0026 (see $\times$'s on Fig. 3.3a). This is consistent with the fact that the proportion of particles in C (on the convex hull) decreases with N. Fig. 3.3b shows that the SMF model generates swarms with a well defined equilibrium extent, R, (and therefore density) which appears to follow a power law $R \sim N^{0.8}$. Hence the SMF model is able to support ordered swarms that remain spatially cohesive in unbounded 3D space; a robust feature of animal swarms.

3.2.2 Order Transition in the SMF model is continuous

A transition between an ordered and disordered state occurs for swarms generated by the SMF model, Fig. 3.4a. The nature and location of the transition is independent of the value of N as is the presence of a smooth transition, see supplementary movies 3.3 and 3.4, confirmed by the monotonic nature of the Binder cumulant[119], $G = 1 - \frac{\langle P^4 \rangle_t}{3\langle P^2 \rangle_t^2}$, Fig. 3.4b. This is very similar to the transition observed for a pure topological Vicsek system (shown as $\times$'s), again confirming that the new surface term

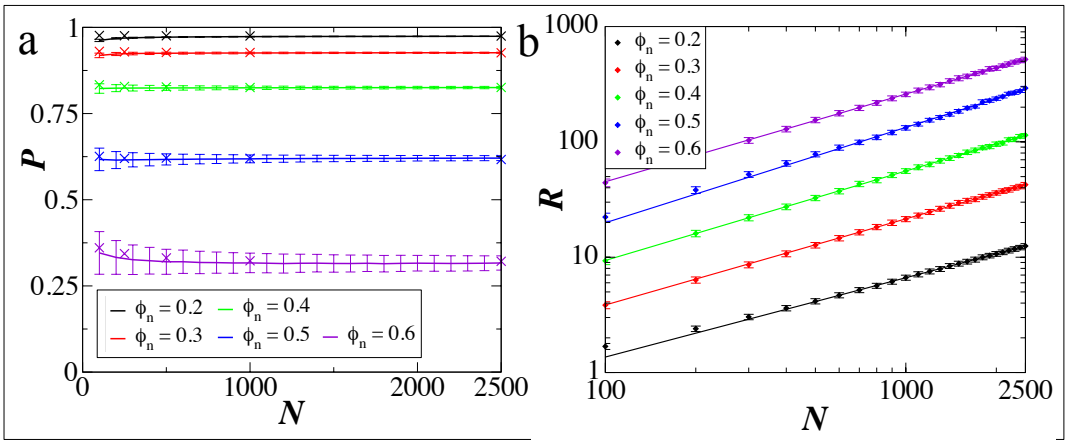

Figure 3.3: Global polarisation of the swarm is independent of the number of particles within the swarm, whereas the radius displays a power law relation. (a) Global order, P, and (b) Swarm spatial extent, R, for swarms containing different numbers of individuals, N, and with varying levels of noise, ϕ_n (the key given in panel (a) also applies to (b). The lines on plot (b) correspond to power law regressions fit to all data points above $N = 500$ giving a relation of $R \sim N^{0.8}$, the origin of this power law relationship is discussed later in section 3.6. Each point on the figures corresponds to an average ($\pm\sigma$, one standard deviation) over 40,000 simulation time steps following a 10,000 time step pre-equilibration period, significantly longer than either the density or order autocorrelation times. The points represented by the $\times$'s in (a) correspond to the values achieved for a pure topological Vicsek model ($\phi_e = 0$) that disperses in space.

controlling the density doesn't compromise the swarms ability to form an ordered (or disordered) state. The continuous nature of the transition is also found to be independent of the choice of ϕ_e, see section 3.7.1.

The fact that the location and continuous nature of the transition are independent of N may mean that a group of swarming animals can occupy the *sweet spot* near the inflection point in the order-disorder transition without the need for any individuals to adjust their behaviour as the number of individuals in the swarm changes. This would seem to be compatible with observations on swarming animals in the wild, which often occupy an intermediate state which displays high local order with a short de-correlation time; this is likely linked to evolutionary fitness, meaning a large group of animals can be both ordered and quick to react.

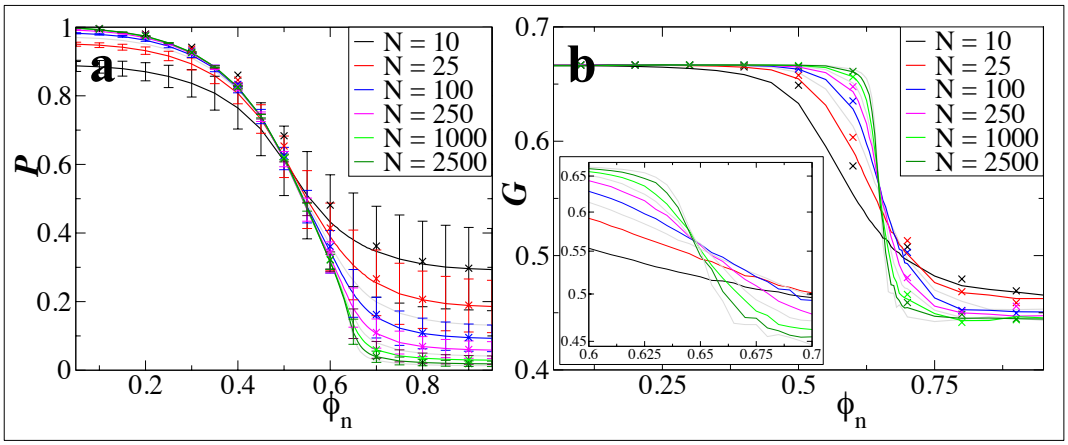

Figure 3.4: (a) Global order, P, and (b) Binder cumulant G[119] as a function of the noise strength ϕ_n and enlarged area near the transition with logarithmic scale (inset). There is a continuous transition from an ordered to a disordered state as the noise increases and this is independent of the number of individuals N.

3.2.3 Finite size scaling analysis of the order transition

The order transition presented in Fig. 3.4 appears to be continuous and approaching some limit as the size of the swarm is increased. Since it is impossible to simulate a swarm of infinite size we can only try to infer what the transition in the limit might be. To do this we use an approach called finite size scaling analysis. Essentially, the polarisation correlation length, ξ, diverges as the system reaches the critical point in the transition. For a finite system, when ξ approaches the system size the behaviour becomes distinct from an infinite system; referred to as a finite size effect. This effect will can seen in various observables, for example the behaviour of the polarisation, P, specifically the location of the critical point, ϕ_{nc}, the susceptibility of the polarisation, χ_P, and the correlation length, ξ. By observing how the behaviour of these observables changes for finite systems of different size, we can infer the behaviour at the infinite size limit.

Since this system is completely topological, our system will have a dimensionless correlation length relating to the number of neighbours between two correlated individuals. Therefore our analogue of "system volume" is given by the number of particles, N, and our analogue of "system length" can be taken as $N^{(1/3)}$. Therefore our measure of susceptibility of the polarisation is given by

$$\chi_{|P|} = \frac{1}{N}(\langle P^2 \rangle - \langle P \rangle^2). \tag{3.5}$$

In the infinite size limit, we expect this to diverge at the critical point of the transition, $\phi_n = \phi_{nc}$, according to the relationship

$$\chi_{|P|} \propto |\phi_n - \phi_{nc}|^{-\gamma}. \tag{3.6}$$

In a finite system, we merely see a maximum in the susceptibility at the apparent critical point for a system of that size, see Fig. 3.5a. The location of the maximum susceptibility does not vary significantly for system sizes over $N = 100$, giving a critical point of $\phi_{nc} = 0.644 \pm 0.002$, this is in agreement with the critical value identified from crossing point of the binder cumulants, $\phi_{nc} = 0.648 \pm 0.004$ (both values are the average estimate $\pm$ 1 S.D.). By using regression to fit a power law to the susceptibility near the critical point it is possible to find the apparent critical exponent for different system sizes, γ_N. This appears to diverge as N is increased following a power law, see Fig.3.5b. Hence it is not easily possible to infer the exact nature of the transition in the infinite size limit and identify a universality class for the system.

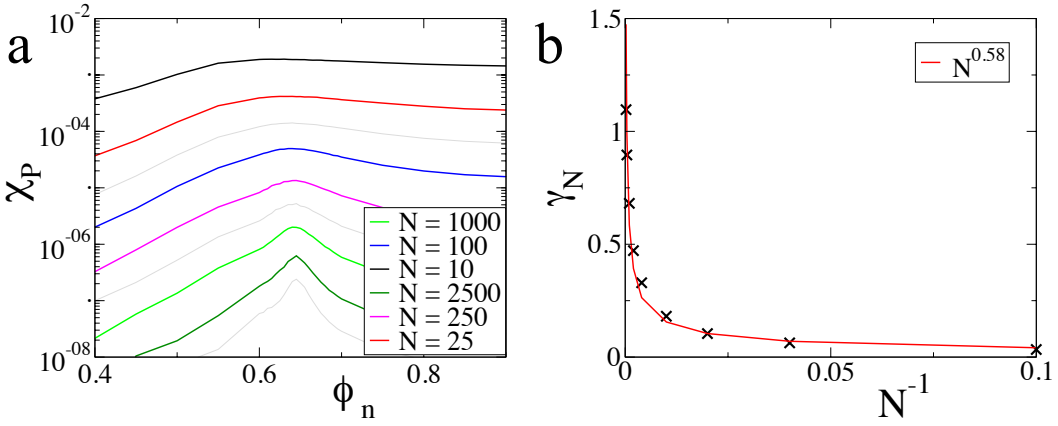

Figure 3.5: (a) Susceptibility of the polarisation of the swarm has a peak at the critical point of the order transition. This point varies very little for different values of N implying a critical point $\phi_{nc} = 0.64$. (b) Estimate of the critical exponent of the susceptibility, γ, for systems of varying size N. As N is increased the critical exponent appears to diverge.

3.3 SMF model recreates scale free velocity correlations

The scale free nature of interactions between starlings within large flocks has been reported by the STARFLAG collaboration[70]. It was found that each bird's velocity is highly correlated with that of a fixed number, N_c, of its nearest neighbours, regardless of the sparseness of the flock, R_1, defined as the average nearest neighbour separation. From this it was inferred that the orientational correlation between two individuals of a flock depends on topological rather than metric distance[71]. This was confirmed by measuring a *topological range*, $N_c^{1/3}$, which was directly observed to be constant for flocks of varying density. By contrast the metric range, defined as the average distance between birds with highly correlated velocities, scales linearly with the sparseness[71;30;70].

In the SMF model, we can define the metric correlation length scale, R_d, as the average distance to the Voronoi neighbors, and the topological correlation length scale as the cube root of the average number of Voronoi neighbours, $N_d^{1/3}$. These are analogous to the quantities calculated from measurements taken on flocks of starlings in the wild[71]. Since the nearest neighbour separation, R_1, is not a parameter that is under direct control in the SMF model, we adjust it by changing the number of members, N, and noise level, ϕ_n, of the swarm and measuring the resulting separation.

Fig. 3.6a shows a linear relationship between the metric range, R_d, and sparseness, R_1. Hence R_d scales with the size of the swarm, a consequence of the metric free nature of the model. Conversely, $N_d^{1/3}$ remains roughly constant as the sparseness of the swarm changes, confirming the fact that the model proposed here is indeed completely metric free, with purely topological interaction ranges. This is in agreement with the analogous quantities for the topological and metric length scales measured in starling flocks[71]. The observed upward trend for denser swarms is due to the fact that these are smaller, $N < 500$; an amorphous swarm has a higher proportion of its members on the surface, which, in turn, have fewer Voronoi neighbours.

3.4 Metric free surface term promotes mixing within the swarm

Observations on starlings suggest that mixing within a flock promotes information flow, particularly from the edge to the bulk[72]. In the topological Vicsek model[86] ($\phi_e = 0$) the voronoi mesh remains largely fixed and mixing within the swarm is very

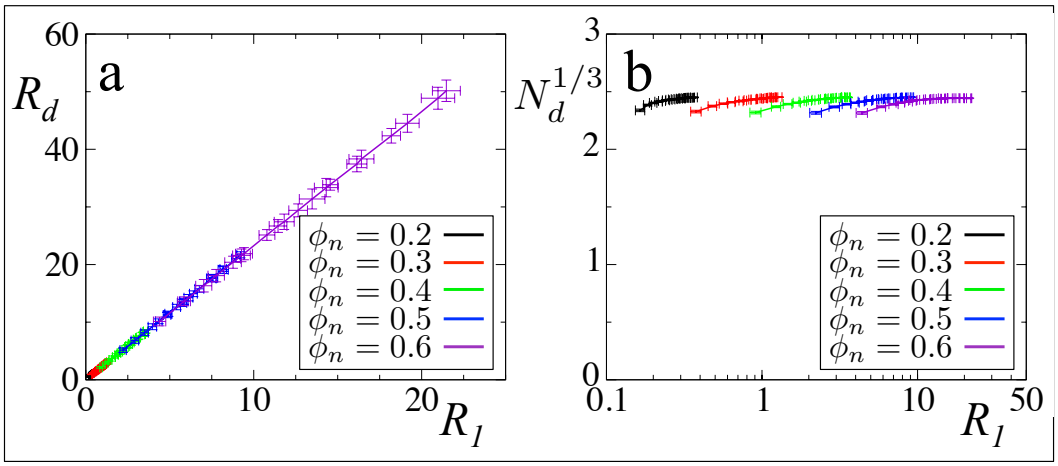

Figure 3.6: The relationship between (a) metric ,R_d, and (b) topological, $N_d^{1/3}$, correlation length scales with the spatial sparseness measured by the nearest neighbour distance, R_1, for varying noise levels. The multiple data points correspond to different values of N which we adjusted to observe different levels of sparseness, R_1. These trends closely agree with data on the metric and topological length scales observed in starling flocks[71].

slow. Most particles in the swarm never get to the edge, and those on the edge never reach the bulk, see Fig. 3.7a. Whereas in the SMF model ($\phi_e = 0.5$) all particles spend some time in both the edge and the bulk, Fig. 3.7a.

We also assess the rearrangement time of the voronoi mesh. In a swarm containing N individuals, each individual can be linked by an edge in the voronoi mesh with any one of the $N-1$ others, hence there are $(N(N-1)/2)$ possible links in the entire swarm. When $\phi_e = 0$ of the $N(N-1)/2$ possible links, most are never observed whereas some persist for up to 100% of the simulation, at least at the timescales accessible here. Therefore most particles very rarely change their neighbours and the voronoi mesh is fixed. However when the inward motional bias is introduced all links occur with a similar frequency implying good mixing within the flock and swift rearrangement of the voronoi mesh, see Fig. 3.7b.

3.4.1 Statistics at the edge of the SMF model

The fraction of time a particle within a given swarm spends on the edge is dependent on the size and noise level of the swarm is shown in Fig. 3.8a. As the noise is increased the amount of time that a particle spends on the edge increases slightly and each time a particle visits the edge it stays longer, Fig. 3.8b,c. One factor that contributes to

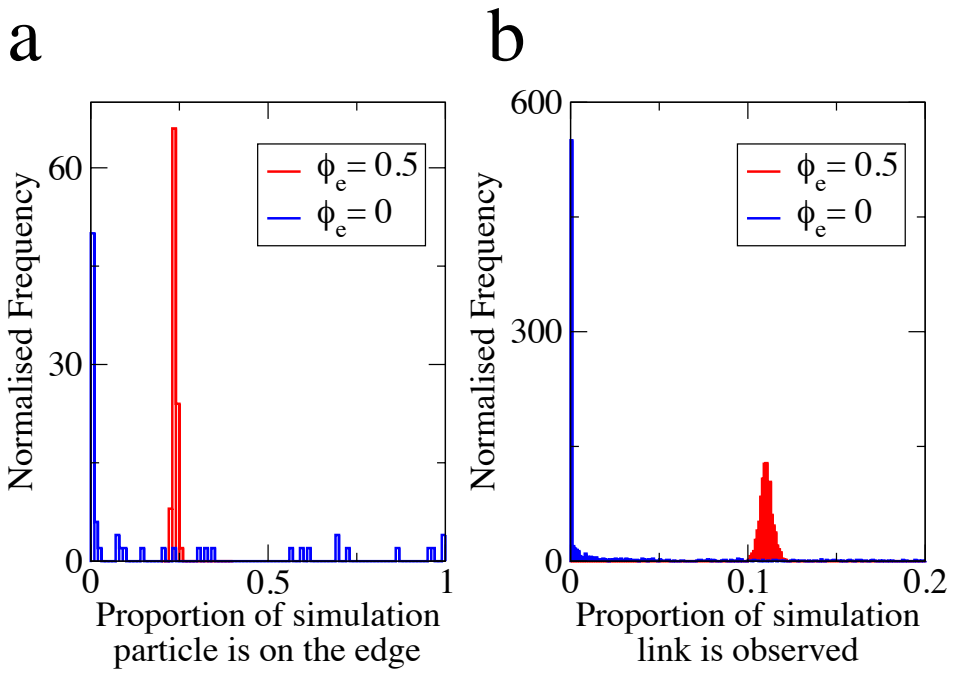

Figure 3.7: (a) Normalised histogram of the proportion of a simulation each particle spends on the edge of the swarm. When the metric free surface term is introduced, $\phi_e = 0.5$, each particle spends $24 \pm 0.6\%$ of the simulation on the edge; the error given here is the standard deviation. (b) Normalised frequency of the proportion of a simulation each possible pairing between two particles occurs. When $\phi_e = 0$ most possible pairings are never seen over the entire duration of the simulation. When the metric free surface term is introduced, $\phi_e = 0.5$, each link occurs for $11 \pm 0.3\%$ of the simulation; the error given here is the standard deviation. Simulation contained $N = 50$ particles and was run for 10^6 time steps.

this is that, as the noise is increased, the swarm takes on a more isotropic and diffuse structure, expanding into a roughly spherical shape. The more spherical shape of these swarms leads to the metric free surface term, $\langle \hat{r}_{ij}^t \rangle_{j \in S_i}$, becoming smaller as the radius of curvature at the edge increases. Hence the inward-pointing component of the vectors connecting particles on the surface becomes smaller on average, see Fig. 3.2. The reduction in density, consistent with Fig. 3.3b, means that it is further for a particle on the edge to travel to pass another particle and re-join the bulk, hence this takes longer. The higher noise also means the effects of the metric free surface term are reduced and a particle on the edge is advocated inwards more slowly. This leads to longer edge residence times. Larger swarms have a higher volume, hence have a lower surface area to volume ratio, therefore a smaller fraction of the swarm

is on the edge, hence the average length of time a particle needs to be on the edge is reduced, Fig. 3.8a. Since larger swarms are more diffuse it takes longer to move from the edge to the bulk leading to longer persistence times on the edge, Fig. 3.8b,c.

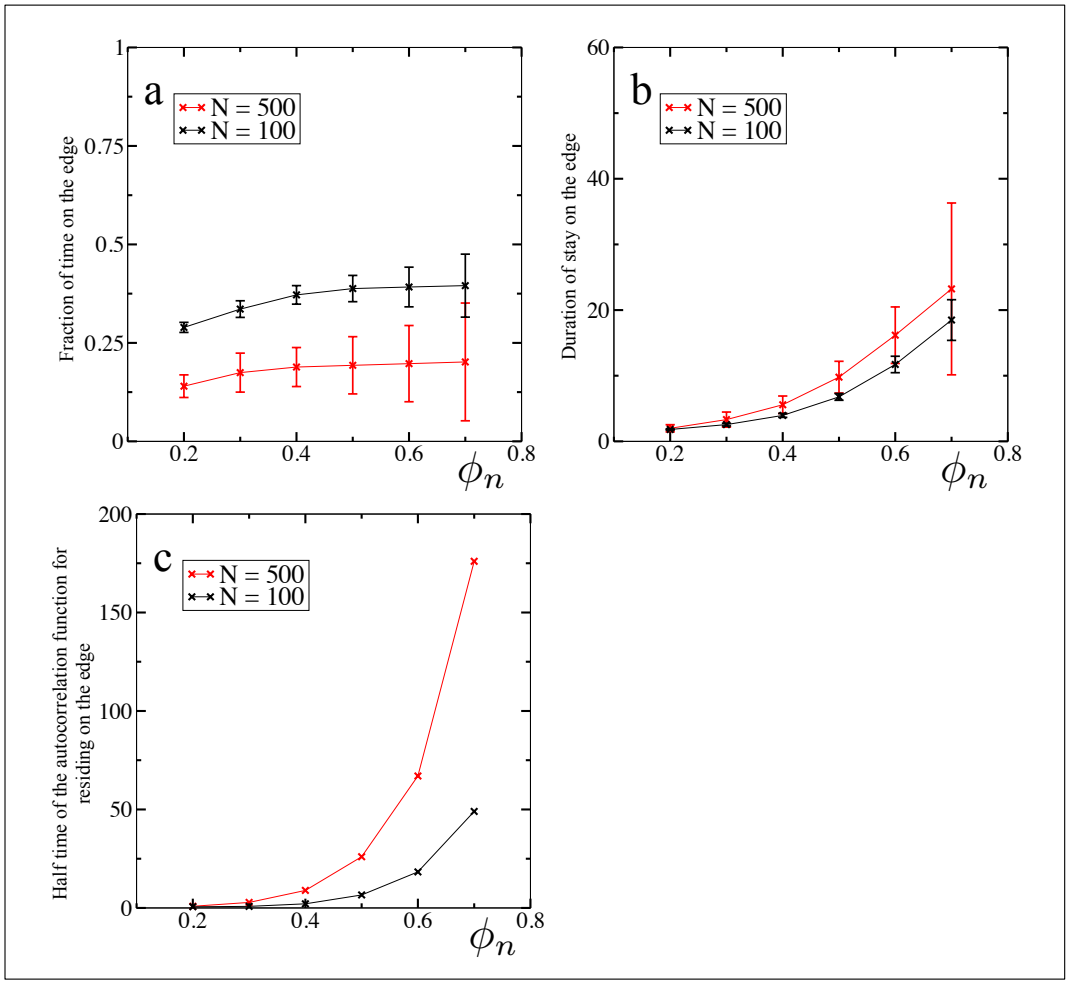

Figure 3.8: (a) Fraction of time a particle spends on the edge of the swarm (b) average duration of each stay on the edge and (c) half-time (in time steps) of the autocorrelation function for a particle residing on the edge of a swarm of size $N = 100$ (black) and $N = 500$ (red) for different noise levels, ϕ_n. Each point is the average over a 10,000 time step simulation following a 10,000 time step equilibration period.

3.5 Speed insensitivity of the SMF model

The model only features one dimensional unit, v_0, which defines the length moved by a particle within a time step. We set v_0 to unity, thereby defining our units of length, but as mentioned previously this is somewhat arbitrary. However, the results are insensitive to the value of v_0 due to the metric free nature of the model itself. To confirm this we ran simulations with values of v_0 that vary by ten orders of magnitude and observed no difference in the behaviour of the model, see Fig. 3.9. The density of the swarm is invariant to the value of v_0 in the sense that even though doubling the speed may result in a doubling of the inter particle distance it also doubles the only unit in which it can be measured, Fig. 3.9a. The polarisation is a function only of the direction of motion of each individual particle, so is speed-invariant, see Fig. 3.9b. Because quantities like the number of Voronoi neighbours and the number of particles on the convex hull are purely topological constructions they are invariant to such rescaling, see Fig. 3.9c,d. The insensitivity of our model to the value of v_0 may simplify the task of constructing continuum models[120;121], although we do not attempt this here. It is worth mentioning that if the model were to be modified to include some kind of inertial effects this could introduce another dimensional unit, changing these conclusions somewhat.

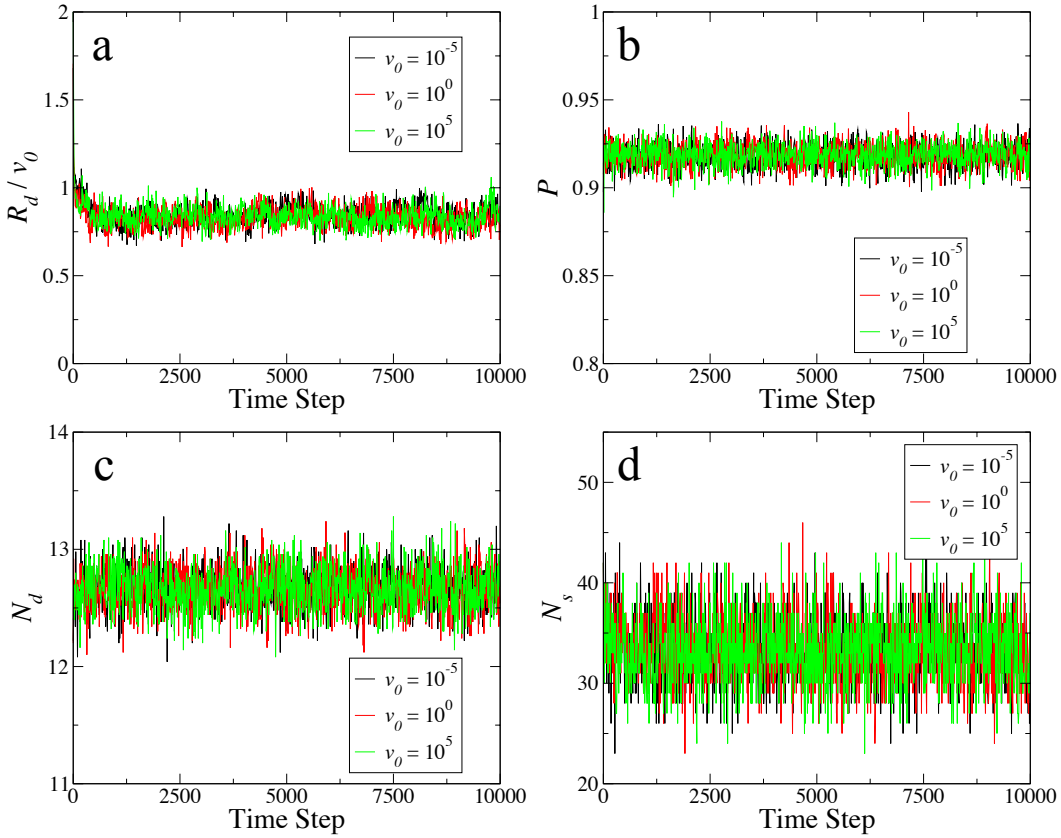

Figure 3.9: Confirmation of the arbitrary nature of the choice of v_0, due to the metric free nature of the model. Panel (a) shows the average distance to Delaunay neighbours, (b) shows the polarisation, (c) the average number of Delaunay neighbours, and (d) the average number of particles on the convex hull, all as a function of time for various choices of v_0, as shown. In every case all measurable quantities are unaffected by a change in v_0 across 10 orders of magnitude.

3.6 Thermodynamic analogy to the SMF swarm

The spatial extent R of SMF swarms follows a power law relationship with the number of particles, N, (Fig. 3.3b). Since the co-alignment of particles may have non-linear effects on the swarm density (connected to the breaking of Galilean invariance by the convention that v_0 is constant) we simplify the SMF model to eliminate co-alignment, i.e. Eq.3.3 becomes

$$\underline{\mu}_i^{t+1} = f_i \langle \hat{\underline{r}}_{ij}^t \rangle_{j \in S_i} \tag{3.7}$$

In this way we hope to gain a clearer understanding of this power law relationship, first via a simple analogy with an ideal gas: In the absence of particle-particle co-alignment each member of the swarm resembles a gas molecule, only feeling an anisotropic average *force* when it reaches the convex hull of the swarm; much like an ideal gas in a bubble.

Starting from the ideal gas law, $pV \sim NT$, and substituting in $p \sim F/A$ for the pressure we arrive at $FV/A \sim FR \sim NT$. Here N and R are naturally the number of individuals and the swarm radius, respectively. The analogue of the total inward force on the swarm, F, is proportional to the number of particles in C (on the surface) N_S, and to the average inward motional bias, $f = \langle\langle \hat{r}_{ij} \rangle_{j \in S_i} \rangle_{i \in C}$. Since the speed v_0 of the particles is fixed, the temperature, T, is assumed to rely only on noise, hence $T(\phi_n)$. Substituting back in for F gives us the relation, $fN_SR \sim NT(\phi_n)$, confirmed for swarms of such gas-like particles, see Fig. 3.10a. The power law relationship between N_S and f with N leads us to expect a similar relationship between R and N, which is confirmed in Fig. 3.10b. The nature of this relationship is surprisingly robust to the introduction of co-alignment between particles, resulting in the power law observed in Fig. 3.3b.

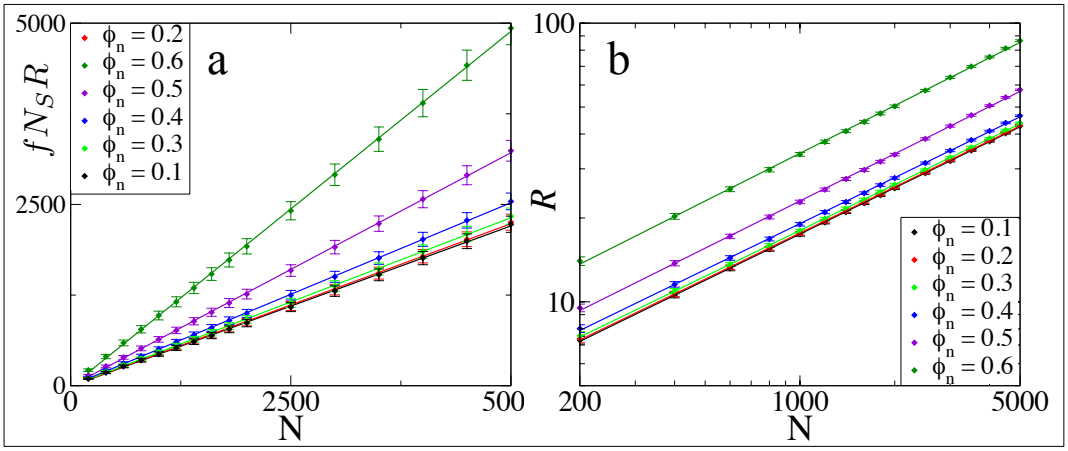

Figure 3.10: (a) For swarms without co-alignment, the number of particles on the surface of the swarm multiplied by the radius of the swarm is seen to scale linearly with the number of particles, ($N_s^{1/2}R \sim N$). (b) This would lead to a power law relationship between R and N which is confirmed by the power law regression giving a relationship of $R \sim N^{0.55}$. As discussed in the text this is closely analogous to the behaviour expected for an ideal gas.

3.7 Further results

3.7.1 Role of parameters ϕ_e and ϕ_n

In order to asses how the properties of the flocks generated by our SMF model depend on the control parameters we simulate swarms for a full range of values for ϕ_e and ϕ_n, controlling the strengths of the "edge" and "noise" terms, respectively. Each point on Fig. 3.11a-d corresponds to a different pair of values for ϕ_e and ϕ_n for which we create 3 independent simulations each 15 000 time steps long, following a pre-equilibration phase of 15 000 time steps (which is higher than the nearest neighbour separation autocorrelation times shown in Fig. 3.11d).

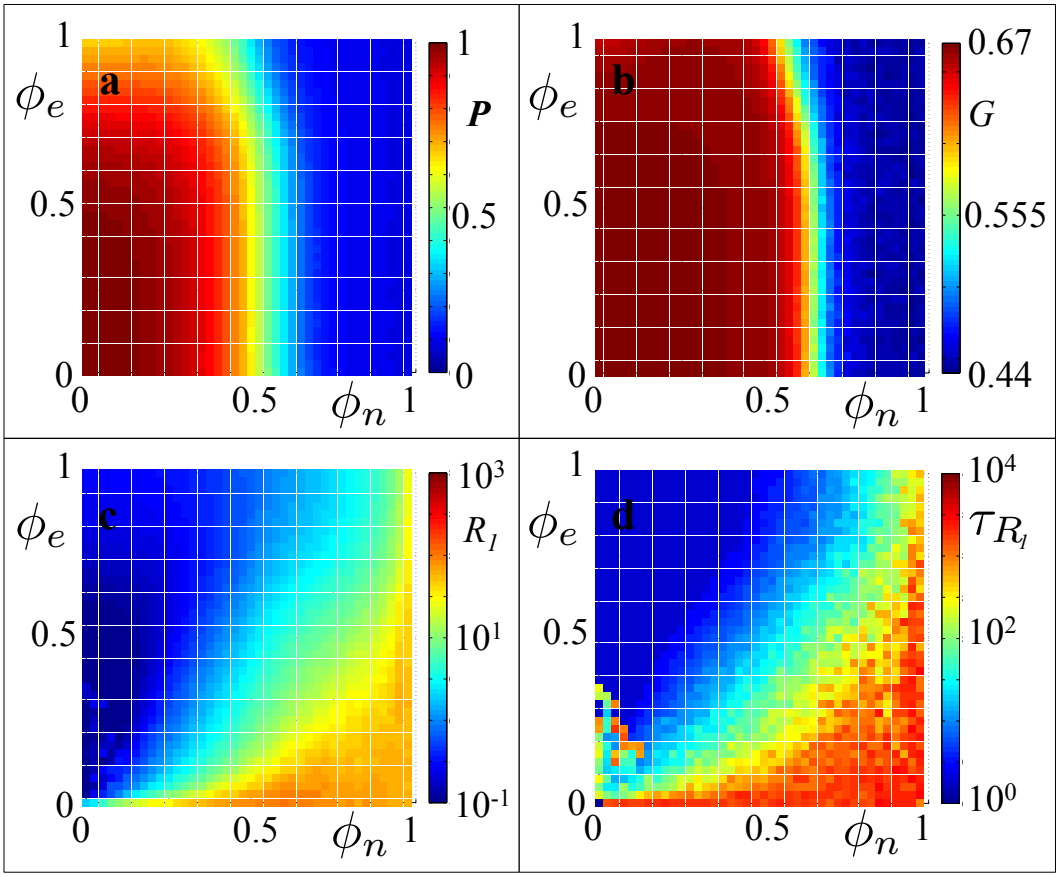

Figure 3.11: Variation of (a) global order parameter P, (b) binder cumulant G, (c) average nearest neighbour separation, R_1 and (d) half time of the autocorrelation function for R_1, τ_{R_1} with ϕ_e and ϕ_n. Each point on the figure corresponds to an average quantity taken over 3 independent simulations of $N = 100$ individuals over 15 000 time steps.

The SMF model exhibits a transition from a disordered to an ordered state around $\phi_n \approx 0.5$; see Fig. 3.11a.

The introduction of inward motional bias, for which $\phi_e \neq 0$, has very little effect on the existence of this transition. Through this transition, the binder cumulant varies monotonically from 1/3 to 2/3 indicating a continuous transition for all values of ϕ_e, see Fig. 3.11b. The position and sharpness of this transition change slightly with ϕ_e: higher values of ϕ_e giving rise to a smoother order-disorder transition, occurring at a lower value of noise. This is due to the fact that the inward motional bias does not lead to polarisation.

However, there is no order-disorder transition associated with variation of ϕ_e alone. Indeed, for low noise, there is a high level of order even when $\phi_e = 1$. This shows that the inward motional bias does not have a significant effect on the ability of the swarm to achieve global order. This is because a high proportion of the swarm are not on the convex hull; for a swarm of 100, this corresponds to between 60 and 80 particles, depending on ϕ_e and ϕ_n.

All simulations featuring a significant surface term ($\phi_e > 0.1$) have a well-controlled swarm density, indicated by the nearest neighbour separation, with low autocorrelation times Fig. 3.11c,d; this indicates no long-term trends or periodicity. In the presence of high noise (disordered state) we see the density decrease and density autocorrelation time increase as the surface term is reduced. In the ordered state, the difference is less pronounced as reduced noise leads to a reduced rate of expansion. If the inward force is switched off entirely, $\phi_e = 0$, then the swarm is still able to achieve a high level of global order but the absence of any binding force means the density drops monotonically in the presence of any noise. Therefore there is no reportable constant density or density auto-correlation time for $\phi_e = 0$, Fig. 3.11c,d

When ϕ_e and ϕ_n are both low, the density and density autocorrelation times both show a region of increase, Fig. 3.11c,d. This is caused by ergodicity breaking in which the swarm occupies fixed configurations that it is unable to escape from within the accessible timescales. For example, when alignment, and therefore global order, is very high the velocity of the centre of mass of the swarm must be very similar to the velocity of an individual. When this is the case, it becomes increasingly difficult for an individual to move relative to the centre of mass of the swarm as all the individuals' velocities are nearly parallel. Therefore it becomes less likely that the swarm will change shape.

3.7.2 Relaxation time of SMF swarms

Due to the metric free nature of the model, there appear to be two different relaxation times in effect. The swarm is able to expand in space until it reaches an equilibrium volume. This volume depends on the values for the parameters in the model, primarily ϕ_e,ϕ_n and N. Noisier swarms in which the effect of the surface term becomes diminished compared to the other terms have higher volumes. Similarly swarms with more individuals are larger. See Fig. 3.12.

Interactions between the particles are entirely topological, and alignment interactions do not depend on the absolute distance between two particles. This leads to the apparent observation of significantly different relaxation times for the ordering and density of the swarm, see Fig. 3.12. Looking only at Fig. 3.12a one might assume that the swarms have reached a steady state after 100 time steps, but at this stage they are still expanding and there could be a subtle difference in the polarisation of the swarm when the expansion stops.

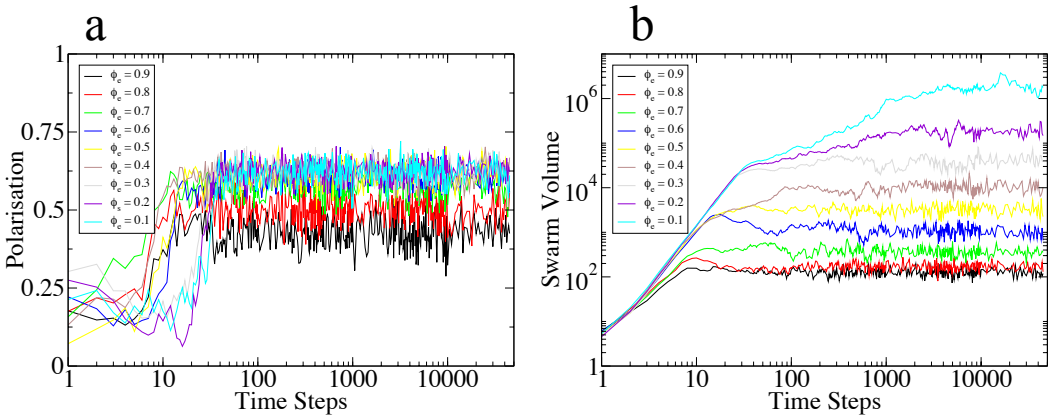

Figure 3.12: (a) Polarisation and (b) Volume of the convex hull of the swarm over the course of 30,000 time steps for varying levels of the surface term ($\phi_e \in (0.1, 0.9), \phi_n = 0.5, N = 100$). After 100 time steps the polarisation would appear to have reached a steady state but the flock is still expanding for a significantly longer time.

3.8 Summary

In this chapter we have shown how the primary features of a flock of starlings, including spatial cohesion, order, low autocorrelation times and metric-free correlation lengths can be generated using a fairly simple, strictly metric free (SMF) model. This

model gives rise to a power law relationship between the spatial extent of the swarm and the number of individuals. This behaviour arises as a result of the different role of individuals on the edge of the swarm.

As well as giving qualitative agreement with observations of animal systems (despite its significant simplifications), this model has the appealing feature that it only requires individuals to perform relatively simple measurements/computations: the relative position and velocity of a finite (and modest) number of nearest neighbours and an awareness of when an individual is itself on the surface of the swarm. These are cognitive tasks that would seem to be within the ability of a large number of swarming animals, in contrast to models that, for example, regulate density using long-ranged (metric based) attraction. These have algorithms that involve $O(N)$ computations per individual, $O(N^2)$ overall, per timestep. This property of the SMF model may help to explain how animals with relatively limited abilities are able to organise themselves into impressive displays of coordinated behaviour.

Chapter 4

Hybrid projection model

Much of the work in this chapter is published in the article 'Role of projection in the control of bird flocks' by Pearce et al.[122].

Many animals employ swarming behaviour as an anti-predation strategy. When under direct attack from a predator this often involves a group of animals appearing to react as one, for example the fast, coordinated turns of a murmuration of starlings avoiding a peregrine falcon. When an entire flock initiates a coordinated turn in a very short amount of time it indicates a rapid transfer of information between all the birds. Local only interactions between individuals result in slow, diffusive information transfer. Information about the approach of a predator would have to propagate inwards, being passed from (the behaviour of) neighbour to neighbour. In this chapter we propose a model in which individuals react to direct, line of sight interactions with the entirety of a swarm. This provides a super diffusive source of information that propagates through the flock at the speed of light. This effectively means that individuals can react *immediately* to perturbations that occur within any visible region of the flock.

The proposition that starlings use line of sight type interactions is consistent with the observations that the primary source of sensory information to them is visual[78]. Recent experiments carried out by the STARFLAG project have observed that starlings within a murmuration respond to the position and velocity of their 7 nearest neighbours[71]. This is supported by experiments suggesting that birds cannot discriminate sets of objects containing more than 7 objects[76]. This indicates it would be unrealistic for a starling to respond to the position and velocity of all visible members of a murmuration, which can contain of the order of 10^5 birds[15]. In

order to make progress we first ask ourselves a simple question, "What does a bird actually see when it is part of a large flock?"

4.1 Defining the visual projection

A birds view out from within a large flock would likely present the vast majority of individuals as merely silhouettes, moving too fast and at too great a distance to be accurately tracked or even discriminated from each other. In our proposed model the basic visual input to each individual is assumed to be simply based on visual contrast: a dynamic pattern of dark (bird) and light (sky) across the field of vision (although it might be possible to extend this to other swarming species and environmental backgrounds, respectively). This has the appealing feature that it is also the projection that appears on the retina of the bird, which we assume to be its primary sensory input[78;79;80]. The two dimensional nature of the projection is also consistent with the fact that starlings in flight have a vey wide viewing angle with minimal stereoscopic vision[77]. A typical individual within a very dense flock would see other, overlapping individuals (dark) almost everywhere it looked. Conversely, an isolated individual, detached from the flock, would see only sky (light). The projected view gives direct information on the *global* state of the flock. It is a much lower dimensional projection of the full $6N$ degrees of freedom of the flock and is therefore more computationally manageable, both for the birds themselves and for the construction of simple mathematical models of swarm behaviour.

This projected pattern carries information. Individuals in a flock that is sufficiently sparse for them to typically see a complex projected pattern of dark and light have much information about the global state of the flock. Such sparse flocks also allow an individual to see out in a significant fraction of all directions, which would allow the approach of a predator, or at least the response of distant individuals to the approach of predator, to be registered. Conversely a dense, completely opaque flock would offer little information, either about the global state of the flock or the approach of predators.

We define the opacity, Θ', of a flock to be the fraction of sky obscured by individuals *from the viewpoint of a distant external observer*. A closely related quantity is the average opacity seen by a typical individual *located within the flock*, written Θ. Crucially, the opacity and density are quite different quantities: Flocks containing large numbers of individuals could be nearly opaque ($\Theta \approx 1$) even for very small densities, corresponding to well separated birds. Such a state corresponds to a complex

projected pattern rich in information.

We first identify those (dark) angular regions where a line-of-sight traced from an individual to infinity intersects one *or more* other members of the swarm. These are separated by (light) domains, see Fig. 4.1.

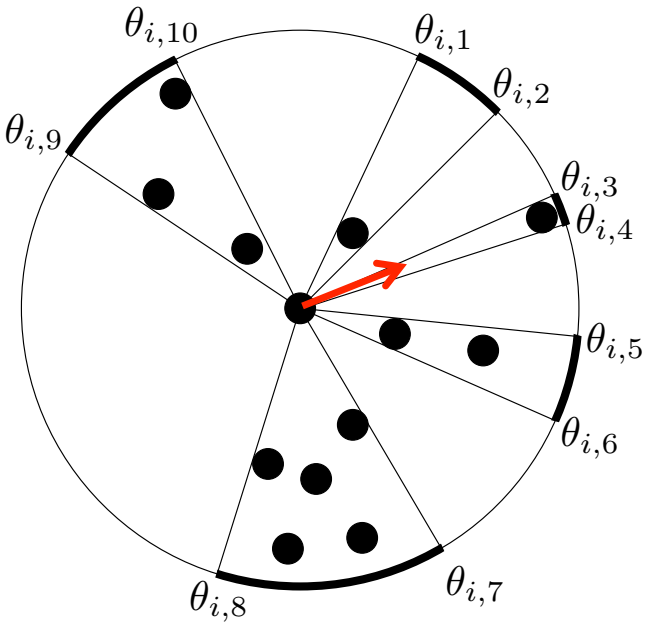

Figure 4.1: Sketch showing the construction of the projection through a 2D swarm seen by the i^{th} individual, which here happens to be one near the centre of the swarm. The thick, dark arcs around the exterior circle (shown for clarity - there is no such boundary around the swarm) correspond to those angular regions where one or more others block the line of sight of the i^{th} individual to infinity. The sum of unit vectors pointing to each of these domain boundaries, at the angles shown, gives the resolved vector $\underline{\delta}_i$, shown in red, that enters our equation of motion.

Each individual is assumed to be isotropic and has a size $b = 1$, that then defines our unit of length. Anisotropic bodies give rise to a projected size that depends on orientation and are explored later in the chapter. In two dimensions the domain boundaries seen by the i^{th} individual define a set of angles θ_{ij}, measured from an arbitrary reference (x) axis, where the index j runs over all the $\mathcal{N}_i$ light-dark (or dark-light) domain boundaries seen by the i^{th} individual, equal to 10 for the central individual shown in Fig. 4.1. These θ_{ij} are a reasonable choice for input to a behavioural model: edge detection like this is known to be performed in the neural hardware of the visual cortex in higher animals[115;116]. We seek a model that takes as input these angles and produces a characteristic direction for the birds,

acknowledging that their actual motion should also include their known tendency to co-align with neighbours and also the effect of some noise.

We take this projection as the input in order to obtain a direction that an individual can follow which will result in flock cohesion. The simplest choices are clearly *'fly towards the dark (or light) areas'*, but this will result in a collapse (or continuous expansion) of the flock, which is unrealistic. Following this, the next simplest, natural, choice for this characteristic direction is to focus on the light-dark domain boundaries, or "edges". Arguably the simplest measure here is the average direction to all boundaries $\underline{\delta}_i$, given by Eq. 4.1.

$$\underline{\delta}_i = \frac{1}{\mathcal{N}_i} \sum_{j=1}^{\mathcal{N}_i} \begin{pmatrix} \cos\theta_{ij} \\ \sin\theta_{ij} \end{pmatrix} \tag{4.1}$$

This can easily be extended to three dimensional flocks, where the light dark boundaries can now be represented as curves on the surface of a sphere and δ becomes the normalised integral of radial unit vectors traced along these curves.

Our model will involve $\underline{\delta}_i$ in such a way as to correspond to birds being equally attracted to all the light-dark domain boundaries. Other choices are possible, but we believe this to be one of the most natural.

4.2 Nearest neighbour selection

We have previously introduced 3 key methods for an individual to selects the neighbours with which it co-aligns. First metric, in which all individuals within a predefined radius are selected. Secondly metric free, in which the nearest n_c individuals are selected, regardless of their absolute separation. Finally, topological, which selects all those within the first voronoi shell.

Here we employ a modified metric free neighbour selection. Namely, all individuals co-align with *visible* local neighbours, assigned in a metric free fashion[71]. We define visible neighbours as those to which there is an unbroken (by another individual) line of sight between the centre of two agents[87;88]. If there are fewer than n_c visible neighbours for an individual, all visible neighbours are selected.

4.3 The Hybrid Projection Model

We incorporate these two characteristic directions, arising from the projection and the orientation of neighbours, into an otherwise standard agent-based model for a

swarm of N particles moving off-lattice with constant speed v_0 ($v_0 = 1$ in all our simulations). For simplicity we treat the individuals as "phantoms", having no direct steric interactions (the effect of introducing steric interactions is explored later in the chapter). The equation of motion for the position $\underline{r}_i^t$ of the i^{th} individual at discrete time t is

$$\underline{r}_i^{t+1} = \underline{r}_i^t + v_0 \hat{\underline{v}}_i^t \tag{4.2}$$

with a velocity parallel to

$$\underline{v}_i^{t+1} = \phi_p \underline{\delta}_i^t + \phi_a \widehat{\langle \underline{v}_k^t \rangle}_{n.n.} + \phi_n \underline{\eta}_i^t \tag{4.3}$$

where $\langle \dots \rangle_{n.n.}$ is an average over the $k \in [1, n_c]$ nearest neighbours to the i^{th} individual ($n_c = 4$ in all simulations), a hat $\hat{}$ denotes a normalised vector and $\underline{\eta}_i^t$ is a noise term of unit magnitude having a different (uncorrelated) random orientation for each individual at each timestep. This equation involves only three primary control parameters ϕ_p, ϕ_a and ϕ_n, the weights of the projection alignment and noise terms, respectively. We further simplify by considering only the relative magnitudes (ratios) of these control parameters which are then taken to obey Eq. 4.4.

$$\phi_p + \phi_a + \phi_n = 1 \tag{4.4}$$

This set of equations introduces only one source of information that the individual draws on that is not directly calculated from the projection, that is the velocity of the nearest neighbours with which it co-aligns. Extracting this information from the projection is explored later.

4.3.1 Numerical Simulations

Simulation of the hybrid projection model involves solving the equations of motion Eqs. 4.2 & 4.3. These were solved iteratively using an algorithm written in C++ by the author. The initial conditions for the N individuals are that they started with random positions in a square region of space of area N^2 (in units of the size of each individual squared) with randomly orientated velocities. So as to eliminate transients associated with these arbitrary initial conditions the swarms are allowed to pre-equilibrate. All simulations were were pre-equilibrated for a period of at least 25,000 time steps. The pre-equilibration period was always longer than the corresponding correlation time (except when $\phi_p = 0$, when the swarm anyway fragments

and disperses to infinity). Phase planes, such as those in Fig. 4.3, show results for 861 different locations in the parameter space, each being the average result of four independent simulations of 100,000 time steps at that particular combination of ϕ_p and ϕ_a.

We now analyse the results of computer simulation of the swarms arising from these equations of motion for given combinations of $\{\phi_p, \phi_a\}$ alone, with ϕ_n given by construction through Eq (4.4).

4.4 The Hybrid Projection Model reproduces key features of a flock of birds

The set of equations that constitute the hybrid projection model can be solved iteratively to recreate trajectories reminiscent of swarming animals, Fig. 4.2.

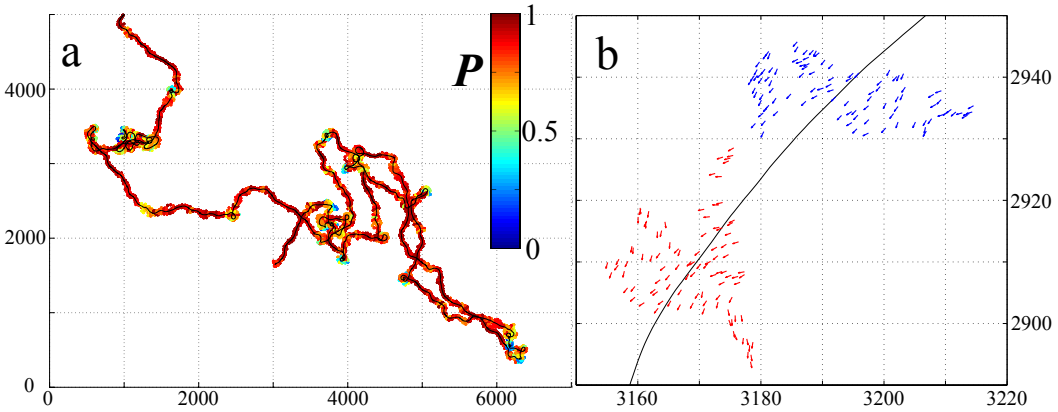

Figure 4.2: An example of a realisation of the equations governing the hybrid projection model with $\phi_a = 0.75$ and $\phi_p = 0.1$. (a) The trajectory of the centre of mass of the flock, coloured with the polarisation, P, at that point in the simulation. (b) a snapshot of the swarm at two different times.

In particular it naturally leads to robustly cohesive swarms capable of high levels of polarisation, see Fig. 4.3, as well as the emergence of *marginal opacity* in large flocks of birds where both Θ and Θ' are neither very close to 0 nor 1, see Fig. 4.4.

The emergence of marginal opacity is a new feature and it is worth emphasising that the model was not constructed to target any particular "preferred" opacity value, rather marginal opacity emerges naturally. Importantly, it arises for swarms of varying size N that are realised with exactly the same control parameters ϕ_p and

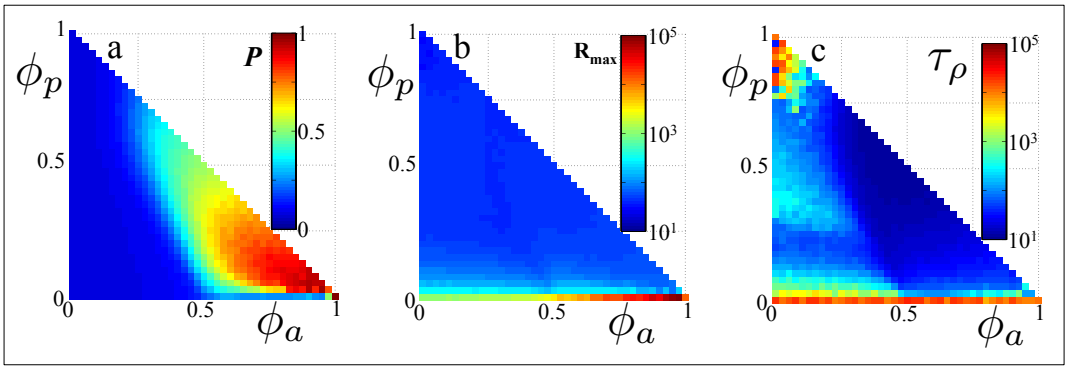

Figure 4.3: Results from repeated computer simulation of a simple hybrid projection model, parameterised by the strength of the response of each individual to the projection through the swarm that they see (ϕ_p) and the strength of the alignment with their 4 nearest neighbours (ϕ_a).Each small coloured square (point), corresponding to a pair of parameter values $\{\phi_a, \phi_p\}$, is an average value over 100,000 timesteps for $N = 100$ individuals. (a) The average speed, P, of the centre of mass of the swarm, normalised by the individual's speed. This is also refereed to as the order parameter. (b) The distance between the two furthest individuals in the swarm, $R_{\max}$, in units of particle diameter - the swarm does not fragment unless $\phi_p = 0$. (c) The swarm density autocorrelation time τ_ρ in simulation time-steps. The upper left corner of this panel represents dynamically "jammed" states that we believe to be unphysical.

ϕ_a. This means that marginal opacity can be maintained without a bird changing its behaviour with, or even being aware of, the size of the flock. Using regression it is possible to estimate the opacity of a swarm following the hybrid projection model in the large N limit, this identifies a value of $\theta_{\text{lim}} \approx 0.73$ (and $\theta'_{\text{lim}} \approx 0.78$). Specifically, we predict that swarms with an infinite size will not be opaque. This implies that the density and morphology of a swarm must vary as it increases in size, a concept we will revisit in more depth later. It is also worth noting that the precise value of θ_{lim} identified here is for a specific set of parameters of the model and we expect it to be somewhat tuneable between 1 and 0 by this selection. Other models, which control the density in a metric fashion[91;90], give rise to values for Θ that approach 1 as the number of individuals in a swarm increases, i.e. they always become fully opaque. In such metric-based models the density of the swarm is fixed by the control parameters. Thus, for any combination of these parameters there will always be a critical size at which the swarm becomes opaque. For the typical models analysed in the literature even rather small flocks with $N < 100$ are already fully opaque. The only possible approach to preventing swarms from becoming opaque with such

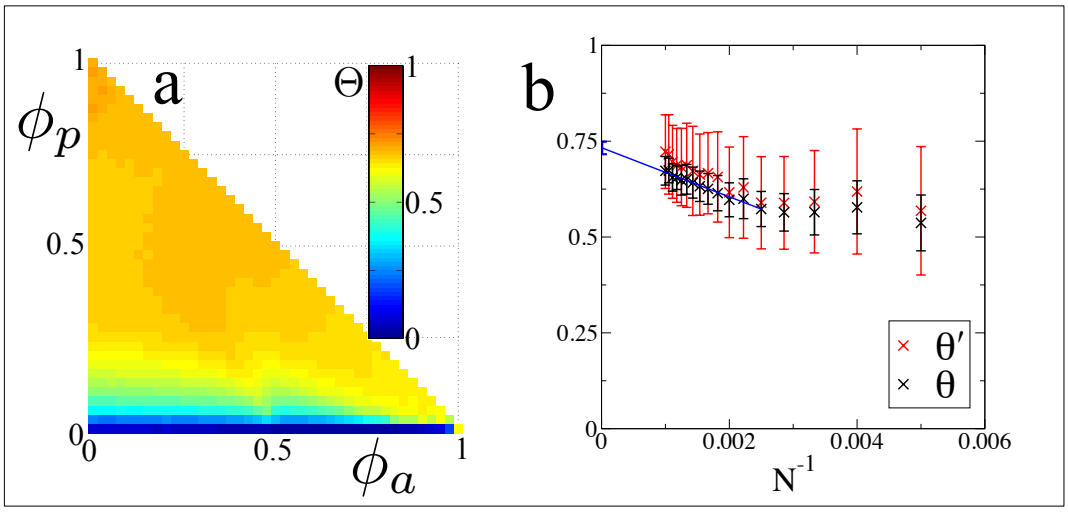

Figure 4.4: (a) The average opacity Θ for different values of $\{\phi_a, \phi_p\}$ (b) The average opacity of swarms of varying size from the point of view of an external (red) and internal (black) observer. Swarms contain different numbers of individuals N (the axis shows $1/N$) with $\phi_p = 0.03$ and $\phi_a = 0.8$ averaged over at least 50,000 timesteps. The linear fit with an R^2 value of 0.97, is to all data points $N \geq 400$.

models would be to continuously modify their control parameters as a function of the swarm size. This would represent a significant proliferation in control parameters from a baseline level that is already typically far higher than in the present work. This is the signature of a class of models that are structurally inadequate to explain marginal opacity.

In Figs. 4.3,4.4a individuals don't respond to the projection at all in the narrow strip where $\phi_p = 0$. Here the swarm fragments/disperses. Provided there is even a very weak coupling to the projection, i.e. $\phi_p > 0$, the swarm no longer dissipates. In Fig. 4.3c the narrow red strip near $\phi_p = 0$ shows that the response of the swarm is slow in the absence of the projection term. Here, even when the swarm does not fragment, the dynamics depend on the exchange of information between nearest neighbours. The correlation time decreases as the strength of response to the projection is turned on. This is because the projection provides a global interaction and can therefore lead to rapid dynamic response, consistent with the fast transients observed in bird flocks. The nature of this model also makes it robust in response to shocks, suck as those caused by predation in animal systems (see Supplementary Movie 4.1).

4.4.1 Projection term leads to flock cohesion

In order to test how flock cohesion is controlled by the presence of the projection term we performed a number of simulations, first with a very small, but non-zero, projection term and then without it. The maximum distance between any two particles within a flock, $R_{\max}$, was recorded as a function of time, see Fig. 4.5. $R_{\max}$ gives a upper bound for the flock diameter, providing a useful metric to demonstrate the effectiveness of the projection term in producing bounded flocks; for an unbounded flock the maximum flock diameter will continually grow over time. Fig. 4.5 shows that the maximum linear size $R_{\max}$ of flocks grows without bound when $\phi_p = 0$. In this case the flock fragments into disconnected clusters that perform independent random walks, hence $R_{\max}$ continually increases (black traces). However, even a very small contribution from the projection term, here $\phi_p = 0.03$, is enough to prevent this from happening (red traces). This result is insensitive to the size of the flock and also to the precise choice of parameter values at the simulation times accessible here. This is evidenced by the stable diameter of all swarms with low autocorrelation times in the parameter sweep (provided $\phi_p \neq 0$), see Fig. 4.3b,c, and the non-zero opacity with finite variance for swarms of varying sizes, see Fig. 4.4b. This can be justified by the heuristic argument that it only takes a very weak coupling to an inward force to prevent the continual expansion of a diffusive system. When ϕ_p is very low the system will be very diffuse. In this scenario the projection term is essentially an inward force for all individuals, which does not diminish as the swarm continually expands, acting to eventually balance diffusion.

4.4.2 Anisotropic nearest neighbour distribution

The closest neighbours of an individual will represent the largest uninterrupted dark regions of the projection, often resulting in a large section of the projection with no light-dark domain boundaries. Therefore the projection term is often slightly biased away from the nearest neighbours. This results in the distribution of the nearest neighbours relative positions, shown in Fig. 4.6. This result is in close agreement with a similar anisotropy observed in birds[71;70] and fish[52;53] which are observed to rarely follow directly behind conspecifics, instead favouring to align themselves slightly off centre.

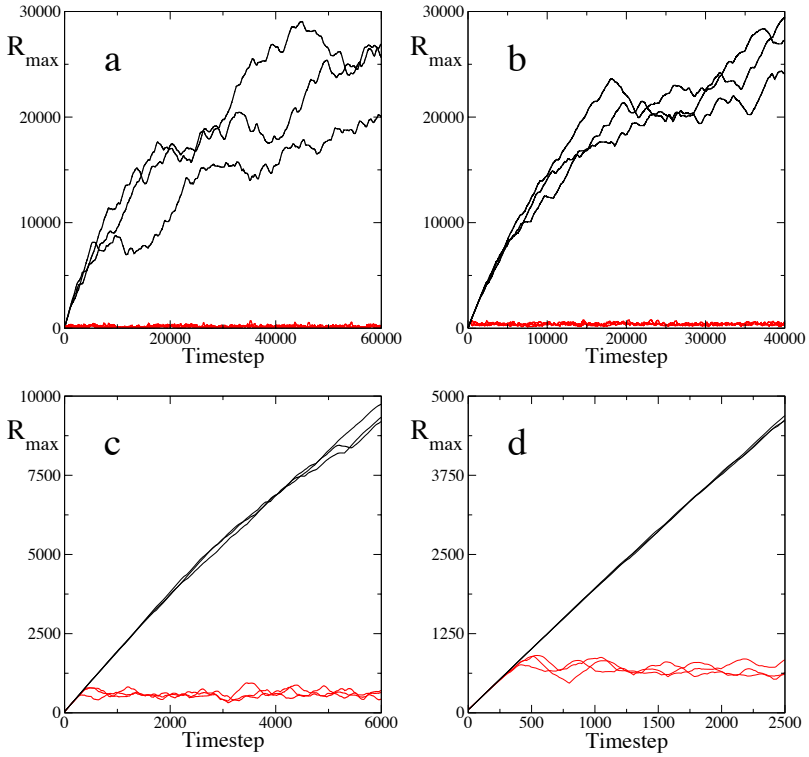

Figure 4.5: Maximum flock diameter for flocks containing (a) $N = 100$, (b) $N = 500$, (c) $N = 1000$ and (d) $N = 1500$ individuals generated by computer simulation of the hybrid projection model with $\phi_p = 0.03$, $\phi_a = 0.8$ and $\phi_n = 0.17$ (red), the same values as those used in Fig.4.4b, and in the absence of projection $\phi_p = 0.0$, $\phi_a = 0.83$ and $\phi_n = 0.17$ (black).

4.4.3 Radial Density of nearest neighbours

The projection term controls the density in such a way that while maintaining a cohesive, high density flock also prevents it from collapsing to an extremely dense state. This is reflected in the radial density of the nearest neighbours, which shows a clear peak separate from the individual, see Fig. 4.7. This is despite the fact there are no steric interactions directly preventing individuals from overlapping. This distribution is very similar to observed radial density of conspecifics within swarms of animals[53;75], which show a peak at the apparent preferred density for a particular swarm which then reduces as the radius is increased. Here we show the tail of the density function has a power law relationship with the radius, this is indicative of a scale free relationship governing the density.

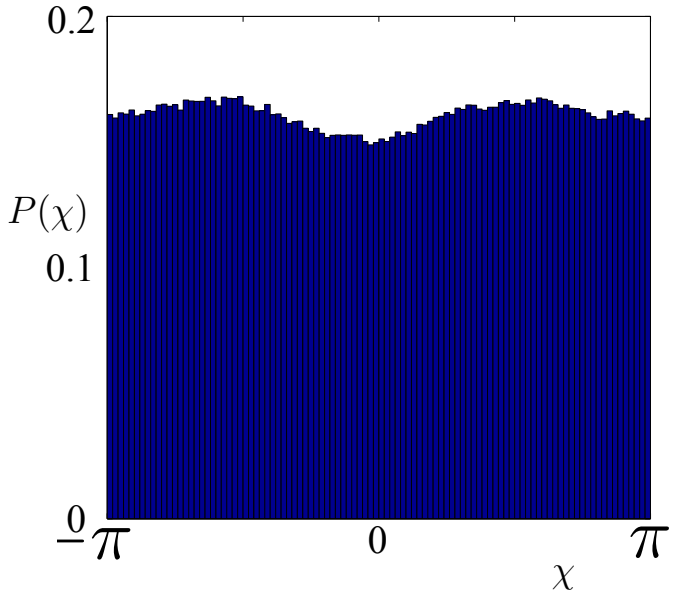

Figure 4.6: Probability density $P(\chi)$ for the angles (χ) between the velocity of (all) of the i^{th} individuals, parallel to $\mathbf{v}_i$, and the vector $\mathbf{r}_{ik}$ to each of its 4 nearest neighbours, labelled by the index k, as in the text. The peaks at $\chi = \pm\pi/2$ indicates that nearest neighbours are preferentially orientated to the sides of the individuals, rather than in front or behind. These results were gathered for a swarm of $N = 100$ isotropic individuals over 10,000 time steps with $\phi_a = 0.85$, $\phi_p = 0.05$.

4.5 Comparison with a typical metric based model from the literature

In order to highlight some of the advantages of a global, metric free model, we compared it to a standard local, metric based model for flocking. The choice of model is somewhat arbitrary; any local repulsion/orientation/attraction model could have been chosen. Because of this we chose a typical model from the literature[90] that includes the core of many established metric models capable of creating coherent flocks[94;36].

In the selected model each particle has three interaction radii, a repulsion from all particles at a distance $r < r_r$, co-alignment with all particles in the region $r_r < r < r_o$, and attraction to all particles in the region $r_o < r < r_a$. Each particle moves with a constant velocity, $v = 1$, and updates its direction and position every timestep, which have duration $dt = 0.1$. Our simulation of this model was coded in C++ and employed simulation parameters $r_r = 1$, $r_o = 10$ and $r_a = 15$ for

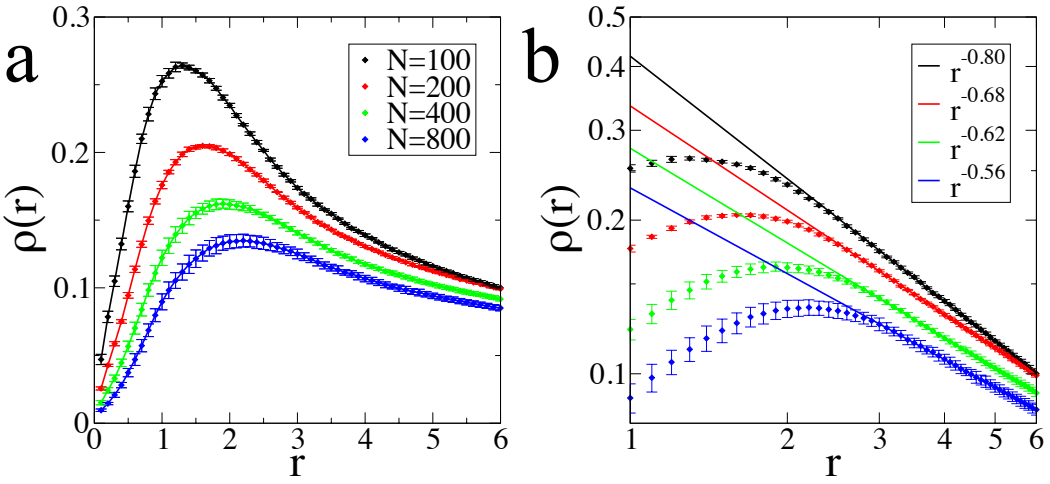

Figure 4.7: a) Average radial density of neighbouring birds relative to an individual (at $r = 0$) for $\phi_a = 0.85$ and $\phi_p = 0.05$. b) Log-log plot of the same data. The straight lines show the power law like behaviour in the tail of the distribution. The density is per unit area, in units where the size of each isotropic individual is unity.

the repulsion, orientation and attraction ranges respectively, shown as all traces in Fig. 4.8a and the red ($N = 300$) and black ($N = 100$) traces in Figs. 4.9, 4.10. Where it was necessary to modify these parameters the green traces on Figs. 4.9, 4.10 correspond to $N = 300$, $r_r = 1$, $r_o = 17$ and $r_a = 26$. The results from this simple attraction-repulsion model are compared with our hybrid projection model in Figs. 4.8, 4.9, 4.10. In order to define an opacity in Fig. 4.10 the size of an individual must be defined. We take this as 0.25 in the same units. This value is chosen because the STARFLAG data shows the nearest neighbour spacing is often around 1m, and the length of a starling is around 0.25m[30]. So there is a factor of 4 between the two units. The dashed lines in Fig. 4.9b are the diameter of the orientation zone $2r_o$, which it is appropriate to compare with $R_{\max}$, the maximum distance across the flock. This, along with the change in units leads to a factor of 8 scaling from $r_o = 10$ and $r_o = 17$, respectively, to the value given in Fig. 4.9b in bird length units.

Although this is an arbitrary choice of model in order to test our hypothesis, the results will be the same (within a scaling factor) for any model that similarly defines metric interaction radii.

4.5.1 Global Interactions result in more robust flocks

Models that include only local interactions produce flocks that can fragment or disperse if the simulation parameters and initial conditions are not carefully chosen. If an agent has a limited, metric-based interaction radius the simulation parameters (such as length of timestep, noise, speed, range(s) etc.) must be selected to prevent moves that could leave an individual disconnected from the flock, i.e. with no other particles within its interaction radius. If this were to happen there would be no mechanism to ensure that it rejoins the flock. Such fragmentation is always a danger when the flock is perturbed, for example by predation, so as to result in a (group of) individual(s) being separated from the flock. It also fails to capture how a flock might form from an initially disperse state. This is characterised in Fig. 4.8, where flocks following the hybrid projection model are shown to recover from an arbitrary perturbation involving a 16 fold metric expansion of the flock while local, metric based flocks fail to re-aggregate. The recovery of the hybrid projection model is independent of the parameters used, provided only that $\phi_p > 0$. In contrast, local metric based models are unable to reliably recover from perturbations that move any (groups of) individual(s) outside the attraction radius.

This effect is also highlighted in supplementary movies 4.1, and 4.2, in which swarms of individuals are introduced to a simple predator (The predator travels at a speed of $2 \cdot v_0$ and is attracted to the centre of mass of the swarm. The individuals react to the predator when it is within $10 \cdot dt \cdot v_0$ and their response is to travel directly away from it at $1.5 \cdot v_0$). In Supp. Mov. 4.1, the predator is unable to separate a swarm of individuals following the hybrid projection model ($\phi_p = 0.2$, $\phi_a = 0.7$). The global nature of the interactions between individuals results in the swarm always reforming. In Supp. Mov. 4.2, individuals have a limited interaction radius. In this case they don't respond to other members of the swarm that are separated by more than $30 \cdot v_0 \cdot dt$. The difference in the cohesiveness is clear from the two movies.

4.5.2 Metric interactions do not scale with the swarm size

The interactions within bird flocks are now understood to be scale free, scaling with the overall extent of the flock[30]. This would seem to be reflected in the failure of metric based models to cope with increasing N unless the behavioural parameters are themselves continually adjusted, see e.g. Fig. 4.9. This is because the metric-based nature of these models effectively fixes the density, through the inter-particle

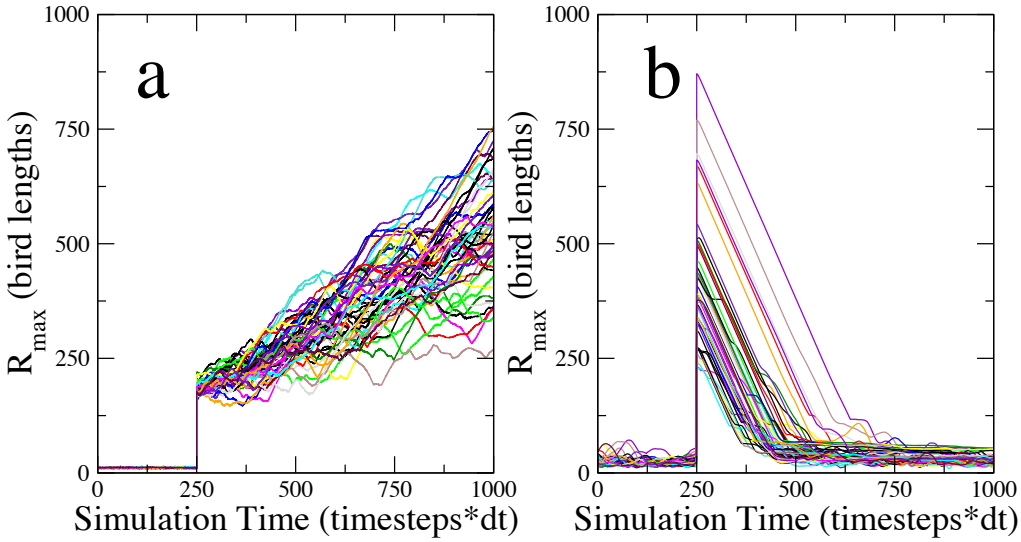

Figure 4.8: Global interactions prevent fragmentation following perturbation. Maximum flock diameter for 50 different simulations (each trace) of a flock of $N = 50$ individuals created using (a) typical local model from the literature and (b) Hybrid Projection Models following a 16× linear expansion in two dimensions. We used typical parameters for a flock of $N = 100$ birds outlined above and a hybrid projection model with $\phi_p = 0.2$, $\phi_a = 0.7$ and $\phi_n = 0.1$. Technical detail: the dimensionless time corresponding to each time step was $dt = 0.1$ in the metric model and $dt = 1$ in the hybrid projection model and so we have scaled the simulation time steps by this factor to obtain a fair comparison of the relative diameters, which would otherwise be different (scaled) by a factor of 10.

spacing, see Fig. 4.10b. As N increases any fixed interaction range will eventually encompass only a small fraction of the flock, leading to a breakdown in transfer of alignment information and loss of global alignment P, see Fig. 4.9a The only way to adjust the model to obtain realistic behaviour is to change the interaction radii accordingly, so that they once again encompass a significant proportion of the flock; essentially the model is *demanding* global interactions. This necessarily leads to a rather complex (highly parameterised) model in which individuals make decisions based on the position and orientation of an ever increasing number of neighbours; for a flock with $N = 300$ each individual responds to the positions and velocities of ~ 270 of its neighbours, as shown in Fig. 4.9c. Many of these are obscured from its view, as discussed in the next section.

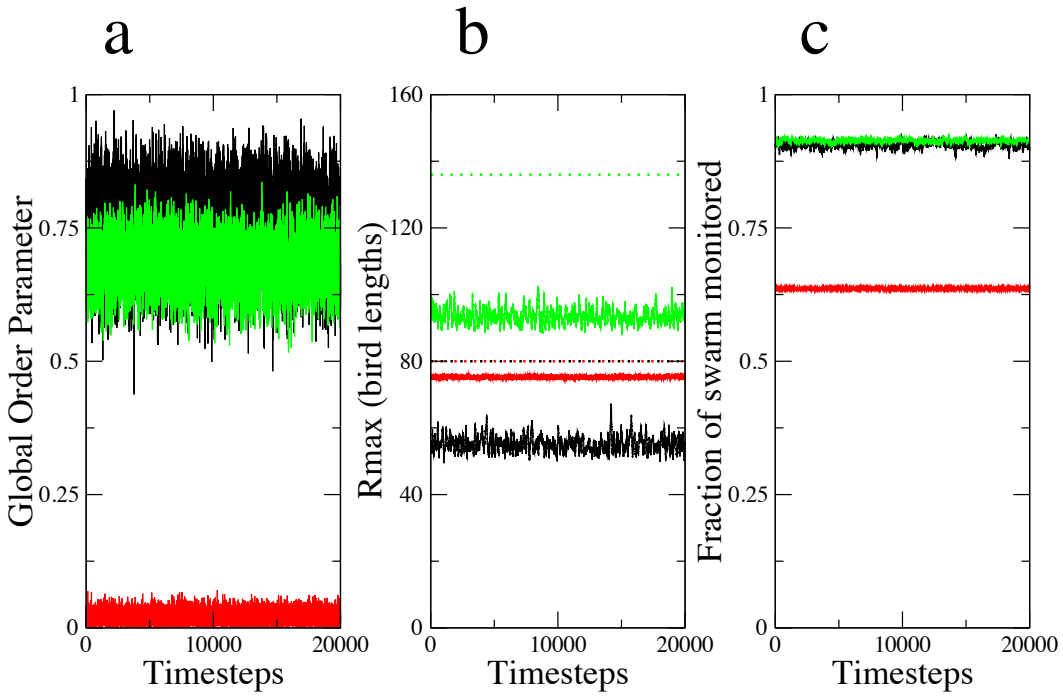

Figure 4.9: Breakdown of a typical local model from the literature. (a) As the number of individuals in the flock is increased from $N = 100$ (black) to $N = 300$ (red) the global order parameter, P, falls to near zero, unless the interaction ranges are extended to the larger values given in the text (green). (b) The alignment interaction diameter (range) in bird length units (dashed line, see text for details) is significantly higher than the maximum extent of the flock ($R_{\max}$) for realistic flocks (black, green) and therefore encompasses almost the entire flock. (c) The increased interaction ranges result in an individual responding to the position and velocity of about 90% of its neighbours (those giving input to the model for that individual's behaviour) for $N = 300$ (green), as was the case for $N = 100$ (black).

4.5.3 Metric based interaction ranges lead to fixed density and opaque flocks

The hybrid projection model results in flocks that are marginally opaque, that is to say that visual information can often pass, uninterrupted, across the entire flock. This is supported by observations (see next chapter). Any model that fixes density, such as through a fixed nearest neighbour distance, must eventually give rise to fully

opaque flocks as more individuals are added (see mean field scaling analysis in the next chapter). In the worst case scenario this could result in behaviour dominated by fictitious interactions between individuals that are completely occluded from one-another. Fig. 4.10a shows that local metric based flocks are almost entirely opaque. This is due to the fact that the individuals essentially form a close packed liquid-like phase with little change in the nearest neighbour separation; see Fig. 4.10b. This results in a large fraction of unphysical phantom interactions, depending on whether one imagines that some (Fig. 4.10c) or all (Fig. 4.10d) of a neighbouring individual must be seen for a realistic interaction to occur. Also, due to the metric nature of the interaction radii, as the flock gets bigger the information transfer across the length of the flock becomes far less efficient. This occurs when the interaction radii become small relative to the extent of the flock. This means that a change in parameters is needed to prevent the flock from entering a solid like state, in which global order is lost.

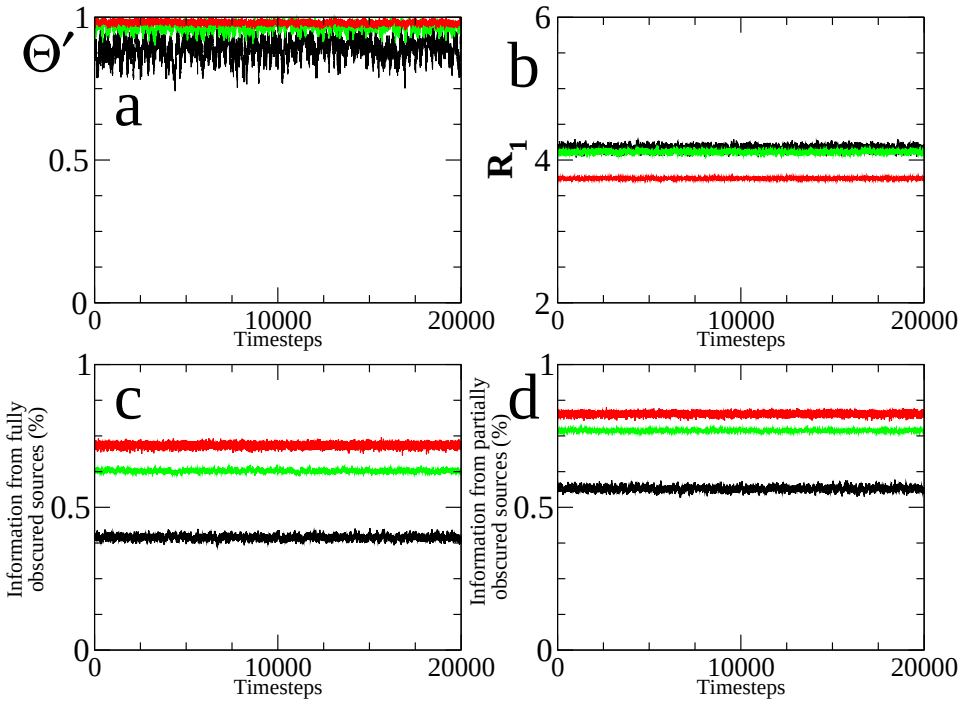

Figure 4.10: Unphysical nature of a typical local model from the literature with the same parameters as used in Fig. 4.9. (a) Flocks remain fully opaque in time from the point of view from an external observer. (b) This is due to the metric nature of the model that fixes the average separation between individuals in time. (c,d) The proportion of neighbours interacting with an individual through this model that are (c) completely and (d) partly occluded from its view remains high throughout.

4.6 Extensions to the hybrid projection model

There are many possible extensions that might be proposed to the hybrid projection model. Here we have chosen some of the more common extensions: a blind angle to the rear of an individual, short ranged repulsion and anisotropic individuals[36;94;35;123].

4.6.1 Effects of steric interactions

We can also introduce a short range repulsion/steric interaction to the model. Whenever the distance between two individuals drops below a threshold they then have a new update rule added to Eq. 4.3 in which they simply move away from neighbours so as to avoid collisions. Such a steric interaction has little effect on the behaviour of the model at the qualitative level. This is because the projection term already acts to prevents the flocks becoming too dense due to the fact that it steers individuals away from opaque (dense) directions. When a steric interaction term in which birds fly away from their nearest neighbours if they get within two length units is introduced there is little observed change in the order parameter, P, linear flock length, $R_{\max}$, and opacity, θ, see Fig. 4.11.

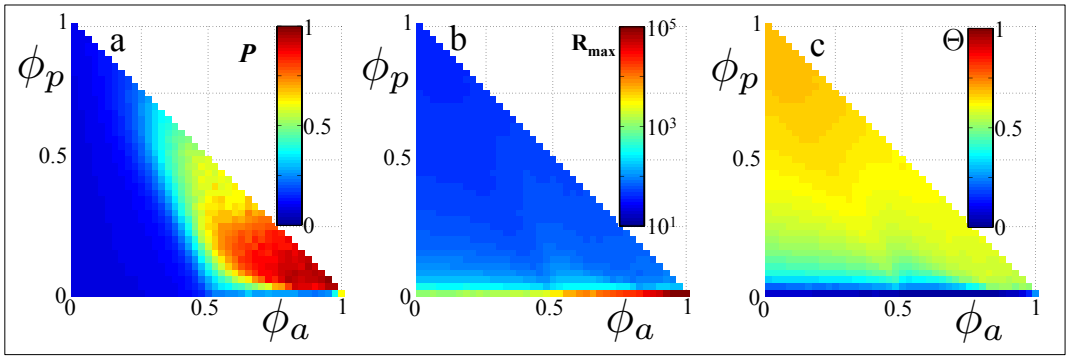

Figure 4.11: (a) The order parameter, P, (b) linear flock length, $R_{\max}$, and (c) opacity, θ, as a function of the parameters ϕ_p and ϕ_a for a flock of 100 isotropic individuals. Featuring a repulsive term to prevent the individuals overlapping.

4.6.2 The effect of anisotropic individuals

The angular size presented to individual i by its neighbour j depends on the physical size of the individual b and vector connecting them $\mathbf{r}_{ij}$. For the isotropic individuals considered in most of the chapter this is defined to be

$$\Delta\theta = 2\arctan\left(\frac{b}{2|\mathbf{r}_{ij}|}\right) \tag{4.5}$$

which approaches $\Delta\theta = b/|\mathbf{r}_{ij}|$ for $r \gg b$. For anisotropic individuals (Figs. 4.13, 4.14, 4.15 and Supplementary Movies, 4.3-4.7, only) the angular size of the j^{th} individual depends on the angle ζ_{ij} between its direction of motion, along $\mathbf{v}_j$, and

the line of sight of the i^{th} individual to it, along $\mathbf{r}_{ij}$. If the aspect ratio is $a \geq 1$ and the long axis is orientated at an angle ψ to the direction of motion ($\psi = 0$ is long-and-thin, $\psi = \pi/2$ is short-and-fat, see Fig. 4.12b and c respectively) the angle subtended at $\mathbf{r}_i$ is defined to be

$$\Delta\theta = 2 \arctan\left(\frac{\tilde{b}}{2|\mathbf{r}_{ij}|}\right) \tag{4.6}$$

with the apparent physical size in this orientation given by

$$\tilde{b} = b\left(\sin^2(\zeta + \psi) + a^2 \cos^2(\zeta + \psi)\right)^{-1/2} \tag{4.7}$$

See Fig. 4.12. This reduces to $\tilde{b} = b$ when $a = 1$, as required,

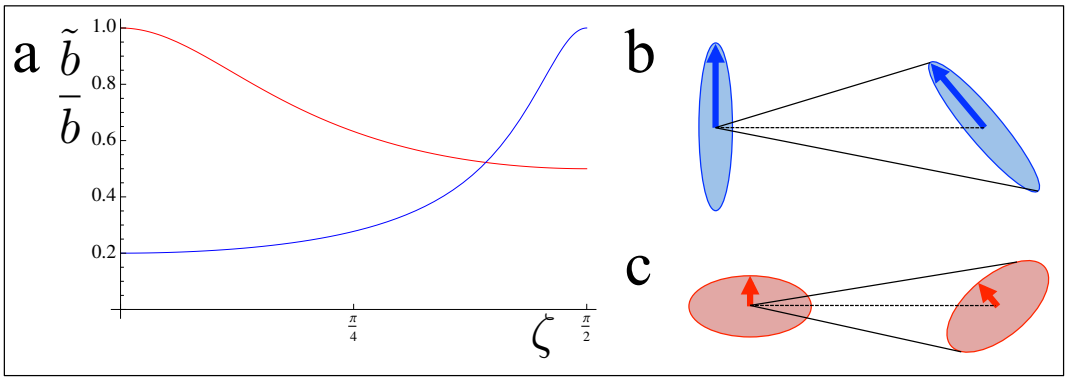

Figure 4.12: (a) The apparent physical size $\tilde{b}$ of an anisotropic individual divided by its (maximum) length b. The individual's velocity is orientated at an angle ζ to the line of sight from the observer. The blue curve represents a long-and-thin individual, with long axis parallel to its velocity ($\psi = 0$) and aspect ratio $a = 5$, shown in (b). The red curve represents a short-and-fat individual, with long axis orientated at an angle $\psi = \pi/2$ to its velocity and aspect ratio $a = 2$, shown in (c).

Phenotypical Behaviour under the Hybrid Projection Model

Fig. 4.13 shows a number of "phenotypes" supported by the hybrid projection model. In this figure the point in parameter space denoted I involves swarms with low global order P and weakly correlated internal dynamics, somewhat reminiscent of a swarm of flying insects, see supplementary movie 4.5. The point F can exhibit circulating vortex-like swarms, somewhat reminiscent of those observed in shoals of

fish[124], see supplementary movie 4.4. This morphology doesn't appear in swarms of isotropic individuals but is seen in these anisotropic individuals that mimic the long-and-thin shape of fish. The point B has a relatively high global order, P, and is similar to many of the swarms seen for isotropic individuals, see supplementary movie 4.3. It is perhaps more reminiscent of migratory flocks of birds or mammals. In each case a corresponding snapshot of a typical swarm configuration is shown. These results lead us to speculate that this model may provide a method to classify swarming behaviour across species, e.g. according to the values of ϕ_p, ϕ_a and n_c (see supplementary movies 4.3-4.5). As discussed below intermediate regions exist in which the entire swarm can switch spontaneously between two distinct behavioural modes, reminiscent of the ability of animals to change their behaviour in response to a threat.

Vorticity of the swarm, milling in fish

The vorticity, ω, of a swarm is here defined as the average tangential component of the velocities with respect to the centre of mass of the swarm according to

$$\omega = \frac{1}{N}\sum_{i=1}^{N} \frac{\delta \mathbf{r}_i}{|\delta \mathbf{r}_i|} \times \frac{\mathbf{v}_i}{|\mathbf{v}_i|} \tag{4.8}$$

with $\delta \mathbf{r}_i = \mathbf{r}_i - \bar{\mathbf{r}}$ and $\bar{\mathbf{r}} = \frac{1}{N}\sum_{i=1}^{N} \mathbf{r}_i$ the centre of mass of the flock. The vorticity satisfies $-1 < \omega < 1$ with $\omega > 0$ for anticlockwise circulation and $\omega < 0$ for clockwise motion. The vorticity autocorrelation time τ_ω is defined by

$$\frac{\langle \omega(t)\omega(t+\tau_\omega)\rangle}{\langle \omega^2 \rangle} = \frac{1}{2} \tag{4.9}$$

Fig. 4.14 shows results obtained for swarms of anisotropic individuals; isotropic individuals tend not to exhibit such high vorticity.

Fig. 4.14b clearly shows a region of increased vorticity corresponding to a region of reduced order (centre of mass velocity), P, in Fig. 4.14a, with a transition between the two states occurring at $\phi_a = 0.55$ when $\phi_p > 0.375$. As can be seen from Fig. 4.14c vorticity decorrelation is observed on computationally accessible timescales. What is the mechanism for this loss of correlation? The trajectory shown in Fig. 4.15 shows that this can arise due to the ability of the swarm to switch between clockwise rotation, anticlockwise rotation and translating phases. The time τ_ω can roughly be associated with the time between switching events.

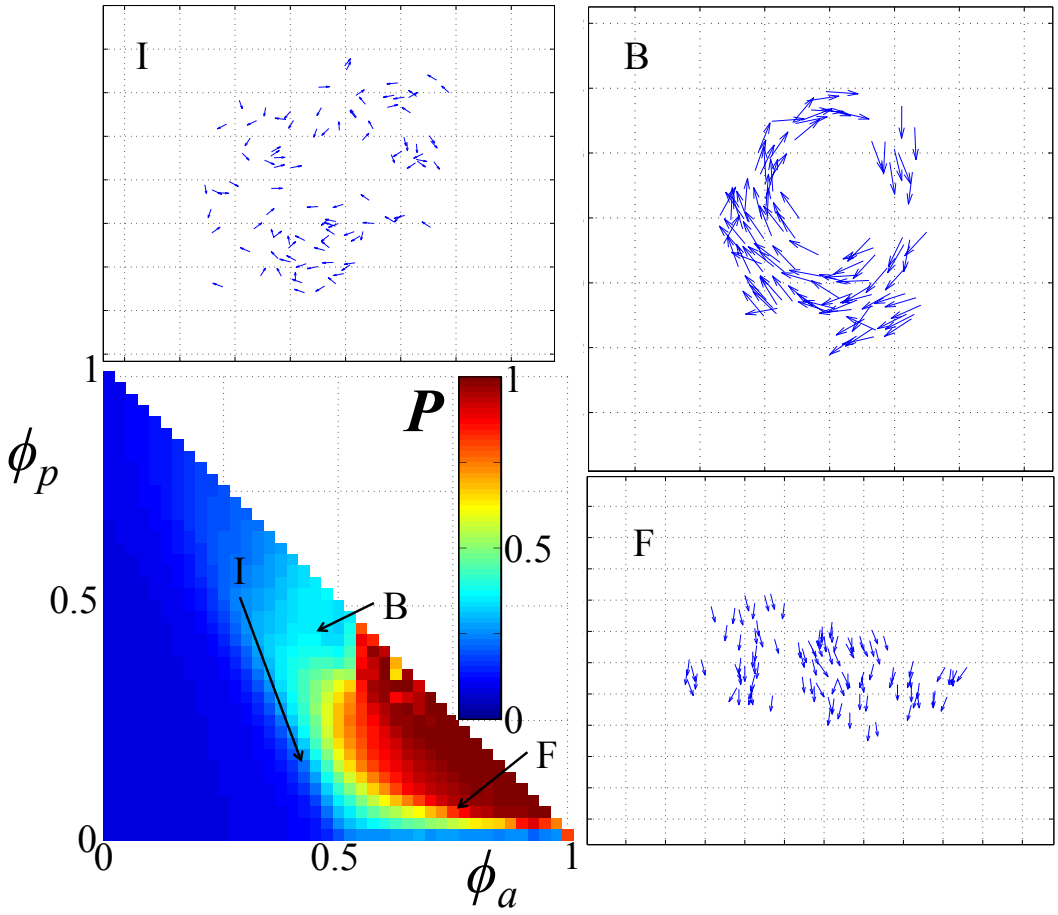

Figure 4.13: Shown in the bottom left is the variation of the global order parameter P for a swarm of 100 anisotropic individuals (10:1 long-and-thin) with the relative weights of the projection ϕ_p and alignment ϕ_a terms (compare with Fig. 4.3 for isotropic individuals). Shown in the other panels are snapshots of the trajectories at each of the corresponding points indicated on the phase plane. Points B, F and I correspond to supplementary movies 4.3, 4.4, and 4.5, respectively.

Significantly, switching occurs with very little change in opacity or average density, although there is an increase in the amplitude of fluctuations about these average values when the swarm enters the translating phase. This is further evidence of the robust nature of the emergence of marginal opacity within our model.

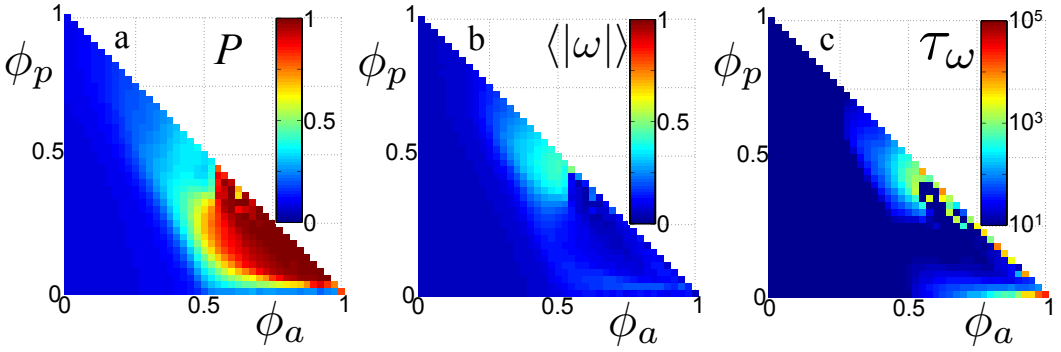

Figure 4.14: (a) The variation of the time averaged magnitude of the polarisation, P, (b) vorticity, $\langle|\omega|\rangle$, and (c) the vorticity correlation time τ_ω in simulation time-steps with the relative weights of the projection ϕ_p and alignment ϕ_a terms. Following the main text all swarms contain $N = 100$ isotropic individuals and each point is an average of 3 simulations over 100,000 time-steps following a 25,000 time-step pre-equilibration period.

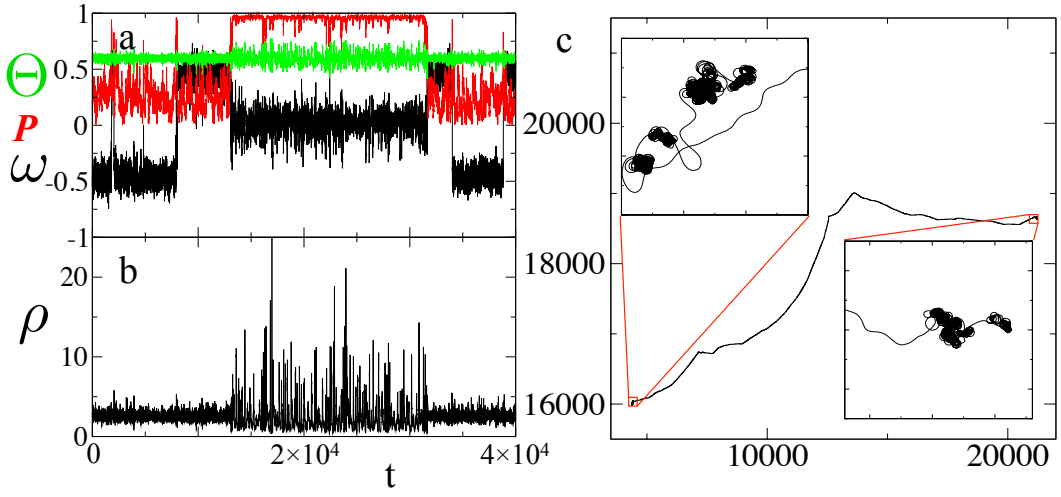

Figure 4.15: The behaviour of a swarm of $N = 100$, 10:1 anisotropic individuals with $\phi_p = 0.4$, $\phi_a = 0.525$. Shown is (a) The time variation of the opacity Θ (green), order P (red) and vorticity ω (black) against simulation time. (b) The time variation of the density ρ, measured in dimensionless units of the inverse squared length of each individual, over the same period. (c) The trajectory of the centre-of-mass of the swarm over a much longer period; inset we zoom in on the apparent kinks in the trajectory, revealing repeated switching between circulating and translating phases, somewhat reminiscent of the run-and-tumble motion of bacteria[125].

4.6.3 Effects of blind angle towards rear of each individual are modest

Birds and other flocking animals do not have fully isotropic vision, e.g. birds cannot see what is directly behind them. In order to study how this might affect the behaviour of the model and the emergence of marginal opacity we introduce a blind angle (γ) behind each individual, outlined in Fig. 4.16. We first define 'behind' as the opposite direction to the velocity (hence $(arg(\underline{v}_i) + \pi)$ for individual i). Any boundary falling within the angular region $(arg(\underline{v}_i) + \pi) \pm \gamma/2$ (shaded in blue on Fig. 4.16) will not contribute to the projection term. For comparison it is worth noting that starlings have a very wide field of vision, with a blind region to the rear that is only 32° ($\approx \pi/6$ rad).

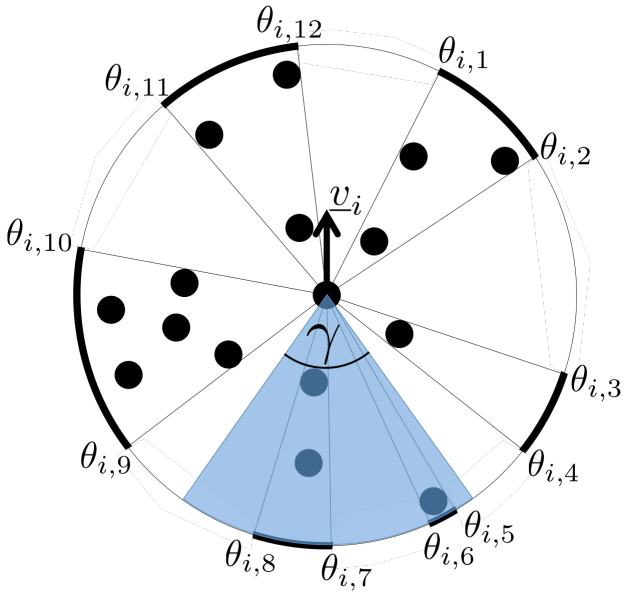

Figure 4.16: Diagram detailing the how the bind angle (γ) corresponds to the angular region directly behind an individual (here i with velocity $\underline{v}_i$) over which the boundaries do not contribute to the projection term (shaded area). In this example the projection term given by Eq. 1(main text) would not include $\theta_{i,5-8}$

.

For values of $\gamma < 4\pi/5$, well in excess of what is realistic (starlings have blind angle of only 32°), marginal opacity emerges robustly and flock cohesion is unaffected. This is shown by the values for opacity (θ) and swarm size ($R_{\max}$)

in Fig. 4.17a,b, where the standard deviations in these values can be seen to be relatively small. There is also very qualitative effect observed on the phenotypes previously described for anisotropic individuals, see supplementary movies 4.6-4.8. As γ becomes unphysically large ($\gamma > 4\pi/5$) the swarm opacity and density are more substantially affected. While the flock now remains strictly cohesive it becomes possible for (groups of) individuals to transiently move directly away from the bulk of the swarm only rejoining it when they have rotated sufficiently to detect it again. This rotation can be slow if there are a substantial number of individuals in any such breakaway group. When this is the case, the maximum separation between two individuals in the swarm becomes a poor measure of the local density, as it is sensitive to outliers that have transiently lost contact with the remainder of the swarm, hence we also show the variation of the average nearest neighbour distance R_{min} in Fig. 4.17c.

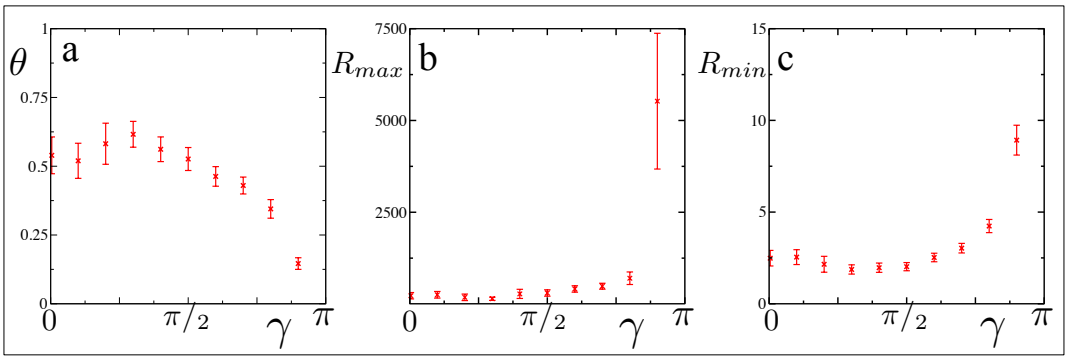

Figure 4.17: (a) Opacity (θ), (b) swarm size ($R_{\max}$) and (c) average nearest neighbour distance (R_{min}) for swarms of $N = 100$ individuals with varying blind angles (γ) within which individuals do not contribute to the projection term in Eq [3](main text). The model parameters are $\phi_a = 0.8$ and $\phi_p = 0.03$, to match those used in Fig. 2b(main text). Results show the mean and standard deviation over 50,000 time steps following a 6000 time step equilibration period.

In fact it is probably more physically realistic that the bird ignores *all* sensory input coming from within the blind angle, i.e. excluding also the co-alignment term. In this case we obtain slightly more dense flocks that are able to remain cohesive and marginally opaque for a greater range of γ, see Fig. 4.18.

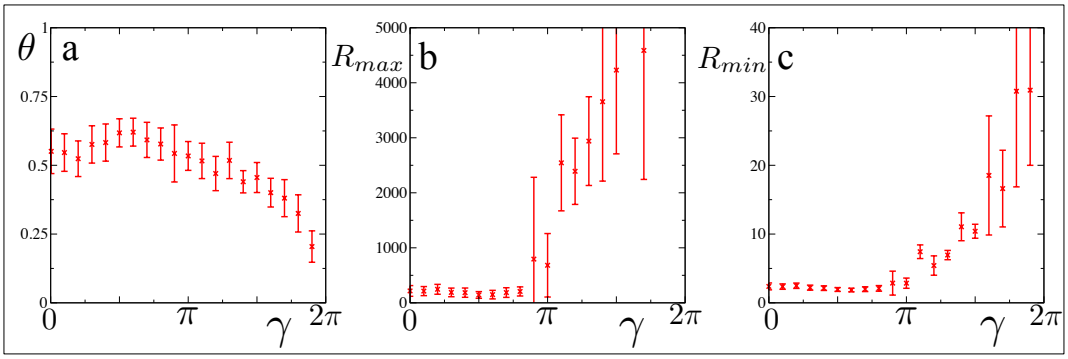

Figure 4.18: (a) Opacity (θ), (b) swarm size ($R_{\max}$) and (c) average nearest neighbour distance (R_{min}) for swarms of $N = 100$ individuals with varying blind angles (γ) within which contributions to *both* the projection term and co-alignment term are ignored. The model parameters are $\phi_a = 0.8$ and $\phi_p = 0.03$, to match those used in Fig. 2b(main text). Results show the mean and standard deviation over 50,000 time steps following a 6000 time step equilibration period.

4.7 Summary

In this chapter we have proposed a minimal swarming model using similar primary inputs to those available to a starling. The proposed hybrid projection model is capable of reproducing primary features of large flocks of starlings, cohesion and ordering. In order to achieve this we employ the projection, essentially line of sight through the swarm. If a bird at any distance were to move into one of the uninterrupted lines of sight, it would immediately become visible. Hence there is no limit to the range of interaction. Therefore interactions relating to the projection are global in scope, provided that a line of sight from any individual has an intermediate probability of reaching the edges of the swam. This is a state we call marginally opaque. This marginal opacity is an emergent feature of the hybrid projection model, by simply employing the update rules outlined above, the intermediate opacity (a bulk property of the swarm) follows. The global nature of the interaction also creates swarms more robust to perturbation such that it is impossible to fracture the swarm making them more resilient to the effects of predation. The hybrid projection model also makes a testable prediction, that flocks should also be marginally opaque from the point of view of a distant observer.

Chapter 5

Marginal opacity observed in starling murmurations

Much of the work in this chapter is published in the article 'Role of projection in the control of bird flocks' by Pearce et al.[122].

The hybrid projection model introduced in the previous chapter adequately reproduces the primary features of a starling murmuration, namely cohesion and order. It also makes an interesting prediction, that a flock will assume the maximum density at which it is still possible for an individual near the centre to see the sky in many directions. If the density and size of a flock were sufficiently high, it would be completely opaque to any individuals near the centre. This would make the visual identification of individual birds significantly more difficult, especially since birds are known to have poor contrast sensitivity relative to mammals[116;126;127]. This could prove unfavourable for the organisation of individuals which, as we have postulated, is based on visual and line of sight type interactions.

So now we come to the final question addressed in the thesis, are bird flocks ever opaque? This would be the simplest way to disprove the central prediction of the last chapter, to find an opaque bird flock.

Datasets for the 3D positions of birds in a flock, such as reported in[30;70], have given us many new insights but there are well known issues associated with particle tracking techniques in high density flocks. This makes using these techniques to obtain unbiased measurements of opacity itself problematic. Instead we chose to study data for 2D projections, this being best suited to test our prediction of projected opacity. This is the most suitable type of data for this analysis since it

is exactly the same as that which a bird in the wild has access to, essentially a 2D projection of its surroundings upon its retina. This is consistent with the fact that during flight starlings have very limited binocular vision, therefore most of their visual information is in the form of a 2D projection[79;80;77].

5.1 Measuring opacity for bird flocks in the wild

In the previous chapter we introduced the concept of opacity Θ as the percentage of an individuals view that was taken up by other individuals, and the closely related quantity Θ', the percentage of a distant external observer's view that is taken up by individuals within a flock.

In order to estimate Θ' from images we don't attempt direct identification of individual birds. Instead each image was converted to an 8-bit greyscale and connected regions of the flock were outlined by eye so as to exclude obvious foreground objects that were not birds (if any) and regions of empty sky outside the flock (if any), see Fig. 5.1. For images that include more than one connected flock region the opacity was computed as the average of the distinct regions of the flock, weighted by their relative size in pixels. All pixels, with greyscale level g_i, $i \in [1, n]$ within the outline were considered to be within the flock. The greyscale distribution was analysed to yield the average $\bar{g} = \frac{1}{n}\sum_{i=1}^{n} g_i$, maximum $g_{\max}$ and minimum $g_{\min}$ pixel greyscale levels (low numbers are darker). The opacity is then given by

$$\Theta' = \frac{g_{\max} - \bar{g}}{g_{\max} - g_{min}} = 1 - \frac{\bar{g} - g_{\min}}{g_{\max} - g_{min}} \tag{5.1}$$

This methodology is simple and has the advantage that it introduces no subjective bias into the image analysis. The error bars shown in Figs. 5.6a-c are computed by using the greyscale levels g_- and g_+, respectively the pixel levels at the $\epsilon/2$ and $(100 - \epsilon/2)$ percentile of the pixel greyscale distribution, where here we choose $\epsilon = 5\%$. This was then used to compute the corresponding upper (Θ'_+) and lower (Θ'_-) bounds for our estimate of the opacity

$$\Theta'_- = \frac{g_+ - \bar{g}}{g_+ - g_{min}} \qquad \Theta'_+ = \frac{g_{\max} - \bar{g}}{g_{\max} - g_-} \tag{5.2}$$

This can be motivated by the heuristic argument that the most extreme 5% of pixels would be a reasonable alternative definition of sky/bird, mitigating the effects of any outlying pixels.

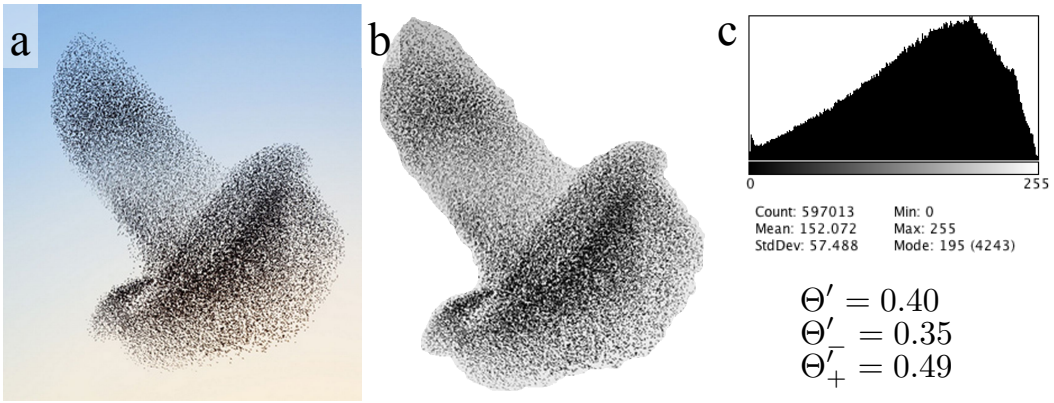

Figure 5.1: Example of how the opacity is measured for a sample picture (a). First the picture is converted to 8bit greyscale and the flock is outlined (b). The distribution of intensities of the pixels making up the flock is then analysed (c) and Eqs. 5.1 and 5.2 are used to obtain values for Θ', Θ'_{-} and Θ'_{+}. All image analysis was performed using imageJ[128].

5.1.1 Camera calibration

We calibrated our camera, and method of image analysis, by creating images of black disks randomly arranged on a white background with a known ratio of black to white pixels, see Fig. 5.2a. This binary image is analogous to our images of birds against sky. These were then printed out and photographed using the HDC-SD600 camera to establish how accurately the camera is measuring the average greyscale, here the fraction of black pixels (bird) in the image, and hence the (flock) opacity. By adjusting the level of optical magnification, distance to the camera and size of the printouts it is possible to vary the size of the feature in the collected images to below the pixel resolution of the camera. In all cases our method is able to reproduce the opacity of the images rather accurately, see Fig. 5.2b. This is even true when the feature size is of the order of (or less than) the size of a pixel, as is often the case for the public domain images (Fig. 5.5) and our collected images (Fig. 5.4).

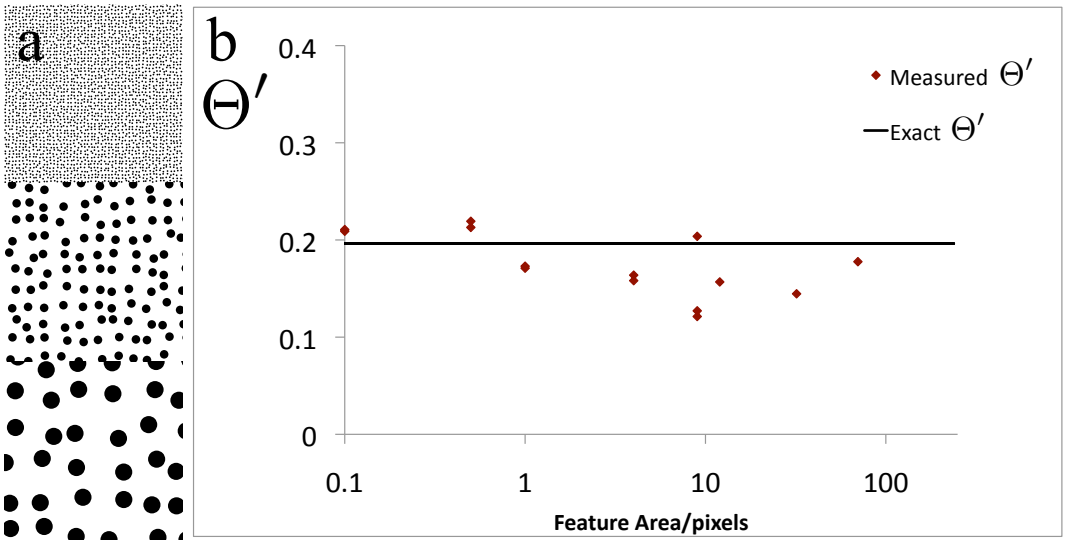

Figure 5.2: (a) Images with a known black to white ratio of pixels, and hence opacity, were created by randomly arranging black discs on a white background. These were created for a range of disc sizes. (b) The camera was used to estimate the opacity of the images by collecting images and using Eq (5.1). The exact value of the opacity is shown as the solid black line.

5.1.2 Image Calibration

The images used in Fig. 5.6b were collected from the public domain and had all been compressed using the jpeg compression algorithm. In order to assess the effect of this compression on the pixel distribution of the images, and therefore measured opacity (Θ'), we processed some of our images with the jpeg compression algorithm. We analysed the average greyscale of an entire image before and after various levels of compression. We find that the measured average greyscale is largely unaffected by compression, see Fig. 5.3c. This is true even when the images are compressed to well below the size (and quality) of any of the images in the public domain set. The analysis of the pixel distribution was performed on the entire image since the high levels of compression can introduce visual artefacts and therefore make the edges of the flock harder to discern; it is worth noting that none of the collected data had this issue as it was not compressed to the same degree.

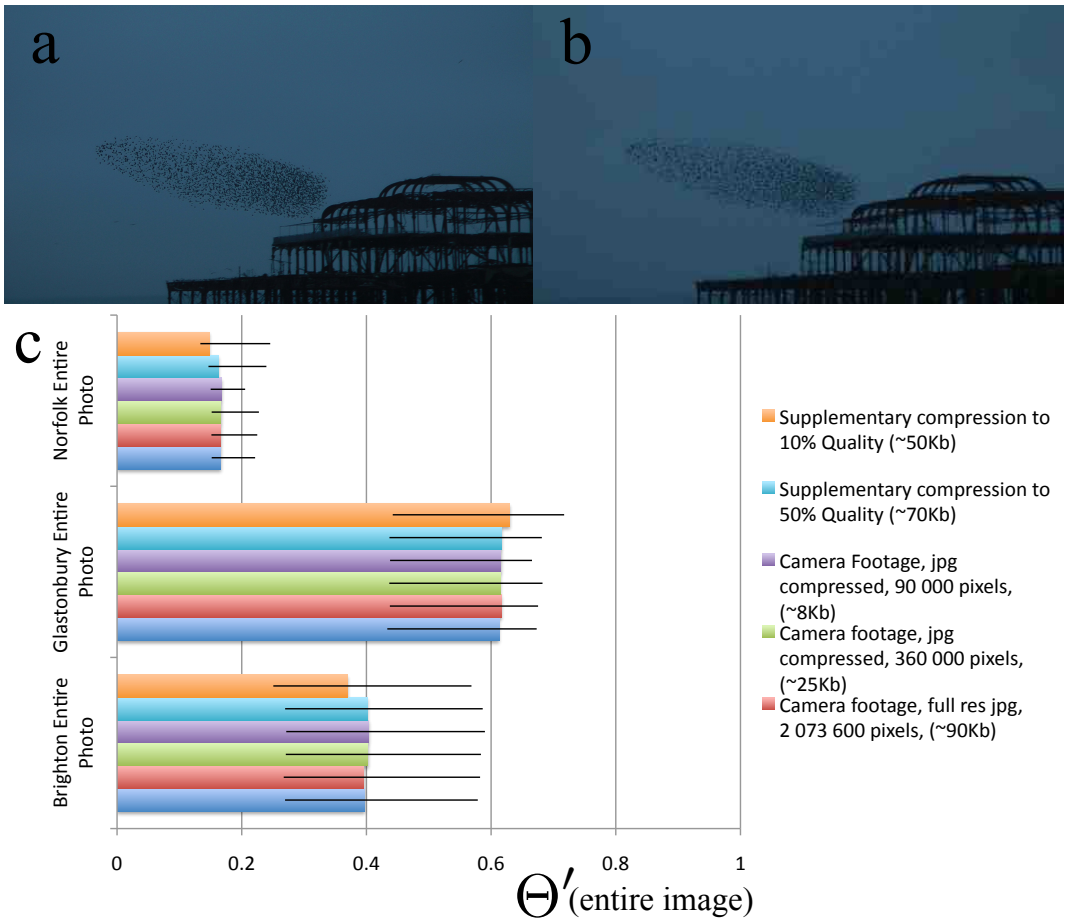

Figure 5.3: Example of an image before (a) and after (b) significant compression in jpeg format. (c) The differences in the calculated opacity (of the entire image) after various levels of jpeg compression and size reduction. The error bars are calculated using Eq (5.2).

5.2 Image collection

5.2.1 Collected data from the UK

Data from the UK was collected at various dates during Autumn 2011, these were:

Strumpshaw, Norfolk, UK. GPS coordinates 52.35515, 1.28122. Date 24/09/2011 Time 17:56 (sunset -66 min).

Glastonbury, Somerset, UK. GPS coordinates 51.157052, -2.73676. Date 05/10/2011 Time 16:48 (sunset -110 min).

Brighton, East Sussex, UK. GPS coordinates 50.816544, -0.136691. Date 10/10/2011 Time 18:10 (sunset -15 min).

Brighton, East Sussex, UK. GPS coordinates 50.816544, -0.136691. Date 14/11/2011 Time 15:40 (sunset -7 min).

Brighton, East Sussex, UK. GPS coordinates 50.816544, -0.136691. Date 14/11/2011 Time 16:10 (sunset -37 min).

A Panasonic HDC-SD600 camera was used to collect 1920 $\times$ 1080 video at 50 progressive frames per second. Frames from the video were analysed as individual images. The video sequences were discarded if they had any obvious obscuring of the flock, not all of the flock was visible, or the background was insufficiently monotone. Examples of collected footage is shown in Fig. 5.4 and supplementary movies 5.1,5.2.

5.2.2 Public domain images

Images selected for analysis in Fig. 5.6b were *all those* returned on the first two pages of a Google image search for the phrase "starling flock" performed on July 27 2011. Images were discarded only if they didn't show a starling flock, had obviously been doctored in some manner, or were composite images. The image number shown on the horizontal axis of Fig. 5.6b corresponds to the ordered number in which that image was returned in the search. The first six of these images are fairly representative and are shown in Fig. 5.5. We believe that the lack of any subjective bias in the selection of these images of flocks, of various sizes under different light conditions, represents a fairly rigorous test of our hypothesis that these flocks adopt a state of marginal opacity, see Fig. 5.6b.

Figure 5.4: Snapshot of the videos that contributed to the histogram in Fig. 5.6a and the light and dark time series Fig. 5.6c.

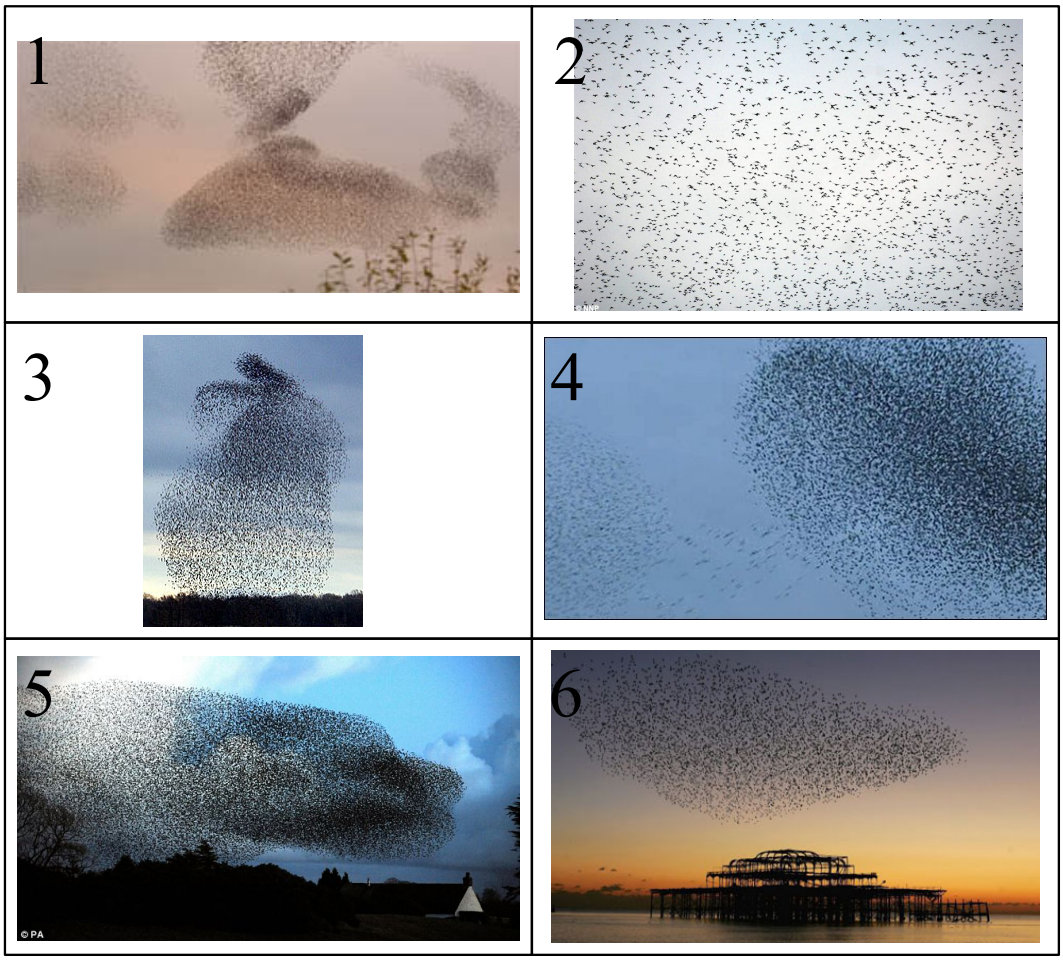

Figure 5.5: The public domain images used to construct the corresponding first six the data points in Fig. 5.6b. These flocks were all found to be marginally opaque.

5.3 Marginal opacity is observed in starling flocks in the wild

Fig. 5.6 shows that all flocks of starlings we observed had an intermediate value of opacity, with an average opacity of $30 \pm 6\%$. This does feature some lower values due to the fact that some of the bird flocks were particularly small (of the order of 10^2 starlings. Fig. 5.6b shows the opacity of the images returned from a public image search, again supporting the marginal opacity hypothesis with an opacity of $41 \pm 1\%$. Fig. 5.6c shows that the opacity of a bird flock is roughly constant over a significant period of time involving the flock changing direction multiple times. It also shows that the opacity of the flock does not change with different light levels, with the two traces being taken $\sim$30 min apart very close to sunset, hence at very different light levels. This supports the hypothesis that the opacity of a bird flock is a robust quantity that remains largely unchanged. The crucial feature in both Fig. 5.6a (our data) and Fig. 5.6b (public domain images) is that the opacity is intermediate, i.e. neither very close to zero nor unity, in spite of the fact that the flocks had very different sizes and were observed under different conditions (the flocks we analysed in Fig. 5.6a are generally smaller than in Fig. 5.6b). This is a feature that, to our knowledge, is not found in any existing models but emerges naturally from our hybrid projection model.

5.4 Opacity is linked to signalling in large starling flocks

The flocks observed in Brighton all made the old burnt pier their home, this meant that it was often also in the background of much of the footage as they constantly fly near to their roosting site, see Fig. 5.4. This meant we had a large, stationary object with which we could triangulate the angular position of the flock relative to the observer.

We first define the centre of mass of the flock within an image as the average position of a pixel making up the flock weighted with each pixels (inverse) intensity; this gives us a coordinate of the flock within the image. Using at least two (here three) easily identified points on the pier we can define an origin and scale to relate this position to, see Fig. 5.7a. This is used to obtain an angular position of the flock. Movement parallel to the line of sight was ignored for two reasons. First, it is also parallel to the direction over which we calculate Θ' and we don't observe as much of an effect. Secondly, the flock is always significantly closer to the pier than it is

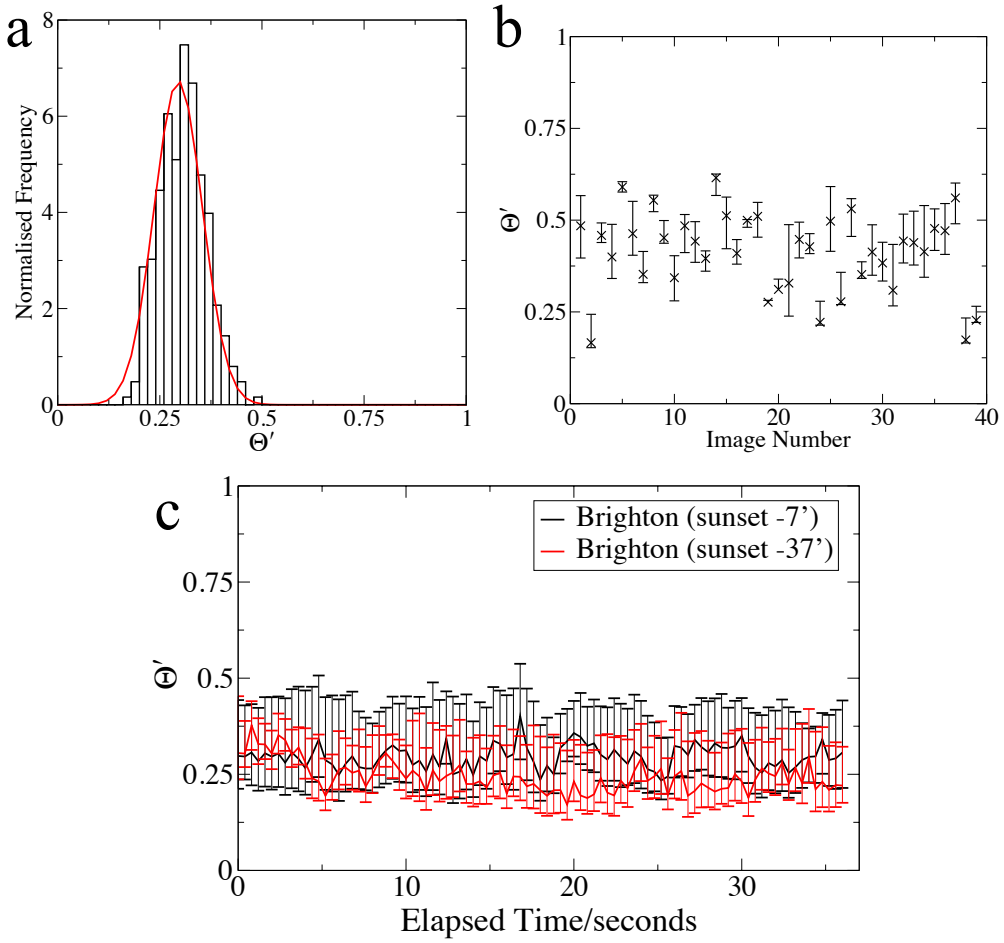

Figure 5.6: (a) Histogram of the opacity Θ' of different Starling flocks from across the UK corresponding to $n = 118$ uncorrelated measurements. The red line displays a gaussian distribution fitted to this data with $\mu = 0.30, \sigma^2 = 0.059$. The null hypothesis that the opacities are drawn from a uniform distribution on [X,1] can be rejected at the 99.99% confidence level for all values of X. These flocks are all *marginally opaque*. (b) The opacity Θ' of images of starling flocks in the public domain ($\mu = 0.41, \sigma^2 = 0.012$). The null hypothesis that the opacities are drawn from a uniform distribution on [X,1] can be rejected at the 99.99% confidence level for all values of X. These flocks are all marginally opaque. (c) Typical time variation of the opacity Θ' of starling flocks observed in dim light (black) and under brighter conditions (red). The fluctuations correspond to moments of rapid acceleration of the flock, see Fig. 5.7b.

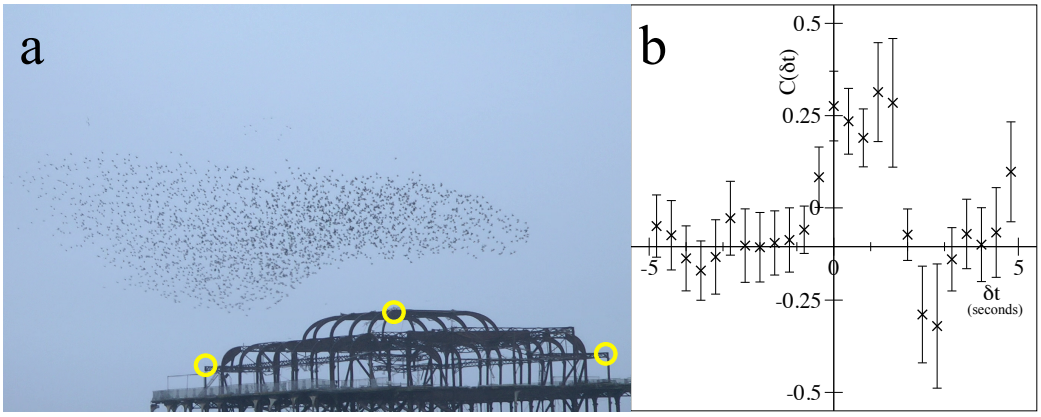

Figure 5.7: (a) Using fixed points on the pier in the images, the relative angular position of the centre of mass of the flock was established. (b) Cross-correlation function of the horizontal acceleration a of the centre of mass of the flock and its opacity $C_{a\Theta'}(\delta t)$ as a function of the delay in seconds (δt).

to the observer, therefore changes in the distance to the flock are hard to quantify whereas angular changes are far easier to analyse.

Fig. 5.7b shows that opacity changes significantly within a few seconds of rapid acceleration and could therefore be implicated in long-ranged information exchange across the flock. Essentially when the flock initiates a turn, the opacity of the flock swiftly increases making the leading edge of the flock suddenly appear far denser to a bird at the rear, this could then be a significant signal to birds that the flock is going into a turn. This has the added of advantage of essentially travelling at the speed of light, rather than the diffusive information transfer of local alignment interactions between nearest neighbours.

5.5 Summary

In this chapter we have presented evidence that supports the hypothesis that bird flocks self organise to a density that still allows individuals in the centre of the flock to see the sky in many directions, a state we refer to as marginally opaque. This is a prediction made in the previous chapter by examining the hybrid projection model. When we compare the hybrid projection model to observations made on starling murmurations in the wild it is clear that the model predicts a higher opacity, $\theta'_{\text{lim}} \approx 0.78$ and $\theta' \approx 0.3$ for the model and bird flocks, respectively. This discrepancy

can be attributed to the fact that the model is not a complete recreation of all aspects of a bird flock, for example many of the parameters are set arbitrarily to unity, the simulations are in two dimensions, and the model does not include terms to account for other factors such as variation amongst individuals, fatigue, gravity, etc. These kind of factors could be introduced to the model so as to more realistically recreate the exact qualities of a flock of birds in the wild, but with the underlying structure of the hybrid projection model remaining unchanged we would still expect marginal opacity to emerge.

The emergence of an opacity that is neither very close to 0 or 1 is a far more significant, and difficult, quality of a bird flock, or model, than one might first assume. It is insightful to consider the following simple mean field argument for the consequences of marginal opacity: Consider a randomly chosen line of sight through, or out from a typical location near the centre of, an idealised homogenous, isotropic flock. Because the probability that any small region is occupied is proportional to its volume multiplied by the density of individuals, the probability that a line of sight reveals "sky" is Poisson distributed according to $P_{sky} \approx e^{-\rho b^{d-1} R}$ with $\rho = N/R^d$ a d-dimensional density, b the effective linear size of an individual and R the linear size of the flock. Our hypothesis of marginal opacity corresponds to P_{sky} being of order unity (a half, say) leading to $\rho \sim N^{-1/(d-1)}$, i.e. $\rho \sim N^{-1}$ in 2D and $\rho \sim N^{-1/2}$ in 3D. Marginal opacity therefore either requires the density to be a decreasing function of N or for the flock morphology to change (or both). There are hints of both of these qualities in some published data[30;70] not inconsistent with the predictions of our model.

Our mean field analysis can also be used to understand why the emergence of marginal opacity is quite such a surprising result. It follows that most spatial arrangements of N finite sized particles are either opaque ($\Theta \approx 1$) or predominantly transparent ($\Theta \ll 1$). The latter obviously occurs whenever the density is very low (and in an essentially infinite space there is plenty of room to achieve this) while the former arises even for a relatively small reduction in the separation between individuals from that found in the marginal state. This is due to the extremely strong dependence of P_{sky} on the flock size R (in 3D it varies *exponentially* with the *square* of R). To illustrate this we consider the effect of a reduction by half of the spacing between individuals, and hence also R. Using $P_{sky} \approx e^{-N(b/R)^2}$ in 3D we find that this leads to a change in opacity from (say) 50% before to 94% afterwards. Thus, the flock becomes almost completely opaque as a consequence of only a halving of the inter-bird spacing. Similar arguments apply if N increases at constant R and

such variations in both density and size are reported in the literature (e.g.[70], table 1), supporting the claim that the marginal opacity apparent in Figs. 5.6a-c is a robust emergent feature.

Chapter 6

Conclusions

Over the course of this study we have highlighted the difficulty in constructing models for collective animal motion. As experiments have shown, it is particularly difficult to directly probe the nature of the interactions between individual animals. There is also a large amount of unconstrained structural freedom in the construction of models that appear to recreate swarming behaviour. Indeed it is relatively easy to hypothesise a set of interaction rules for an individual agent to follow that would result in collective behaviour qualitatively similar to that seen in large animal aggregates. This is compounded by the fact that so many areas of the animal kingdom perform this type of behaviour, with each species having its own unique set of abilities and limitations. Not to mention the diverse environments these animals inhabit that can be of different dimensionality, media and involve varied methods of motility. In short, it may be unrealistic to construct a model for how animals interact in large groups that is correct for all swarming species. Although similarities can be drawn between different species, a complete model must be tailored to the species of interest. This lead us to focus primarily on models recovering a few key defining features of animal aggregates: polarisation, cohesion and rapid information transfer. We have also limited ourselves to comparison with a limited number of species, primarily starling flocks.

We first addressed the degeneracy in models by introducing a new method to distinguish between very similar candidate models. By confining the swarms to periodic channels and allowing adjacent channels to interact we are able to frustrate the system, much like the frustration observed between spins on a geometrically frustrated antiferromagnet. When different swarms are frustrated in this manner we observe distinct behaviour depending on the nature of the underlying model.

This highlights a new transition for metric based swarming models in this geometry. The swarms can either have a permanently locked direction of polarisation or a rapidly switching polarisation for intermediate or high interaction range, respectively (for a sufficiently low interaction range no net polarisation is observed). This new transition, or the rapidly switching polarised state, is not observed in the metric free model. We also saw the emergence of different behavioural traits. Metric swarms are more prone to clumping into high density bands that can either avoid each other by occupying different areas of the channel which we denoted "trains", or meet each other and regularly reverse polarisation, which we denoted "shuttles". Both metric and metric free models can form well dispersed swarms with long persistence times. By taking advantage of the binary like nature of the polarisation (clockwise or anticlockwise) and the linkage observed between swarms in adjacent channels it is possible to mimic the responses of a logic gate. We have shown that a universal NOR gate can be created, hence it is possible to create a Turing machine.

Next we addressed the issue of cohesion in swarms, the second of our identified primary features. Following observations on starling murmurations it has been concluded that the interactions governing the swarm should be metric free. Highly polarised swarms are possible using metric free interactions, but controlling the density is not as simple. By starting from the topological Vicsek model, which uses co-alignment between agents connected in a delaunay triangulation, we introduced a metric free inward motional bias to the agents that were identified as being on the edge of the swarm. The resultant model is able to reproduce highly polarised swarms with a well defined density in a completely scale free manner. Appealingly it only features two free control parameters, the relative weightings of the inward motional bias and the noise. This model gives a power law relationship between the radius of a swarm and the number of individuals within it that can be explored by a direct analogy with an ideal gas. This model also gives good agreement with the correlation length scales observed in flocks of starlings. It is the first completely scale free model with cohesion, wherein there is no associated length scale, and all behaviour is completely independent of the (arbitrary) length scale used in simulations.

We next adapted our swarming model to more accurately recreate the information available to (and capabilities of) a starling, which are primarily visual. By modelling the individuals' eye view of the rest of the flock we are able to replace the metric free inward motional bias with the projection term. This takes as its input the silhouette of the rest of the swarm from the point of view of an individual and gives a direction toward the area containing the most information, i.e. the most

boundaries between light and dark. This model reproduces the primary features of a flock of starlings, polarisation and cohesion, but also gives rise to the complex morphologies observed in starling flocks. The global nature of the projection term makes the hybrid projection model more robust to perturbation, indeed it is impossible for the swarm to become fragmented or the flow of information through the swarm to be severed. By comparison to a standard metric model, we confirmed that these features are exclusive to the hybrid projection model. A naturally emergent feature of the hybrid projection model is that swarms target the density at which the projection of the swarm presents a complex pattern rich in information, hence containing many light and dark areas. Therefore the hybrid projection model also makes a testable prediction: bird flocks should be marginally opaque, i.e. a bird is able to see areas of sky and bird within its view at all times. The emergence of an intermediate opacity appears to be independent of the size of the swarm. This is achieved by a density that scales with the size and implies that the swarm would not become opaque even as the swarms become infinitely large.

The prediction of marginal opacity can be extended to an observable quantity. It follows that if a bird can always see a mix of bird and sky from its position within a murmuration, then an external observer should always be able to see a similar mix. We confirmed this by capturing video of starling flocks from around the UK and calculating their opacity (from the point of view of an external observer), which was always observed to have an intermediate value. Though not immediately apparent, this constrains the density and morphology of the flock to a considerable degree. The variation in the number of birds within a starling murmuration can vary by 3 orders of magnitude, for the opacity to remain constant the murmuration would have to adjust its density and morphology significantly.

The hybrid projection model, and the prediction of marginal opacity, represent a significant change in the way we think about swarming animals. The idea of using an analogue of the visual stimulus available to an individual is the key insight of the model, and is central to why it reproduces marginally opaque swarms. We believe that marginal opacity is a fundamental feature of many swarming animals, and must be taken into account when judging models for this behaviour. We also believe that opacity may be related to fitness in flocking animals. The marginally opaque state has the highest density (offering protection) that is consistent with an individual being able to see out directly and also to monitor the behaviour of most others across the flock, in case they first observe an approaching predator. Thus projection-based models that give rise to such states would seem evolutionarily fit.

It would also appear to be cognitively plausible, indeed birds eyes are particularly well adapted to the task of edge detection, which is the key process required by the projection term in the model. Since hybrid projection model uses the boundary between two distinct areas ("bird" and "sky") within the vision of an individual, it is not effected by their relative colour or brightness. As long as the two areas are distinct, and identifiable as such by an individual, it should be able to perform the necessary actions to form a flock. For a bird this would imply that there must be a sufficient contrast between areas of bird and sky for a murmuration to be possible. Birds are known to have poor contrast awareness, this could explain the fact that while large murmurations form at dusk, they cease before dark. Perhaps when the sky becomes dark, the contrast between sky and bird eventually becomes sufficiently small that it becomes impossible to form a murmuration. This would of course depend on the specific capabilities of the animal in question, for example bats often swarm at night and have significantly different vision and echolocation capabilities than birds.

Modern humans also need to rapidly extract useful information from high dimensional datasets. A generic approach to this is to present information through lower dimensional projections. This is reminiscent of the approach that we are proposing has been adopted by flocking animals. Here a $6N$-dimensional phase space (or $4N$ for 2D), consisting of the spatial coordinates and velocities of all N members of the flock, is projected onto a simple pattern on a surface (or line for 2D). Perhaps the use of such simplifying projections is more widespread in nature than previously suspected?

The interactions and motions of swarming animals are so complex that we can only claim to have a rudimentary understanding. Due to this there is a multitude of ways this current work could be expanded upon. There are obvious extensions to more accurately represent the reality of birds forming swarms in the real world such as flight physics, gravity, three dimensions, fatigue, etc. Many previous models have attempted this, using the hybrid projection model as a foundation it may be possible to recreate an even more realistic recreation of swarming animals. These additions may well improve final recreation of a swarm, but do not necessary improve our understanding of how animals form swarms.

On a more fundamental level, it might be possible to change the way in which an individual uses the information in the projection to derive its velocity. The proposed hybrid projection model is one of the simplest ways to form a direction from the projection, it is not unlikely that a swarming animal actually uses a more

complex algorithm to determine its velocity. One example would be for the individual to move toward the region of the projection with the highest entropy, which would be represented by the most complex part of the projection. This would be similar to being attracted to the region of the projection that contains the most information. Another possible extension would be to include dynamic terms. Currently only the projection at the current time step is considered, but including terms that react to how the projection changes over time could be included. This has a particular interest when a swarm reacts to predators, where the rapid changes of the flock might be indicative of an attack.

There are also methods by which you could further compare simulated swarms to groups of animals, for example how they react to perturbations. In the thesis we observed how robust the swarm is to artificial predators and expansive shocks, this could easily be expanded to examine more complex attack patterns of multiple predators. It would also be possible to explore this area further by performing a more rigorous examination of how the response corresponds to a quantifiable perturbation. By applying statistical mechanics techniques from fluctuation dissipation theory it would be possible to compare the response of the swarm to small perturbations and infer possible analogues of statistical mechanics quantities such as temperature.

Bibliography

[1] S. J. Portugal, T. Y. Hubel, J. Fritz, S. Heese, D. Trobe, B. Voelkl, S. Hailes, A. M. Wilson, and J. R. Usherwood, Nature **505**, 399 (2014).

[2] J. D. Shepherd, Behavioral Ecology and Sociobiology **11**, 77 (1982).

[3] *Wikimedia commons*, `http://commons.wikimedia.org/wiki/Main_Page`.

[4] G. White, *The Natural History and Antiquities of Selborne* (Benjamin White, 1789).

[5] I. Vine, Journal of Theoretical Biology **30**, 405 (1971).

[6] R. C. Miller, Ecology **3**, 122 (1922).

[7] J. Krause and G. D. Ruxton, *Living in groups* (OUP Oxford, 2002).

[8] U. d. V. Pienaar, Koedoe **12**, 108 (1969).

[9] C. D. Fitzgibbon, Animal Behaviour **39**, 1116 (1990).

[10] W. D. Hamilton, Journal of theoretical Biology **31**, 295 (1971).

[11] L. J. Morrell, G. D. Ruxton, and R. James, Behavioral Ecology **22**, 16 (2011).

[12] A. J. King, A. M. Wilson, S. D. Wilshin, J. Lowe, H. Haddadi, S. Hailes, and A. J. Morton, Current Biology **22**, R561 (2012).

[13] W. Foster and J. Treherne, Nature **293**, 466 (1981).

[14] J. K. Parrish, Animal Behaviour **38**, 1048 (1989).

[15] A. King and D. Sumpter, Curr. Biol. **22**, 112 (2012).

[16] D. C. Krakauer, Behavioral Ecology and Sociobiology **36**, 421 (1995).

[17] M. Milinski, Animal Behaviour **32**, 1157 (1984).

[18] C. Schradin, Ethology **106**, 691 (2000).

[19] S. D. Gillett, P. J. Hogarth, and F. Jane Noble, Animal Behaviour **27**, 592 (1979).

[20] S. Neill and J. Cullen, Journal of Zoology **172**, 549 (1974).

[21] L. Landeau and J. Terborgh, Animal Behaviour **34**, 1372 (1986).

[22] H. R. Pulliam, Journal of theoretical Biology **38**, 419 (1973).

[23] L. Conradt, Nature **471**, 40 (2011).

[24] A. J. Ward, J. E. Herbert-Read, D. J. Sumpter, and J. Krause, Proceedings of the National Academy of Sciences **108**, 2312 (2011).

[25] S. Goss, S. Aron, J.-L. Deneubourg, and J. M. Pasteels, Naturwissenschaften **76**, 579 (1989).

[26] T. Pitcher and A. Magurran, Animal Behaviour **31**, 546 (1983).

[27] D. Grünbaum, Evolutionary Ecology **12**, 503 (1998).

[28] I. D. Couzin, C. C. Ioannou, G. Demirel, T. Gross, C. J. Torney, A. Hartnett, L. Conradt, S. A. Levin, and N. E. Leonard, Science **334**, 1578 (2011).

[29] S. Camazine, *Self-organization in biological systems* (Princeton University Press, 2003).

[30] A. Cavagna, A. Cimarelli, I. Giardina, G. Parisi, R. Santagati, F. Stefanini, and M. Viale, Proc. of Nat. Acad. Sci. **107**, 11865 (2010).

[31] W. Cresswell, Animal Behaviour **47**, 433 (1994).

[32] T. C. Roth II, S. L. Lima, and W. E. Vetter, Behavioral Ecology and Sociobiology **60**, 195 (2006).

[33] T. D. Seeley, American Scientist **77**, 546 (1989).

[34] A. J. King and G. Cowlishaw, Communicative & Integrative Biology **2**, 147 (2009).

[35] T. Vicsek and A. Zafeiris, Physics Reports **517**, 71 (2012).

[36] I. Giardina, H.F.S.P. Journal **2**, 205 (2008).

[37] *Food and agriculture organisation of the united nations*, `http://www.fao.org/`.

[38] P. Ceccato, K. Cressman, A. Giannini, and S. Trzaska, International Journal of Pest Management **53**, 7 (2007).

[39] A. D. Chapman, Department of the Environment, Water, Heritage and the Arts, Canberra (2009).

[40] B. Hölldobler and E. O. Wilson, *The superorganism: the beauty, elegance, and strangeness of insect societies* (WW Norton & Company, 2009).

[41] R. Baker, The Journal of Animal Ecology pp. 703–746 (1969).

[42] J. Buhl, D. Sumpter, I. Couzin, J. Hale, E. Despland, E. Miller, and S. Simpson, Science **312**, 1402 (2006).

[43] W. H. Gotwald Jr et al., *Army ants: the biology of social predation.* (Cornell University Press, 1995).

[44] S. Bazazi, J. Buhl, J. J. Hale, M. L. Anstey, G. A. Sword, S. J. Simpson, and I. D. Couzin, Current Biology **18**, 735 (2008).

[45] S. Bazazi, C. C. Ioannou, S. J. Simpson, G. A. Sword, C. J. Torney, P. D. Lorch, and I. D. Couzin, PloS one **5**, e15118 (2010).

[46] V. Guttal, P. Romanczuk, S. J. Simpson, G. A. Sword, and I. D. Couzin, Ecology Letters **15**, 1158 (2012).

[47] B. Uvarov, Population Dynamics (Cambridge Univ. Press, Cambridge, 1977) (1977).

[48] T. Vicsek, A. Czirók, E. Ben-Jacob, I. Cohen, and O. Shochet, Phys. Rev. Lett. **75**, 1226 (1995).

[49] E. Shaw, American Scientist pp. 166–175 (1978).

[50] G. C. Williams, Publ. Mus. Mich. State Univ. Biol. Ser **2**, 349 (1964).

[51] D. Weihs, in *Swimming and flying in nature* (Springer, 1975), pp. 703–718.

[52] B. Partridge, T. Pitcher, J. Cullen, and J. Wilson, Behav. Ecol. Sociobiol. **6**, 277 (1980).

[53] B. Partridge, J. Johansson, and J. Kalish, Environ. Biol. of Fishes **9**, 253 (1983).

[54] T. Pitcher and B. Partridge, Marine Biology **54**, 383 (1979).

[55] O. A. Misund, A. Aglen, and E. Frønæs, ICES Journal of Marine Science: Journal du Conseil **52**, 11 (1995).

[56] J. K. Parrish, S. V. Viscido, and D. Grünbaum, The biological bulletin **202**, 296 (2002).

[57] C. Becco, N. Vandewalle, J. Delcourt, and P. Poncin, Physica A: Statistical Mechanics and its Applications **367**, 487 (2006).

[58] N. Abaid and M. Porfiri, Journal of The Royal Society Interface **7**, 1441 (2010).

[59] Y. Katz, K. T. m, C. Ioannou, C. Huepe, and I. Couzin, Proc. of Nat. Acad. Sci. **108**, 18720 (2011).

[60] A. E. Magurran and A. Higham, Ethology **78**, 153 (1988).

[61] J. Krause, D. Hoare, S. Krause, C. Hemelrijk, and D. Rubenstein, Fish and Fisheries **1**, 82 (2000).

[62] A. J. Ward, D. J. Sumpter, I. D. Couzin, P. J. Hart, and J. Krause, Proceedings of the National Academy of Sciences **105**, 6948 (2008).

[63] L. Conradt and T. J. Roper, Nature **421**, 155 (2003).

[64] S. G. Reebs, Animal behaviour **59**, 403 (2000).

[65] P. F. Major and L. M. Dill, Behavioral Ecology and Sociobiology **4**, 111 (1978).

[66] R. Budgey and S. Hutton, International Bird Strike Committee (September)(IBSC24/WP 12) (1999).

[67] H. Pomeroy and F. Heppner, The Auk pp. 256–267 (1992).

[68] A. Cavagna, I. Giardina, A. Orlandi, G. Parisi, A. Procaccini, M. Viale, and V. Zdravkovic, Animal Behaviour **76**, 217 (2008).

[69] A. Cavagna, I. Giardina, A. Orlandi, G. Parisi, and A. Procaccini, Animal Behaviour **76**, 237 (2008).

[70] M. Ballerini, N. Cabibbo, R. Candelier, A. Cavagna, E. Cisbani, I. Giardina, A. Orlandi, G. Parisi, A. Procaccini, M. Viale, et al., Animal Behaviour **76**, 201 (2008).

[71] M. Ballerini, R. C. N. Cabibbo, A. Cavagna, E. Cisbani, I. Giardina, and V. Zdravkovic, Proc. of Nat. Acad. Sci. **105**, 1232 (2008).

[72] A. Cavagna, I. Giardina, and F. Ginelli, Phys. Rev. Lett. **110**, 168107 (2013).

[73] A. Attanasi, A. Cavagna, L. Del Castello, I. Giardina, T. S. Grigera, A. Jelić, S. Melillo, L. Parisi, O. Pohl, E. Shen, et al., Nature Physics **10**, 691 (2014).

[74] G. Dell'Ariccia, G. Dell'Omo, D. P. Wolfer, and H.-P. Lipp, Animal Behaviour **76**, 1165 (2008).

[75] R. Lukeman, Y. Li, and L. Edelstein-Keshet, Proc. of Nat. Acad. Sci. **107**, 12576 (2010).

[76] H. Zeigler and E. H.J. Bischof, *Beyond sensation: visual cognition in pigeons.* (M.I.T. Press, 1993).

[77] G. R. Martin, Journal of Comparative Physiology A **159**, 545 (1986).

[78] V. Tisdale and E. Fernández-Juricic, Behavioral Ecology **20**, 936 (2009).

[79] K. V. Fite and S. Rosenfield-Wessels, Brain, Behavior and Evolution **12**, 97 (1975).

[80] M. P. Jones, K. E. Pierce Jr, and D. Ward, Journal of Exotic Pet Medicine **16**, 69 (2007).

[81] C. W. Reynolds, ACM SIGGRAPH Computer Graphics **21**, 25 (1987).

[82] H. Hildenbrandt, C. Carere, and C. Hemelrijk, Behav. Ecol. **21**, 1349 (2010).

[83] C. Hemelrijk and H. Hildenbrandt, Interface Focus **2**, 726 (2012).

[84] K. Bhattacharya and T. Vicsek, N. J. Phys. **12**, 093019 (2010).

[85] M. Moussaïd, D. Helbing, and G. Theraulaz, Proc. of Nat. Acad. Sci. **108**, 6884 (2011).

[86] F. Ginelli and H. Chaté, Phys. Rev. Lett. **105**, 168103 (2010).

[87] M. Camperi, A. Cavagna, I. Giardina, G. Parisi, and E. Silvestri, Interface Focus **2**, 715 (2012).

[88] H. Kunz and C. K. Hemelrijk, Applied Animal Behaviour Science **138**, 142 (2012).

[89] A. Okabe, B. Boots, K. Sugihara, S. Chiu, and D. Kendall, *Spatial Interpolation, in Spatial Tessellations: Concepts and Applications of Voronoi Diagrams, 2nd Ed.* (John Wiley & Sons, Inc., 2008).

[90] I. Couzin, J. Krause, R. James, G. Ruxton, and N. Franks, J. Theor. Biol. **218**, 1 (2002).

[91] G. Grégoire, H. Chaté, and Y. Tu, Physica D **181**, 157 (2003).

[92] M. D'Orsogna, Y. Chuang, A. Bertozzi, and L. Chayes, Phys. Rev. Lett. **96**, 104302 (2006).

[93] C. K. Hemelrijk and H. Hildenbrandt, PloS ONE **6**, e22479 (2011).

[94] J. Schellinck and T. White, Ecol. Modell. **222**, 1897 (2011).

[95] J. Toner and Y. Tu, Phys. Rev. E. **58**, 4828 (1998).

[96] G. Grégoire and H. Chaté, Phys. Rev. Lett. **92**, 025702 (2004).

[97] H. Chaté, F. Ginelli, G. Grégoire, and F. Raynaud, Phys. Rev. E. **77**, 046113 (2008).

[98] G. Baglietto and E. V. Albano, Phys. Rev. E **78**, 021125 (2008).

[99] G. Baglietto, E. V. Albano, and J. Candia, Interface focus (2012).

[100] M. Nagy, I. Daruka, and T. Vicsek, Physica A: Statistical Mechanics and its Applications **373**, 445 (2007).

[101] H. Chaté, F. Ginelli, G. Grégoire, and F. Raynaud, Physical Review E **77**, 046113 (2008).

[102] G. Baglietto and E. V. Albano, Physical Review E **80**, 050103 (2009).

[103] J. Toner and Y. Tu, Phys. Rev. Lett. **75**, 4326 (1995).

[104] M. Aldana, V. Dossetti, C. Huepe, V. Kenkre, and H. Larralde, Phys. Rev. Lett. **98**, 095702 (2007).

[105] G. Baglietto, E. V. Albano, and J. Candia, International Journal of Modern Physics C **25** (2014).

[106] A. Ramirez, Annual Review of Materials Science **24**, 453 (1994).

[107] D. J. Pearce and M. S. Turner, arXiv preprint arXiv:1408.1593 (2014).

[108] D. Sumpter, J. Buhl, D. Biro, and I. Couzin, Theory in biosciences **127**, 177 (2008).

[109] Z. Li, M. A. Rosenbaum, A. Venkataraman, T. K. Tam, E. Katz, and L. T. Angenent, Chemical Communications **47**, 3060 (2011).

[110] Y.-P. Gunji, Y. Nishiyama, A. Adamatzky, T. E. Simos, G. Psihoyios, C. Tsitouras, and Z. Anastassi, Complex Systems **20**, 93 (2011).

[111] A. Andreanov, J. T. Chalker, T. E. Saunders, and D. Sherrington, Physical Review B **81**, 014406 (2010).

[112] J. Reimers, Physical Review B **45**, 7287 (1992).

[113] V. Narayan, S. Ramaswamy, and N. Menon, Science **317**, 105 (2007).

[114] D. J. Pearce and M. S. Turner, New Journal of Physics **16**, 082002 (2014).

[115] W. Geisler and D. A. et al., Visual neuroscience **14**, 897 (1997).

[116] H. Zeigler and E. H.J. Bischof, *Vision, Brain and Behavior in birds* (M.I.T. Press, 1993).

[117] A. Cavagna, S. D. Queirós, I. Giardina, F. Stefanini, and M. Viale, Proc. R. Soc. B **280** (2013).

[118] CGAL, *Computational Geometry Algorithms Library*, http://www.cgal.org.

[119] K. Binder, Rep. Prog. Phys. **60**, 487 (1997).

[120] P. Degond and S. Motsch, Mathematical Models and Methods in Applied Sciences **18**, 1193 (2008).

[121] A. Czirók and T. Vicsek, Physica A: Statistical Mechanics and its Applications **281**, 17 (2000).

[122] D. J. Pearce, A. M. Miller, G. Rowlands, and M. S. Turner, Proc. of Nat. Acad. Sci. **111**, 10422 (2014).

[123] N. Shimoyama, K. Sugawara, T. Mizuguchi, Y. Hayakawa, and M. Sano, Phys. Rev. Lett. **76**, 3870 (1996).

[124] J. Parrish and L. Edelstein-Keshet, Science **284**, 99 (1999).

[125] H. Berg., *E.Coli in Motion.* (Springer, 2004).

[126] M. M. Ghim and W. Hodos, Journal of Comparative Physiology A **192**, 523 (2006).

[127] J. Hirsch, Nature **300**, 57 (1982).

[128] W. Rasband, *imagej* (1997-2014), `http://imagej.nih.gov/ij/`.

Appendices

Appendix A

List of Supplementary Movies

All movies included with the thesis are the results of the simulations described in the text. All simulations were performed using software written by the author in C++. The resulting trajectories were plotted using MATLAB. In all movies each frame is a single time step.

A.1 Chapter 2: Distinguishing methods of nearest neighbour separation

Movies 2.1-2.4 show simulations of systems of 3 frustrated channels while Movie 2.5 shows the Logic gate described in main text and in Fig. 2.6. All movies are plotted after a co-ordinate transformation that maps the motion in linear periodic channels onto a circular channel. Rings that appear to touch in a movie share a boundary in the simulation, see Fig. 2.1.

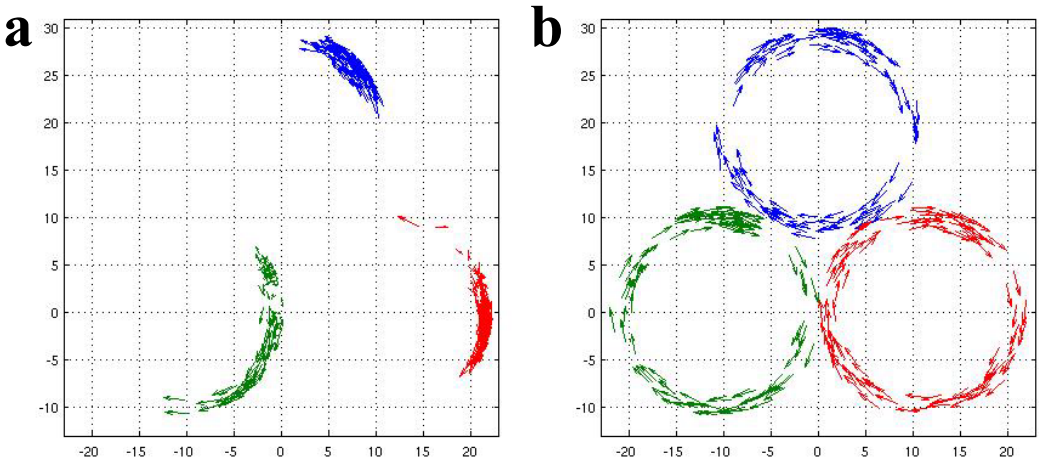

Figure A.1: (a) **Movie 2.1** Semi-frustrated system with metric-based particle interactions. Shown is the motion of particles in a system of 3 channels, each containing $N = 100$ particles with metric interactions of range $R = 4$ and noise level of $\phi_n = 0.3$. Each channel has a window with each of the other channels over a third of its length. This movie shows the *trains* phenotype. (b) **Movie 2.2** Semi-frustrated system with metric-free particle interactions. Shown is the motion of particles in a system of 3 channels, each containing $N = 100$ particles with metric-free interactions, $N_c = 45$ neighbours and a noise level of $\phi_n = 0.3$. Each channel has a window with each of the other channels over a third of its length.

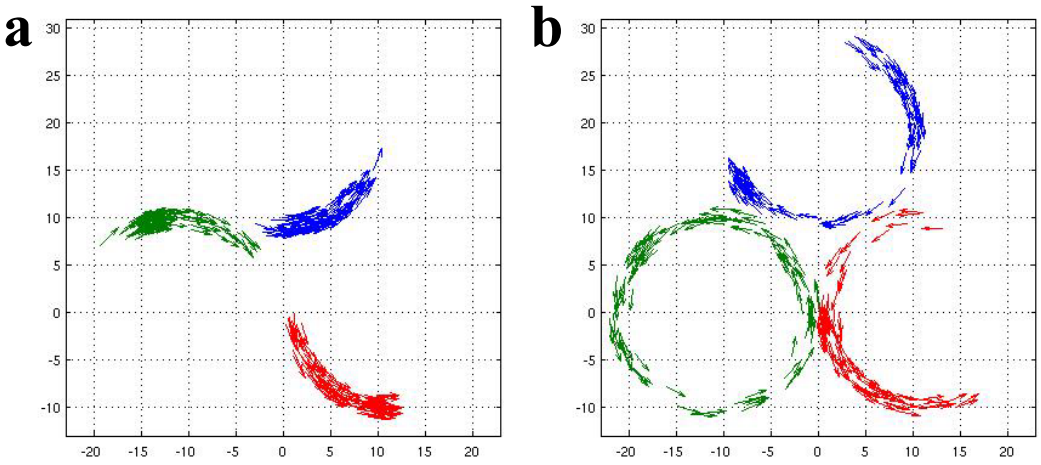

Figure A.2: (a) **Movie 2.3** Fully frustrated system with metric-based particle interactions. Shown is the motion of particles in a system of 3 channels, each containing $N = 100$ particles with metric interactions of range $R = 4$ and noise level of $\phi_n = 0.3$. Each channel has a window with each of the other channels over its entire length. This movie shows the *shuttles* phenotype. (b) **Movie 2.4** Fully frustrated system with metric-free particle interactions. Shown is the motion of particles in a system of 3 channels, each containing $N = 100$ particles with metric-free interactions, $N_c = 45$ neighbours and noise level of $\phi_n = 0.3$. Each channel has a window with each of the other channels over its entire length.

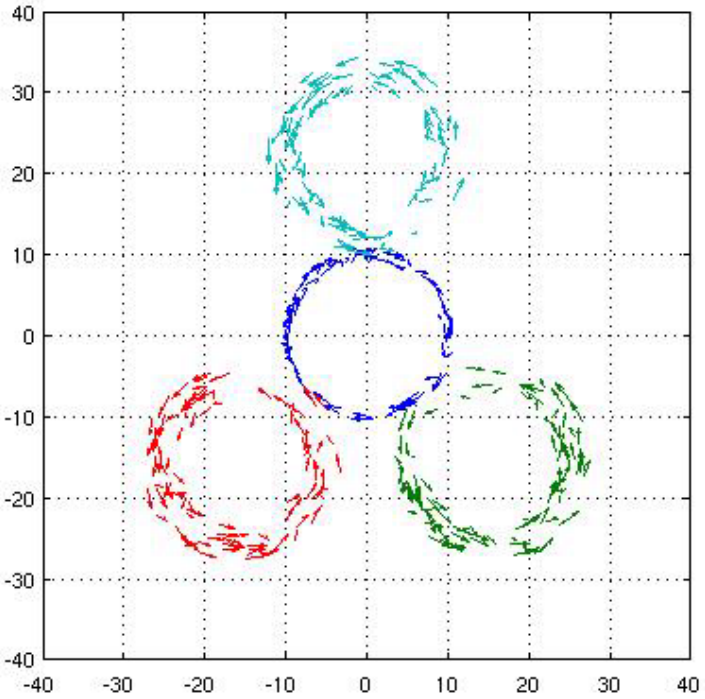

Figure A.3: **Movie 2.5** System of 4 channels acting as a logical OR gate. The central (blue) ring gives the *Output*, the other rings being two *Inputs* (red and green) and a similar *Locked* channel (cyan) in which the circulation is always anticlockwise (one can think of its window being a one-way mirror). The direction of particles in the In channels are manually switched at intervals of 500 time steps to explore all combinations of inputs. The Out channel spontaneously reverses its polarisation as necessary to mimic the behaviour of an OR gate.

A.2 Chapter 3: Strictly metric free density regulation

Movies 3.1 and 3.2 show typical swarms with $\phi_n = 0.5$ and $N = 100$ and $N = 500$, respectively. Movies 3.3 and 3.4 show a swarm going through the order transition and back for $N = 100$ and $N = 500$, respectively (see captions for details).

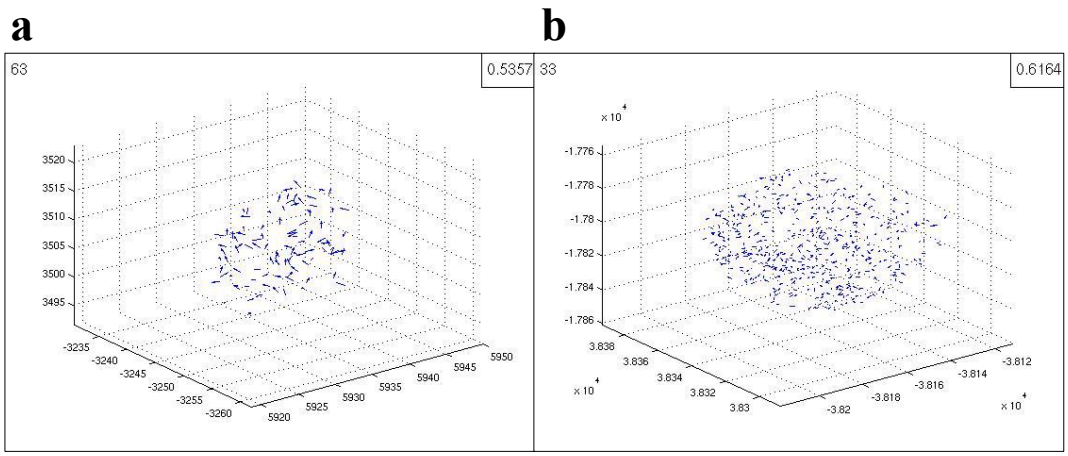

Figure A.4: (a) **Movie 3.1** shows a swarm of 100 particles with $\phi_n = 0.5$ resulting in a polarisation around $P = 0.6$. (b) **Movie 3.2** shows a swarm of 500 particles with $\phi_n = 0.5$ resulting in a polarisation around $P = 0.6$. The number in the top left shows the time step, and the polarisation is shown in the top right.

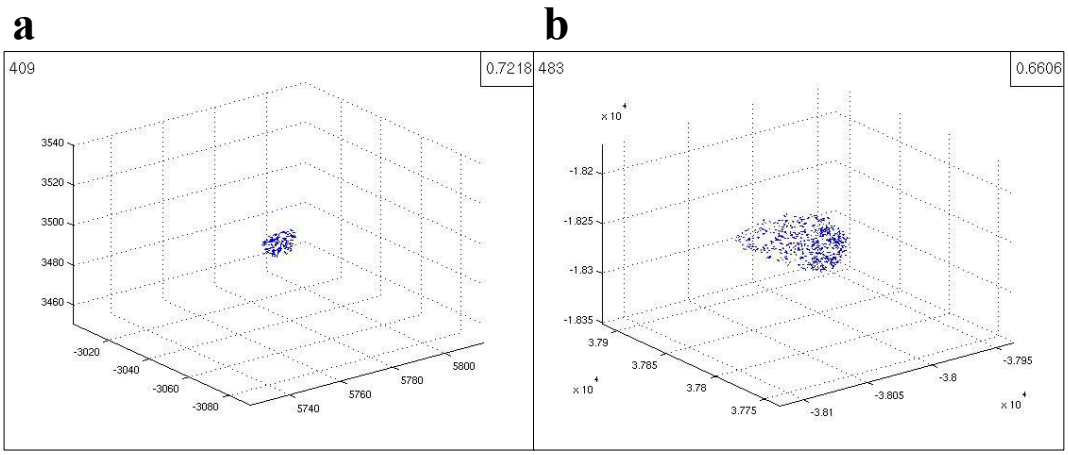

Figure A.5: (a) **Movie 3.3** shows a swarm of 100 particles starting with $\phi_n = 0.15$, increasing slowly until $\phi_n = 0.85$ at the middle of the movie and then decreasing back to $\phi_n = 0.15$ for the end of the movie. (b) **Movie 3.4** shows a swarm of 500 particles starting with $\phi_n = 0.15$, increasing slowly until $\phi_n = 0.85$ at the middle of the movie and then decreasing back to $\phi_n = 0.15$ for the end of the movie. These movies show the behaviour of the swarm through the order transition.

A.3 Chapter 4: Hybrid projection model

Movies 4.1 and 4.2 feature $N = 100$ individuals with $\phi_p = 0.2$, $\phi_a = 0.7$. The predator travels at a speed of $v_p = 2 * v_0$ and is attracted to the centre of mass of the swarm. The individuals react to the predator when it is within $r_p = 10 * dt * v_0$ and their response is to travel directly away from it at $v_{response} = 1.5 * v_0$. In Movie 4.2 individuals only react to other members of the swarm within $r_{limit} = 30 * dt * v_0$.

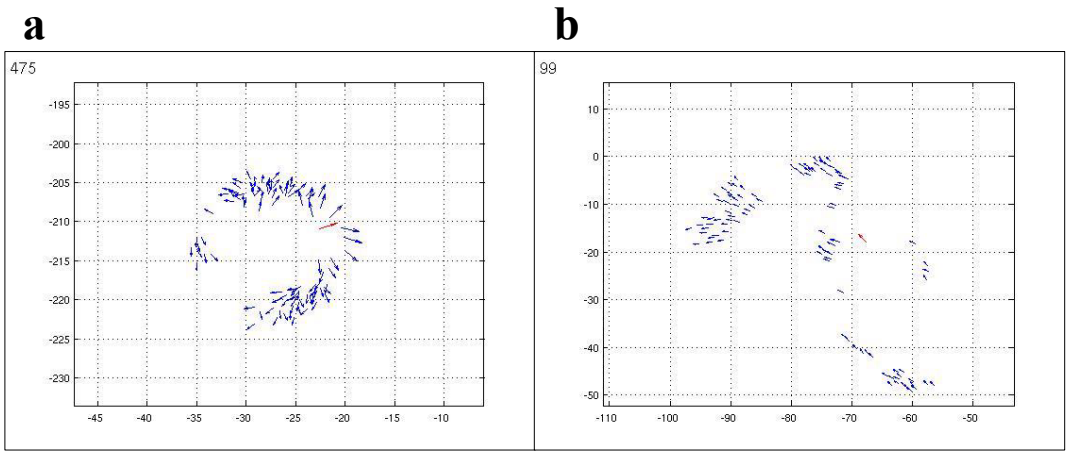

Figure A.6: (a) **Movie 4.1** shows the robustness of the hybrid projection model (blue arrows) under attack by a simple predator (red arrow) trying to split up the swarm. Due to the global nature of the interactions between individuals, the flock is always able to reform after the predator's attacks. (b) **Movie 4.2** shows how a swarm responds to the same predator when the interactions between individuals have a limited range. This means it becomes possible for the predator to completely sever interaction between two regions of the swarm resulting in a far less cohesive swarm that cannot guarantee that it will reform after becoming scattered.

Movies 4.3, 4.4 and 4.5, show the behaviour of a swarm of $N = 100$, 10:1 anisotropic (long and thin) individuals within our hybrid projection model. These movies show the distinct behavioural phenotypes observed with a change in the parameters ϕ_p and ϕ_a, highlighted in Fig. 4.13.

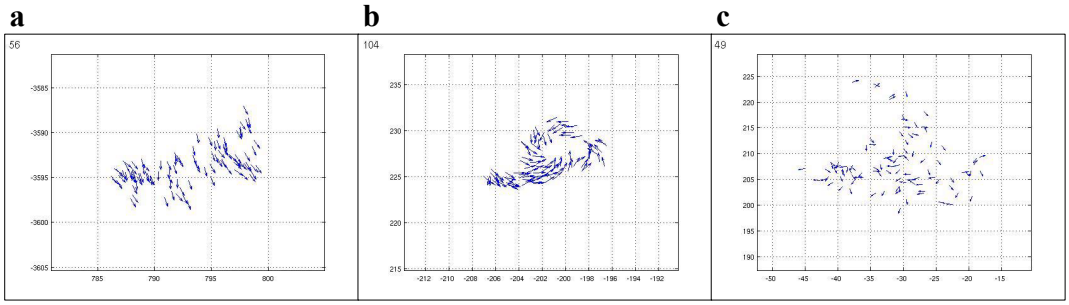

Figure A.7: (a) **Movie 4.3** is obtained for $\phi_p = 0.1$, $\phi_a = 0.75$, point B in Fig. 4.13; this shows a phenotype displaying a high level of orientational order similar to that seen in migratory animals. (b) **Movie 4.4** is obtained for $\phi_p = 0.45$, $\phi_a = 0.45$, point F in Fig. 4.13; this shows a phenotype displaying a high swarm vorticity much like the milling behaviour observed in fish. (c) **Movie 4.5** is obtained for $\phi_p = 0.175$, $\phi_a = 0.45$, point I in Fig. 4.13; this shows a phenotype with lower order in which there is a higher variation in the density of the swarm reminiscent of the swarming behaviour observed in insects.

Movies 4.6, 4.7 and 4.8 show the qualitative effects of the introduction of a "blind angle" behind each individual. This means that the projection term does not respond in any way to individuals within a $\pi/8$ cone directly behind them. Movies 4.6, 4.7 and 4.8 show simulations with exactly the same parameters as movies 4.3, 4.4 and 4.5, respectively, and highlight the modest effect of the blind angle on the behaviour.

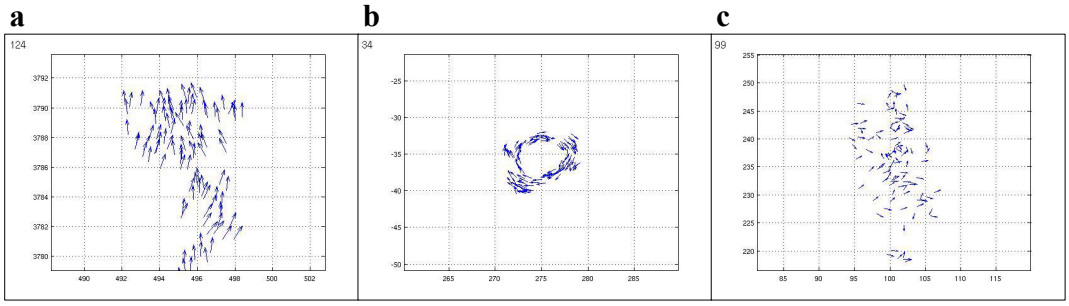

Figure A.8: Movies showing the effects of a blind angle behind each individual. (a) **Movie 4.6** is obtained for $\phi_p = 0.1$, $\phi_a = 0.75$, point B in Fig. 4.13; this shows a phenotype displaying a high level of orientational order similar to that seen in migratory animals. (b) **Movie 4.7** is obtained for $\phi_p = 0.45$, $\phi_a = 0.45$, point F in Fig. 4.13; this shows a phenotype displaying a high swarm vorticity much like the milling behaviour observed in fish. (c) **Movie 4.8** is obtained for $\phi_p = 0.175$, $\phi_a = 0.45$, point I in Fig. 4.13; this shows a phenotype with lower order in which there is a higher variation in the density of the swarm reminiscent of the swarming behaviour observed in insects. The parameters of these movies are exactly the same as those used in Movies 4.3, 4.4 and 4.5. Individuals in these simulation do not respond in any way to anything within a $\pi/8$ directly behind them.

A.4 Chapter 5: Marginal opacity observed in starling flocks in the wild

Movies 5.1 and 5.2 are of the starling flocks shown in the red and black traces of Fig. 5.7c, respectively. These were taken at Brighton, East Sussex, UK on 14/11/2011 between 15:30 and 16:30. These are typical of the type of footage captured of Starling flocks.

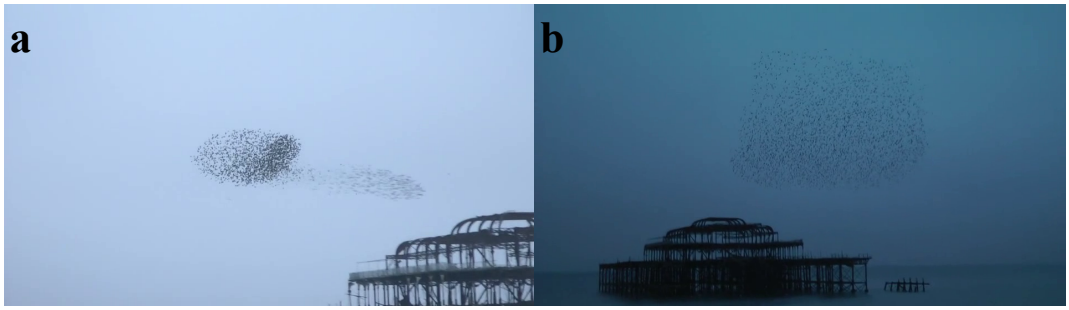

Figure A.9: **Movie 5.1** and **Movie 5.2** show typical footage of a starling flock taken at Brighton, East Sussex, UK on 14/11/2011 at (a) 1540 and (b) 1610 GMT.